UNIVERSITÀ DEGLI STUDI DI FERRARA

Dottorato di Ricerca in
FISICA
CICLO XXXV

Coordinatrice Prof. Luppi Eleonora

Study of the $e^+e^- \to \pi^+\pi^-\psi(2S)$ reaction at centre-of-mass energies above 4.600 GeV and search for the charged $Z_c(4430)$ exotic state at BESIII

Settore Scientifico Disciplinare FIS/01

Dottorando:
Scodeggio Marco

Tutore:
Dr. Cibinetto Gianluigi

Co-Tutore:
Dr. Mezzadri Giulio

Anni 2019/2022

Contents

List of Figures

List of Tables

Introduction

Introduced in the past century, the Quark Model has been fundamental in the classification of standard mesons and baryons. Till 2003, despite Quantum Chromodynamics allowing more complex structures, no clear signatures of exotic hadrons had been found. The Belle collaboration opened a door with the $X(3872)$ discovery. Since then, many new hadrons that do not fit the standard Quark Model prediction have been discovered. These hadrons are collectively dubbed XYZ states. From a theoretical side, many interpretations came forth using phenomenological approaches and non-relativistic effective field theories or lattice QCD calculations. Yet, despite all these theoretical and experimental inputs, the scientific community seems to be far from understanding the nature of these states.

The BESIII collaboration has been at the forefront of the XYZ sector studies since the dawn of the first discoveries and this thesis wants to contribute to the understanding of the XYZ sector by studying the $e^+e^- \to \pi^+\pi^-\psi(2S)$ process with BESIII data both to probe the $Y(4660)$ nature and to search for the $Z_c(4430)$ state. The BESIII collaboration has already seen the $Y(4660)$ in this channel, but measuring the $e^+e^- \to f_0(980)\psi(2S)$ contribution to the whole $e^+e^- \to \pi^+\pi^-\psi(2S)$ process might give some insights over the $Y(4660)$ states interpretations. Furthermore, the direct search for the $Z_c(4430)$ state at the BESIII experiment is fundamental as its discovery would be an important step ahead to understanding this resonance as only the Belle and LHCb collaborations saw the $Z_c(4430)$ state and exclusively in B decays.

This work aims to study the $e^+e^- \to \pi^+\pi^-\psi(2S)$ process using six data samples with a total integrated luminosity of $\sim$5 fb^{-1} collected by the BESIII detector at centre-of-mass energies ranging from 4.6121 GeV to 4.6984 GeV. The $e^+e^- \to f_0(980)\psi(2S)$ sub-process is studied as well and its contribution to the to-

tal cross-section is estimated. Finally, a search for the charged $Z_c(4430)$ tetraquark state is performed.

This work is divided into five chapters which are developed as follows:

- **Chapter 1** carries out a brief introduction to Quantum ChromoDynamics and the Quark Model. The charmonium system is described as well, emphasising the $h_c(1^1P_1)$ pseudovector resonance;
- **Chapter 2** will focus on the XYZ exotic states describing some of the latest and most important experimental measurements and introducing some of their phenomenological interpretations;
- In **Chapter 3** BESIII detector and its components are described;
- In **Chapter 4**, **Chapter 5**, **Chapter 6**, and **Chapter 7** this thesis' analysis is introduced and described, and its results are presented and discussed;
- **Chapter 8** describes the systematic uncertainties of this analysis and presents the thesis' outlook.

Chapter 1

Quantum ChromoDynamics and Charmonium Spectroscopy

For almost a century, the physics community has agreed that the structure of ordinary matter, encountered or created in high-energy physics (HEP) experiments, is made of fermions interacting via exchanging bosons. The elementary fermions are leptons and quarks, while the bosons are the mediators of the forces with which the aforementioned fermions interact. Aside from gravity, three are the forces, probed in HEP experiments, fermions interact with: the electromagnetic, the weak, and the strong interaction. This theory (and its extension to include the Higgs boson) goes by the name of the Standard Model (SM) [1]. The mathematical modelisation of these interactions is described by relativistic quantum field theories.

Quantum ChromoDynamics (QCD) is the SM theory that describes strong interaction (*i.e.*, the dynamics of quarks and gluons), as it will be made clear throughout this Chapter, many of its predictions have been tested successfully in a broad range of energies. Though, despite its successes in describing the strong interaction, the free QCD Lagrangian does not model the binding of the quarks and gluons into hadrons. This modelisation is taken care of by the Quark Model, introduced by Gell-Mann [2] and Zweig [3] in 1964.

The initial effective theory proposed contained only three quark *flavours* (*up*, *down*, and *strange*), but the additional hadrons discovered since its first formulation needed three additional elements (*charm*, *bottom*, and *top*).

Since their discovery in 1974 [4–6], the *charm* (c) quark and its $c\bar{c}$ bound states have been an important test bench for understanding and testing the QCD. Indeed, due to the relatively high mass of the $c\bar{c}$ systems, perturbative QCD (pQCD) and effective theories (*e.g.*, the non-relativistic potential model) can be employed, providing

also insights on the non-perturbative structure of this theory.

1.1 Quantum ChromoDynamics

QCD is a non-abelian $SU(3)_C$ quantum field theory, where the symmetry properties are encapsulated in the *colour*-charge and each of the quarks can take one of three values of charge (*R, G, B*). The Yang-Mills QCD Lagrangian [7] can be written as follows:

$$\mathcal{L} = -\frac{1}{4}(F^a_{\alpha\beta})^2 + \sum_f \bar{\psi}_f(i\not{D} - m_f)\psi_f, \tag{1.1}$$

where $F^a_{\alpha\beta}$ is the field strength tensor which is obtained from the gluon field A^a_α as

$$F^a_{\alpha\beta} = \partial_\alpha A^a_\beta - \partial_\beta A^a_\alpha + g_s f^{abc} A^b_\alpha A^c_\beta, \tag{1.2}$$

with f^{abc} the $SU(3)_C$ structure constants and g_s the strong coupling constant. The *non-abelian feature* of the QCD (*i.e.*, the possibility for the gluons to self-interact) is encoded by the last term in Eq. (1.2). The ψ_f ($\bar{\psi}_f$) multiplet describes the quark (antiquark) spinor field of flavour f with mass m_f in the given representation r of SU(3). The index sum in Eq. (1.1) runs over the six flavours (*u, d, c, s, t, b*), while the index a refers to the QCD colour charge (technically, the sum over the 8 generators of the SU(3) group is implied). The mass m_f is not the mass of the quark constituting the hadrons but the bare mass of the free fermion. Finally, the QCD covariant derivative $\not{D}$ is explicitly written as:

$$\not{D} = \gamma^\mu(\partial_\mu - ig_s A^a_\mu t^a_r). \tag{1.3}$$

The t^a_r are the eight 3×3 generator matrices of SU(3) written in a given representation r. These matrices are connected to the structure constants f^{abc} via the $[t^a, t^b] = if^{abc}t^c$ relation.
Variating the QCD Lagrangian (Eq. 1.1), it is possible to estimate the QCD Feynman diagrams. From the first three non-linear terms, the three QCD vertices, shown in Fig. 1.1, are obtained:

- the fermion-gluon vertex;
- the 3-gluon vertex;

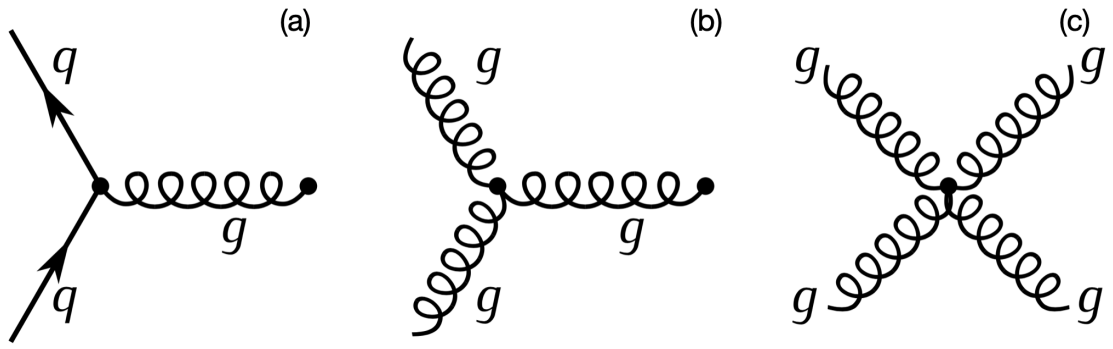

Figure 1.1: QCD vertices that can be estimated from the QCD Lagrangian: Fig. (a) is the fermion-gluon vertex, while the 3- and 4-gluon vertices are shown in Figs. (b) and (c), respectively.

- the 4-gluon vertex.

The last two vertices are the explicit result of the non-abelian algebra, which relates to the fact that gluons carry a colour charge. This feature is fundamental in describing another property of QCD (and more generically of all non-Abelian gauge theories), the asymptotic freedom (and its specular counterpart, the confinement). Related to this is the particular behaviour of the strong interaction coupling constant (α_s). The running of the coupling constant happens as well in Quantum ElectroDynamics (QED) and it derives from loops correction, which might give divergent contributions, to the tree-level Feynman diagrams, like the ones presented in Fig. 1.1). The peculiarity of QCD, due to the non-abelian nature allowing bosonic loops, is that α_s decreases at higher energies. More specifically, below the scale Λ_{QCD}, experimentally determined to be ~ 0.2 GeV [1], $\alpha_s \sim 1$ and the confinement property of QCD is observed[1].

Before arising from the structure of the theory itself, asymptotic freedom was experimentally requested as a consequence of the *parton model* (developed by Bjorken [8] and Feynman [9]). In the mentioned model, introduced for explaining the observations in the Deep Inelastic Scattering experiments, the nucleons are described as bound systems of *partons* (quarks and gluons), each carrying part of the nucleons' momentum. The conclusions of this model (cf., Bjorken scaling [8]) stated that the

[1]The discussion of α_s and its implications are merely qualitative here. The quantitative origin of α_s derives from the renormalisation of QCD. For a more organic explanation please refer to Ref. [7].

interactions between *partons* have to "*switch off*" at relatively short time scales; put it in better words, when confined in a bound system *partons* have to be essentially free. This regime can use a perturbative expansion to study the strong interaction (pQCD). On the other hand, if one considers energies smaller than Λ_{QCD} one gets the so-called "confinement". In this case, the strong coupling constant is ~ 1 and higher-order contributions become important, hence a perturbative approach cannot be pursued. This energy region corresponds to the separation of colour-singlet particles greater than about 1 fm; the energy cost to separate coloured objects grows proportionally to the separation. If coloured particles are separated at a distance longer than 1 fm, quark-antiquark pairs are excited from the vacuum to create a less energetic system. Indeed, in high-energy collisions, we observe particles' jets, which are the products of hadronization: the rapid, in terms of strong force time scale, formation of hadrons starting from free-coloured particles.

1.1.1 Potential Model

The properties of QCD introduced in the previous section allow for building an effective model, taking the form of a potential describing both confinement and asymptotic freedom. This theoretical model was proposed after the J/ψ and $\psi(2S)$ discoveries [10–13] and relies on the charm quark mass ($\gtrsim$1 GeV/c^2). Due to its mass, the momentum of a confined charm quark is $m_c v_c^2 = 0.3$ GeV, implying that, in natural units, $m_c >> m_c v_c >> m_c v_c^2$ and giving the possibility at first order to neglect the relativistic effects[2].

The potential model takes the following form [13]:

$$V(r) = -\frac{\alpha_s}{r}\left[1 - \left(\frac{r}{a}\right)^2\right], \tag{1.4}$$

with a being the scale at which the confinement becomes important. In analogy to QED, the first term (the so-called Coulombian) represents a single gluon exchange and describes asymptotic freedom. On the other hand, the linear term is an effective description of the flux tube which comes to formation when one tries to separate colour-singlet states; this term, describing a multi-gluon exchange, models quarks confinement.

[2]This model holds also for the bottomonium ($b\bar{b}$ bound state) and, potentially, for any hypothetical system made by quarks heavy enough to neglect relativistic effects.

1.2 Quark Model

As mentioned earlier in this Chapter, the free QCD Lagrangian does not model the binding of quarks and gluons into hadrons. This modelisation was carried out independently by Gell-Mann [2] and Zweig [3] in 1964. The underlying idea is that the experimentally observed colour-neutral hadrons could be described by starting from elementary constituents. These constituents are nowadays referred to as Gell-Mann first named them, *i.e.*, *quarks*. The original model is built around three flavours of quarks: up (u), down (d), and strange (s). With the discovery of additional hadrons, the Quark Model has been extended adding the last three quark flavours: charm (c), bottom (b), and, potentially, top (t), though a top-containing bound system has not yet been observed. In this model, mesons are interpreted as quark-antiquark pairs and (anti)baryons as bound states of three (anti)quarks; it comes naturally that for this model quarks need to have fractional electric charges. In its first formulation, the quarks are organised into multiplets of *isospin*, *i.e.*, the degree of freedom of the flavour $\mathrm{SU(3)_F}$ symmetry; assuming that the up and down quarks have identical masses and interactions, they form an isospin doublet, while the strange quark is left in an isospin singlet. With this information, it is possible to relate the electric charge of the quarks (in units of the electron charge) to the third component of the isospin (I_3) and the baryon number (B):

$$Q = \frac{B+S}{2} + I_3, \tag{1.5}$$

where I_3 is ($\frac{1}{2}$, -$\frac{1}{2}$, 0) for the (u, d, s) flavours and S is the strangeness (-1 if the hadrons contain an s-flavoured quark)[3]. Moreover, considering mesons have a baryon number equal to 0, while it is 1 for baryons, quarks must have $B = \frac{1}{3}$, and the opposite holds for antibaryons and antiquarks. It is evident that, with these quantum numbers, quarks do have a fractional electric charge.

Despite this model does not take into account spins, angular momentum, and their interactions, one can construct, assuming SU(3) flavour symmetry, mesons and baryons multiplets with the same flavour symmetry, but with different quantum numbers.

[3]This formula can be extended to include the three other additional quark flavours (c, b, t) by adding the corresponding terms $[C + \tilde{B} + T]$.

Mesons are formed by combining quark-antiquark pairs, each in one of the three possible flavours (*i.e.*, in a fundamental representation of $\mathrm{SU(3)_F}$). As such, one has $3 \otimes \bar{3} = 1 \oplus 8$, obtaining a flavour octet and a singlet.

Baryons are built in a similar manner combining triplets of quarks, *i.e.*, $3 \otimes 3 \otimes 3 = 1_\mathrm{A} \oplus 8_\mathrm{M} \oplus 8_\mathrm{M} \oplus 10_\mathrm{S}$, getting an antisymmetric flavour singlet, a symmetric decuplet, and octets of mixed flavour symmetry.

Despite SU(3) flavour symmetry being assumed, it is not an exact symmetry. As such, within the same multiples, the different mesons and baryons have different masses. These differences can be explained by the fact that the constituent quarks do not have the same masses ($m_{up} \sim m_{down} << m_{strange}$). On top of this, one must consider spins, angular momentum, and their interactions; different multiplets of different total angular momenta will have different masses for the same quark content, due to quarks interactions modifying the hadron's mass (notably, this is the case of the pseudoscalar π meson and the vector ρ state). Finally, quarks are electromagnetically charged particles, hence, the symmetry is furtherly broken by the electromagnetic interaction (*e.g.*, the different masses of neutron and proton).

Now that we have the Quark Model on one side and the QCD Lagrangian on the other, how do they connect? How one justifies the other? The connection between these two ideas came to explain the existence of the Δ^{++}, the Δ^{-}, and the Ω^{-} baryons (uuu, ddd, and sss bound states). These three states are symmetric under spin (as they all are spin-3/2 particles) and flavour interchange and they are the lowest-lying S-wave decuplet states, implying that these baryons' spatial wavefunctions are symmetric. Though quarks, being spin-1/2 particles, obey the Fermi-Dirac statistics, hence they must carry an additional degree of freedom to justify the Δ^{++}, Δ^{-}, and Ω^{-} baryons existence. This additional degree of freedom is nonetheless that the *colour*-charge discussed at the beginning of Sec. 1.1.
The existence of coloured quarks is confirmed by the so-called R-ratio, which is the ratio between the $e^+e^- \to$ hadrons cross-section and the $e^+e^- \to \mu^+\mu^-$ one. At the leading order, the R-ratio is calculated to be proportional to 3 times the squared sum of the quarks' electric charges, where the sum is performed over the contributing flavour at the centre-of-mass energy ($\sqrt{s}$) at which the R-ratio is calculated. The experimental confirmation of the R-ratio is proof of the existence of a hadronic substructure made of fractional electric charges and *colour*-charge contributions.

1.3 Charmonium Spectroscopy

As mentioned, thanks to the Glashow, Iliopoulos and Maiani (GIM) [14] mechanism the *charm* quark was predicted. This mechanism was introduced to solve a puzzling feature introduced by the "Cabibbo mixing", a theory proposed by Cabibbo [15] to explain the differences in the proton and hyperion β-decay cross-sections. The theory, as it was proposed, implied that Flavour Changing Charged Currents must have the same probability as Flavour Changing Neutral Currents, which are instead suppressed in the experimental observation. The addition of a quark and the GIM [14] mechanism allows for explaining the observations.
Few years later, an indirect confirmation of the *charm* quark existence arrived. Simultaneously, at BNL, in a $p + Be \rightarrow e^+e^- + X$ experiment, and at SLAC, in the $e^+e^- \rightarrow$ hadrons (leptons) reaction, a narrow resonance called J/ψ was discovered [4, 5]. That year, the latter experiment discovered also the ψ' resonance [6].
Both the experiments measured the same J/ψ mass (~ 3.1 GeV/c^2) and SLAC provided the width of the two resonances and the $\psi(2S)$ mass. The features of these resonances could not be explained in terms of u, d, s bound states. Only by using the *charm* quark, the particle's mass could be explained. Moreover, their widths were a clear indication that a new type of quark had been produced. Following the prescription of the Okubo, Zweig, and Iizuka (OZI) selection rule, decays described by diagrams with unconnected quark lines are suppressed concerning the connected ones. Indeed, the decay towards charmed mesons (*i.e.*, containing only one c quark) is forbidden by energy conservation as J/ψ and $\psi(2S)$ states lay below the $D^0\bar{D}^0$ threshold (3.73 GeV [1]), hence these resonances can only decay into non-charmed hadrons.

Since their discovery, charmonia ($c\bar{c}$ states) have been fundamental tools for understanding the strong interaction and testing QCD. In particular, due to the high mass of the constituent quarks, relativistic corrections can be neglected at the first order so that pQCD and effective field theories (*e.g.*, non-relativistic potential model) can be employed. The spectrum of the charmonium resonances is shown in Fig. 1.2 and the subsequent sections will be dedicated to its description.

Fig. 1.2 wants to provide a pictorial explanation of the charmonium spectrum before and after the discovery by the BELLE collaboration [17] of the $X(3872)$ state, the first non-standard charmonium ever found. Before 2003, the knowledge of the states above the $D^0\bar{D}^0$ threshold was very limited, mostly due to the relatively low

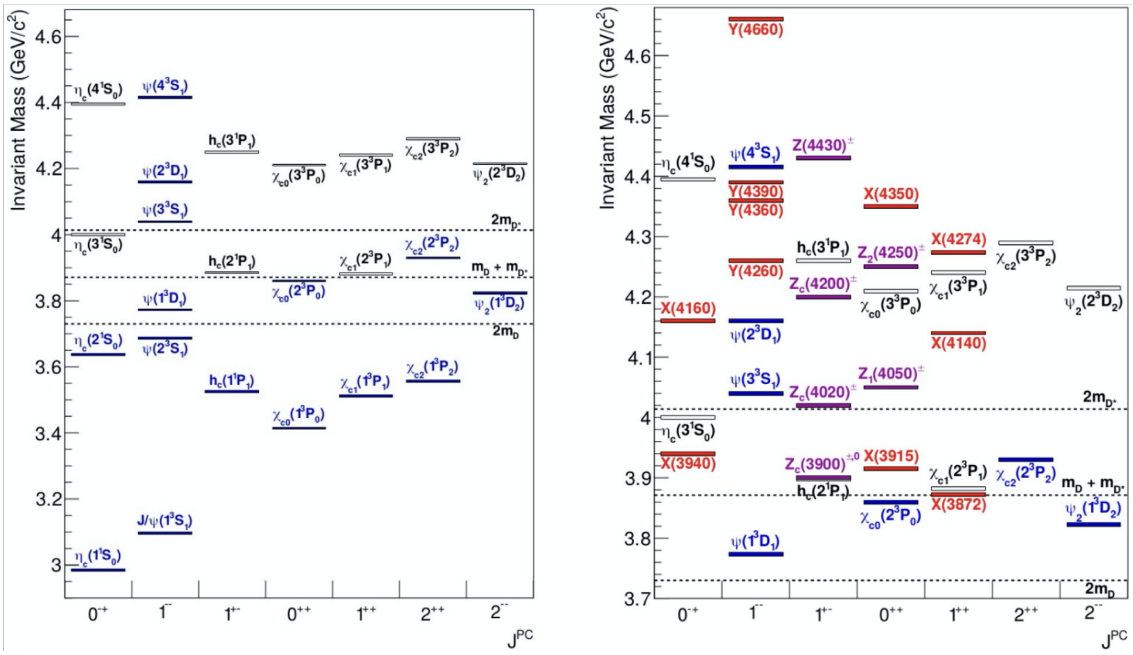

Figure 1.2: States populating the charmonium spectrum: on the left, the full charmonium spectrum is shown with the knowledge above the $D^0\bar{D}^0$ threshold previous to 2003; on the right, the charmonium spectrum above the $D^0\bar{D}^0$ threshold with the present knowledge [1] is depicted. The blue boxes show the predicted and discovered charmonium states; the grey boxes represent the predicted conventional charmonia, but not yet discovered; the red boxes represent the neutral non-conventional XYZ states, while the magenta boxes show the charged non-conventional states. Ref. [16].

precision caused by the large widths of the charmonia that populate this energy reason. Since the discovery of the $X(3872)$ [17] particle, the region above the open-charm threshold has become a subject of interest for "non-standard" physics and it has grown overpopulated with new states. The newly discovered particles do not all fit in the standard charmonium description; these exotic states were then dubbed XYZ to recognise their still-elusive nature and are the topic of this thesis.

1.3.1 The Potential Model Strikes Back

Drawing from conclusions of Sec. 1.1.1 and the potential in Eq. (1.4), it is possible to write the non-relativistic Hamiltonian as

$$H = 2m_c + \frac{p_c^2}{m_c} - \frac{\alpha_s}{r}\left[1 - \left(\frac{r}{a}\right)^2\right], \tag{1.6}$$

and solve its associated Schrödinger equation.
As this model is put to test in the charmonium spectrum description, the Hamiltonian in the Eq. (1.6) formulation is not entirely adequate to describe all of the charmonium spectrum states, as it does not take into account the quarks' spins (S), angular momenta (L), and their interactions. Hence, to Eq. (1.6) one has to add additional terms (cf., Ref. [18]):

$$\widetilde{H} = V_{SS} + V_{LS} + V_{tens}. \tag{1.7}$$

These additional corrections describe the spin-spin interaction (V_{SS}), the spin-orbit interaction (V_{LS}), and tensor interaction (V_{tens}). They depend on whether the interaction arises from the exchange of a single gluon or an effective scalar object (*i.e.*, a modelisation of a multi-gluon exchange); the Fourier transform of the transition matrix element of these exchange processes allows ones to obtain the vectorial ($V_V(r)$) and scalar ($V_S(r)$) terms, from which the three correction factors depend on. Indeed, higher orders of effective interactions are also possible. Hence, one can relate the three terms of Eq. (1.7) to these two additional interaction terms as follows:

- For the Spin-Spin interaction, one has

$$V_{SS} = \frac{\bar{\sigma}_q \cdot \bar{\sigma}_{\bar{q}}}{6 m_q m_{\bar{q}}} \Delta V_V(r), \tag{1.8}$$

  where $\bar{\sigma}_q$ ($\bar{\sigma}_{\bar{q}}$) and m_q ($m_{\bar{q}}$) are the Pauli matrix, encoding the spin, and mass of the constituent (anti)quark, respectively. The $\bar{\sigma}_q \cdot \bar{\sigma}_{\bar{q}}$ product is equal to $+1$ for triplet states and -3 for singlet ones and V_{SS} is nonzero (at leading order) only between S states [18].

- For the Spin-Orbit interaction, one obtains

$$V_{LS} = \frac{\mathbf{L} \cdot \mathbf{S}}{2 m_q m_{\bar{q}} r} \left(3 \frac{dV_V(r)}{dr} - \frac{dV_S(r)}{dr} \right), \tag{1.9}$$

  where $\mathbf{L}$ and $\mathbf{S}$ are the angular momentum and spin operators, respectively. The $\mathbf{L} \cdot \mathbf{S}$ product is trivially 0 for S-wave states and is calculated to be (1, -1, -2) for the ($^3P_2$,$^3P_1$,$^3P_0$) ones.

- For the Tensor interaction, one gets

$$V_{tens} = \frac{2[3(\mathbf{S}\cdot\hat{\mathbf{r}})^2 - \mathbf{S}^2]}{12 m_q m_{\bar{q}}} \left(\frac{1}{r}\frac{dV_V(r)}{dr} - \frac{d^2V_S(r)}{dr^2}\right), \tag{1.10}$$

  where $3(\mathbf{S}\cdot\hat{\mathbf{r}})^2 - \mathbf{S}^2$ is non-zero only for non-S states and its expectation values are $(-2/5,\ 2,\ -4)$ for the $(^3P_2, ^3P_1, ^3P_0)$ states.

These additional corrections allow describing the charmonium spectrum in complete analogy with the Hydrogen system. Hence, three quantum numbers are necessary to describe the $c\bar{c}$ states: total angular momentum J = L + S, parity P = $(-1)^{\mathrm{L}+1}$, and charge conjugation C = $(-1)^{\mathrm{L+S}}$.

The potential model has proven to be successful in describing and predicting charmonium and bottomonium resonances. The model works strikingly well with the resonances below the $D^0\bar{D}^0$ threshold. Above the open charm threshold, calculations are more difficult, due to many threshold openings (*e.g.*, DD^*, D^*D^*, D_sD_s, and $D_s^*D_s^*$), which couple to $c\bar{c}$ bound states modifying their properties. The potential model can be still used as a blueprint to identify non-standard charmonia, as it has been clear since the observation of many unpredicted exotic states in this energy region.

1.3.2 States below Threshold

Below the $D^0\bar{D}^0$ threshold, eight states can be encountered. Of these, the most well-measured and studied are the vector resonances, as they can be directly produced in e^+e^- colliders. The least-known charmonium, to which the next Section is dedicated, is the $h_c(1\ ^1\mathrm{P}_1)$ state. This resonance has been also the object of an analysis I concluded during my PhD work. The Sec. 1.3.2.1 briefly describes the $h_c(1\ ^1\mathrm{P}_1)$ state importance and outlines the main results of my analysis.

1.3.2.1 The $h_c(1^1P_1)$ State: a Special Mention

Due to its $J^{PC} = 1^{+-}$ quantum numbers, knowledge of the singlet state $h_c(1^1P_1)$ is sparse. It is not possible to produce this resonance directly in leptonic colliders, and the $\psi(2S) \to h_c$ production branching ratios are relatively small ($\sim 10^{-4}$). Its features are of importance inside the theoretical framework of the potential model as

the V_{SS} term is crucial in the estimation of the 1P mass splitting Δ_{hyp} = M(c.o.g.) - M(h_c), where

$$M(\text{c.o.g.}) = \frac{M(\chi_{c0}) + 3M(\chi_{c1}) + 5M(\chi_{c2})}{9}, \tag{1.11}$$

is the centre-of-gravity mass of the three $\chi_{cJ}(1\ ^3\mathrm{P}_J)$ states. As already mentioned, predictions [18] state that the splitting should be 0 at the leading order. Hence, big deviations from $\Delta_{hyp}(1P) = 0$ would put at stake the short-range Coulomb-like nature of the strong interaction. For this purpose, measurements of its mass (cf., Table 1.1) have been performed by the BESIII [19, 20], the CLEO [21], and the E835 [22] collaborations, but a better precision is desirable as the uncertainty on $\Delta_{hyp}(1P)$ is still much bigger than its value.
Moreover, of this state only nine decay modes have been observed, with the E1 (i.e, electric dipole) transition $h_c \to \gamma\eta_c$ being the predominant one, with a branching fraction of $(50 \pm 9)\%$ [1]. Its hadronic transitions, though, still add up to only 10^{-4} of its total decay width [1], suggesting that a lot of studies are still missing.
The $\psi(2S) \to \pi^0 h_c(1^1P_1)$ production mechanism is also known with a relatively large uncertainty [1].
Finally, only one measurement of its width had existed before 2022 [23], provided by the BESIII experiment [20] using the $h_c \to \gamma\eta_c$ process, with the η_c resonance reconstructed into 16 different decay modes.
A more precise knowledge of the $h_c(1^1P_1)$ resonance parameters is needed in the light of the discoveries in the XYZ (cf., Section 2) sector as the h_c resonance is an intermediate state [24, 25] of these exotic states transitions.

Mass [MeV/c^2]	Width [MeV/c^2]	Δ_{hyp} [MeV/c^2]	Experiment
$3525.8 \pm 0.2 \pm 0.2$	$0.5 < \Gamma < 1.1$	-	E835 [22]
$3525.20 \pm 0.18 \pm 0.12$	-	$0.02 \pm 0.19 \pm 0.13$	CLEO-c [21]
$3525.40 \pm 0.13 \pm 0.18$	< 1.44	$-0.10 \pm 0.13 \pm 0.18$	BESIII [19]
$3525.31 \pm 0.11 \pm 0.14$	$0.70 \pm 0.28 \pm 0.22$	$-0.01 \pm 0.11 \pm 0.15$	BESIII [20]

Table 1.1: Summary [1] of the h_c mass and width, and Δ_{hyp} measurements. The shown results are the ones used by the PDG for "*for averages, fits, limits, etc.*". The PDG provides the following h_c average mass: $\mathrm{M(h_c)} = 3525.38 \pm 0.11$ MeV/c^2.

The latest study on the $h_c(1^1P_1)$ resonance, namely Ref. [23] by the BESIII collaboration, provides its parameters via the $\psi(2S) \to \pi^0 h_c(1^1P_1) \to \pi^0\gamma\eta_c$ transition, using the world's largest $\psi(2S)$ data sample. The branching fractions of the involved decays ($\psi(2S) \to \pi^0 h_c(1^1P_1)$, $h_c(1^1P_1) \to \gamma\eta_c$, and the whole decay chain) are measured as well.
Besides providing the second-ever measurement of the $h_c(1^1P_1)$ width with a similar uncertainty as the other BESIII estimate [20], Ref. [23] increased the branching fractions precision by two and three times concerning the PDG values [1]. All of the aforementioned values are extracted from the fit to π^0 recoil mass spectra presented in Fig. 1.3.
Finally, Ref. [23] estimated Δ_{hyp} finding it to be consistent with 0 as the prediction states it to be at the leading order [18].

1.3.3 States above Threshold

Above the $D^0\bar{D}^0$ threshold, the experimental knowledge of charmonium resonances is limited by the statistics and due to the complexity of the threshold effects and the mixing between the states lying in this region. Nonetheless, this energy region is bustling with new interesting discoveries as many of the found states have dubious or unknown quantum numbers and nature. As shown in Fig. 1.2, above threshold eight canonical $c\bar{c}$-states have been observed[4]: four in D-wave ($\psi(1^3D_1)$, $\psi_2(1^3D_2)$, $\psi_3(1^3D_3)$, and $\psi(2^3D_1)$), two in S-wave ($\psi(3^3S_1)$ and $\psi(4^3S_1)$), and two in P-wave ($\chi_{c0}(2^3P_0)$ and $\chi_{c2}(2^3P_2)$).
The first established charmonium state, called $\psi(3770)$ (or $\psi(1^3D_1)$), was discovered by the LGW collaboration [26] decaying into hadrons. Indeed, with a width of ~ 100 MeV/c^2, the $\psi(3770)$ decays mainly ($\gtrsim$90% [1]) to $D\bar{D}$ pairs as a further confirmation of the aforementioned OZI selection rule.

The energy region above the open-charm threshold is both theoretically challenging and experimentally exciting due to the discoveries within the XYZ exotic family. These states, to which Chapter 2 is dedicated, do not have a "conventional" structure as their masses are not accommodated into the potential model, despite showing an internal charmonium structure. These exotic resonances point toward

[4]Ref. [1] reports more than seven hypothetical charmonia above the $D^0\bar{D}^0$ threshold. Though the quantum numbers of these states are not yet fully determined, their masses and widths do not match theoretical predictions.

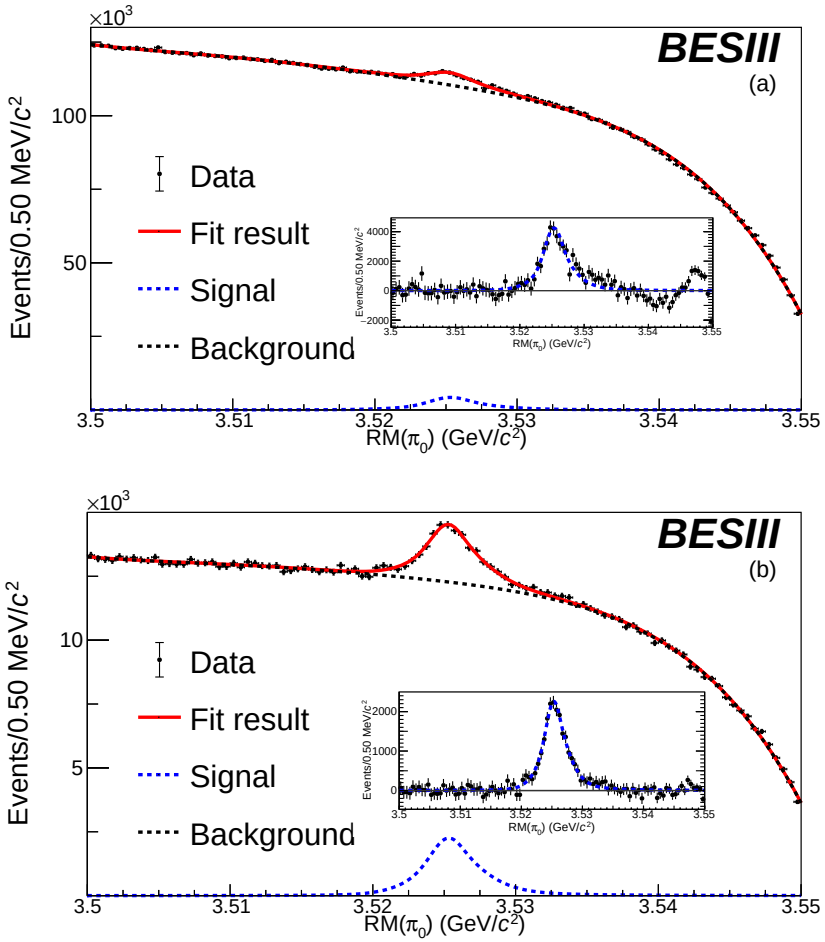

Figure 1.3: Fits to the π^0 recoil mass spectra for the (a) inclusive ($\psi(2S) \to \pi^0 h_c(1^1P_1)$ decay) and (b) tagged ($\psi(2S) \to \pi^0 h_c(1^1P_1) \to \pi^0\gamma\eta_c$ transition) data-samples. Red solid lines denote the fit results, while the black dots with error bars are the data. The blue dashed lines represent the signal component and the black dashed lines are the background. Insets show the background-subtracted data with the signal shape overlaid. Additional studies were performed to understand the trough and bump in the inset (a). All the studies confirmed that no additional state or resonance made that feature possible, the trough and bump are just statistical fluctuations.

the Gell-Mann [2] and Zweig [3] predictions as their theory does not forbid additional colourless combinations such as glueballs (states with no valence quarks), hybrid meson (*i.e.*, with an additional valence gluon), and multiquark states (tetraquarks, and higher).

The first state discovered belonging to this new category was the $X(3872)$ by the

Belle collaboration in 2003 in the $B^{\pm} \to K^{\pm}\pi^{+}\pi^{-}J/\psi$ decay [17] in the $\pi\pi J/\psi$ invariant mass. This narrow state (cf., Ref. [1]) can be described by several models such as a conventional $c\bar{c}$ resonance, a $D\bar{D}^{*}$ molecule [27], a tetraquark state or a $c\bar{c}$-gluon hybrid.

1.4 Experimental Methods for Charmonium Production

The charmonium spectrum can be studied using different production ways. Indeed not only leptonic and hadronic colliders can shine a light on $c\bar{c}$ resonance; as already mentioned, the first $c\bar{c}$ state was discovered by a fixed target experiment [4].
The first studies of charmonium spectroscopy were performed mainly at $e^{+}e^{-}$ colliders. In these machines, the $c\bar{c}$ production proceeds mainly through intermediate virtual photons, $\gamma\gamma$ fusion channel, initial state radiation (ISR), B-meson decays, and double charmonium production. Several experiments in the past years have used leptonic colliders to study the $c\bar{c}$ states such as Mark [28, 29], TPC [30] and Crystal Ball [31] experiments at SLAC; the DASP [32] and PLUTO [33] collaborations at DESY; CLEO [34] and CLEO-c [35] at the Cornell Storage Ring; the four LEP experiments; the BES experiments [36, 37] at IHEP; and the B-factories BaBar [38] and Belle [39] at SLAC and KEK-B, respectively.
Charmonia can be produced at fixed target experiments and $pp/p\bar{p}$ colliders with the same production techniques (apart from the ISR method). Indeed, the B-meson decay method is employed by the LHCb collaboration [40] at CERN to produce and study charmonia.

Apart from the aforementioned methods $pp/p\bar{p}$ colliders can profit from other production techniques. One, originally proposed in Ref. [41], can overcome the relatively low statistics for the non-vector states in $p\bar{p}$ colliders, where C-even or C-odd states are produced via two and three-gluon fusion, respectively. The use of $p\bar{p}$ collisions was employed by the E835 [42] experiment at Fermilab, aside from the two Tevatron ones, and is programmed for the PANDA [43] experiment at FAIR.
At hadronic colliders, charmonia are also produced by hadroproduction, *i.e.*, via strong interaction of quarks and gluons of colliding nucleons. This method is typically employed by ATLAS [44], CMS [45] and the ALICE [46] collaborations.

Finally, charmonia can also be produced in electron-proton colliders such as HERA [47] and at the electron-ion colliders such as the planned EIC [48].

A description of the production channels employed at leptonic colliders is presented below (cf., Ref. [49]).

Direct Formation An e^+e^- pair annihilates into a virtual photon (cf., Fig. 1.4). Due to the boson quantum numbers, it is possible to produce only $\mathrm{J}^{PC}_{c\bar{c}} = \mathrm{J}^{PC}_{\gamma} = 1^{--}$ states, such as the J/ψ, the $\psi(2S)$, and the $\psi(3770)$. The experimental advantage of direct production is that high-precision measurements can be obtained once the accuracy of the energy beams is set. All the other non-vector states can be produced via radiative or hadronic decays [1], increasing the importance of the detector resolution effects.

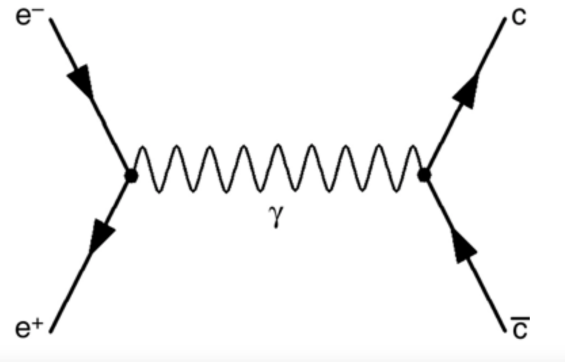

Figure 1.4: Feynman diagram for the $e^+e^- \to c\bar{c}$ process.

$\gamma\gamma$ Fusion e^+e^- annihilations can also produce J-even (and C-even) charmonia through two virtual photons fusion as shown in Fig. 1.5. Being a higher-order process, the production rate scales down by a factor of α^2_{EM} compared to the direct formation rate; hence, despite possible in principle, the observation of the direct production of a C-even state is possible at high-luminosities facilities as pointed out by Ref. [50]. Indeed, only recently, the BESIII collaboration observed for the first time the direct production of a C-even state, namely the $\chi_{c1}(1^3P_1)$ resonance [51].

Initial State Radiation As illustrated in Fig. 1.6, a photon is radiated by a lepton before annihilating, diminishing the effective $\sqrt{s}$. As for the direct formation,

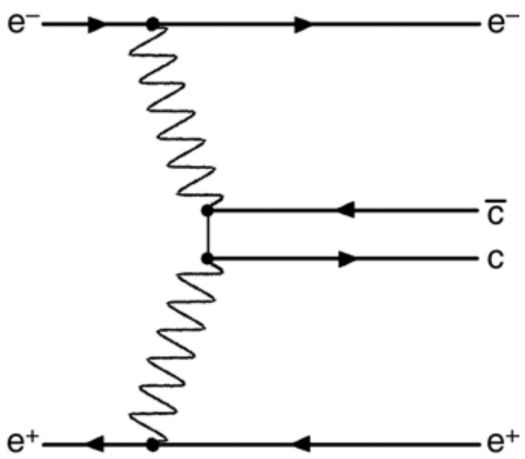

Figure 1.5: Feynman diagram for the $e^+e^- \to e^+e^- + c\bar{c}$ process.

only vector states can be produced, but exploring a large mass range (down to the production threshold) makes it fundamental for searching for new vector states.

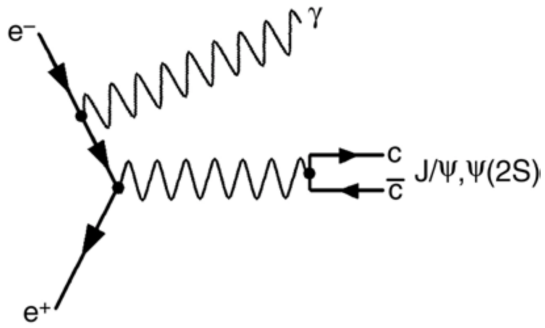

Figure 1.6: Feynman diagram for an ISR process.

B **Meson Decays** Thanks to the weak decay of the B meson b-quark ($b \to c$), states of any quantum number can be formed in a relatively clean production environment. Typically, the so-produced c-quark combines with quarks from the "flavour sea" to form a charmonium state. This approach is employed at B-factories for studying known states and searching for new resonances. This production mechanism allowed the discovery of the $\eta_c(2S)$ resonance [52] and the exotic state $X(3872)$ [17].

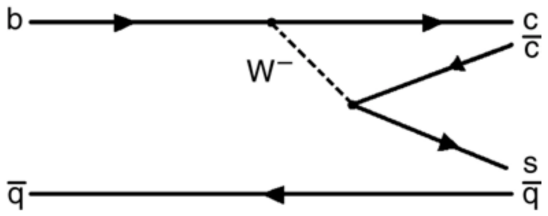

Figure 1.7: Feynman diagram of a B meson decay to $c\bar{c}$.

Double charmonium Discovered by the Belle collaboration [53], it allows the production via a virtual photon of a charmonium pair. This process was found at centre-of-mass energy $\sqrt{s} = 10.6$ GeV studying the recoil mass spectrum of the J/ψ in the $e^+e^- \to J/\psi + X$ process. This production mechanism is of particular interest as its cross-section is a benchmark for non-relativistic QCD calculations as discussed in Refs. [54, 55].

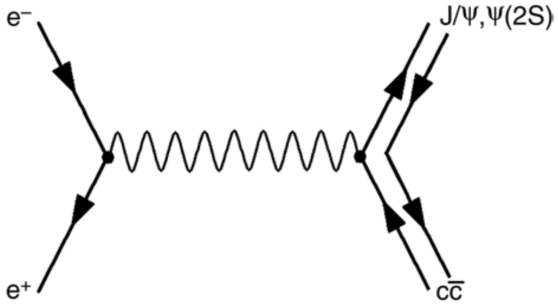

Figure 1.8: Feynman diagram of a double charmonium production process.

1.4.1 Towards the XYZ States

After this introductory part on QCD and charmonia, one can move towards a tentative way to bring some order to the phenomenological chaos of the XYZ states. This introduction's purpose is to define the framework within which this thesis moves and is thought. Several phenomenological models (*e.g.*, the Heavy Quark Effective Field Theory [56]) were not discussed and even the results of Lattice QCD [57][5], despite promising, were left untouched.
The next Chapter will be entirely dedicated to these exotic resonances, both from

[5] A non-perturbative approach in solving QCD and in predicting hadrons features formulated on a *lattice* of space-time points.

an experimental point of view and the analysis of their theoretical interpretation. The main protagonist of this thesis is, indeed, the charged $Z_c(4430)$ state, observed by the BELLE collaboration [58] in the $\pi\psi(2S)$ system from the B meson decays and confirmed by the LHCb experiment [59].

Chapter 2

Brief Review of Charmonium-like Structures

The Quark Model used to describe the experimental observations in the charmonium spectrum revealed itself as a powerful tool to identify exotic states. The concept of exotic hadron is based on whether the aforementioned phenomenological description accommodates the observed state, even though both Gell-Mann [2] and Zweig [3] predicted that more complex structures than the standard hadrons could satisfy the colour neutrality requirement. Despite the experimental efforts, no clear evidence of exotic states was found in the light quark sector. However, in 2003, the first clearly-exotic state was found in the charmonium spectrum. The first state not fitting this scheme was dubbed $X(3872)$ and was observed by the Belle collaboration as a structure in the $\pi\pi J/\psi$ invariant mass [17]. This discovery sparked an era of searches in which more hadrons were found in processes with properties at odds with those of ordinary charmonia.
Apart from not fitting the Quark Model predictions, it must be stressed that there is no general rule for whether a state should be defined as "exotic" or just an ordinary charmonium one. However, all states below the lowest DD^* threshold are typically considered ordinary $c\bar{c}$ states. Above said threshold, the situation is unclear as mixing can take place among standard charmonium states complicating the description and the impact of the opening of thresholds on states is not well modelled.

Assuming a novel physical origin, and not coming from thresholds or coupled channel effects, exotic states can be grouped into two big families of structures following their valence content, they might contain gluons or additional quarks concerning the standard hadronic picture. The former group contains those states

referred to as hybrids (standard mesons with gluonic degrees of freedom) or glueballs (states of pure gluons), while for the latter a more complex description than adding quarks to the standard hadrons is necessary. The multiquark states contemplate structures whose building blocks can be colour-neutral, like in hadronic molecules where single mesons are bound by QCD Van-der-Waals-like forces, or coloured, such as in the hadroquarkonium and compact tetraquark pictures. An intuitive and graphical representation of these phenomenological scenarios is shown in Fig. 2.1. Towards this chapter's end, these phenomenological models are treated in more detail.

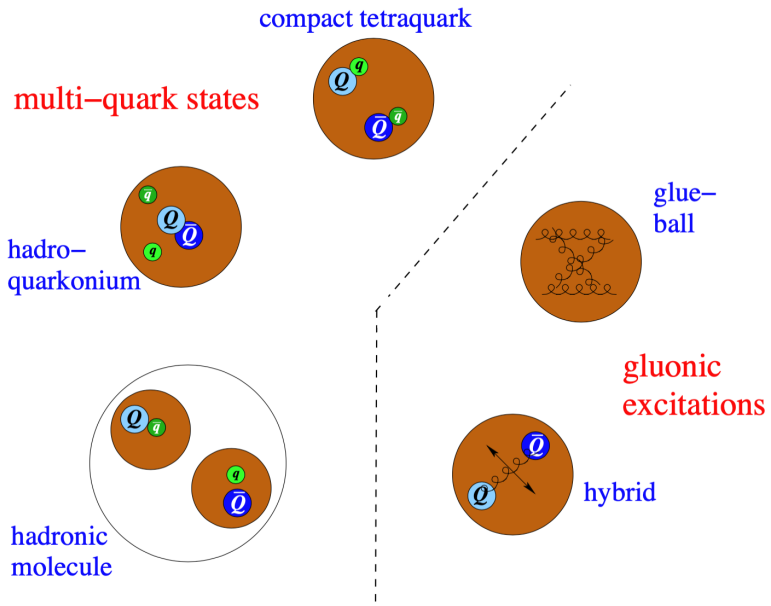

Figure 2.1: Pictorial representation of the discussed phenomenological structures proposed for the exotic states [60].

This Chapter outlines some of the main features of the XYZ states and does not want to be a compendium of all the possible exotic states and of their theoretical interpretations (c.f., Refs [16, 60]). The focus is directed on six exotic states, three of which are experimentally well-established despite their nature is still a matter of debate (*i.e.*, the $X(3872)$, the $Y(4260)$, and the $Z_c(3900)$). The other three states are discussed as two of them are the protagonists of this thesis work (*i.e.*, the $Y(4660)$ and the $Z_c(4430)$) and one is the latest addition to this family of states, the $Z_c(3900)$ strange-flavoured partner (*i.e.*, the $Z_{cs}(3985)$).

2.1 Order from Chaos: Nomenclature

Traditionally, after the XYZ's mysterious nature, the collaborations dub the exotic states' candidates either $X(mass)$, $Y(mass)$, or $Z(mass)$ following the subsequent scheme:

- the Z states are charged (most likely isovector[1]) structures;
- the Y resonances are vector states (*i.e.*, with $J^{PC} = 1^{--}$);
- the X structures are all those states not described by the previous two cases.

To bring order to a growing number of discoveries, the PDG [1] proposed a new naming scheme; essentially extending the scheme used for standard quarkonia, the new names carry the information on the J^{PC} and on the mass of the states as a label in brackets. The new naming scheme does not state the nature of the labelled states, it is just a mere description of their observed properties. The Y states, thus, become ψ ones, and the $X(3872)$ resonance is renamed $\chi_{c1}(3872)$. Considering their charged nature and their manifest charmonium content impose a minimum quark content of four, the Z states are the only exception. This exception is generalised in a new naming scheme for all the I = 1 states (*e.g.*, the pseudoscalar $X(4240)$ is dubbed $R_{c0}(4240)$). The same naming scheme applies to the XYZ resonances found in the bottomonium spectrum with the prescription of using the subscript "$_b$".
Finally, more recently (*i.e.*, in summer 2022) the LHCb collaboration proposed a new naming scheme [61] extending the PDG conventions. Throughout the text, though, the historical names are used to be consistent with respect to the original papers.

2.2 A Non-Standard Quarkonium? The $X(3872)$ Structure

As Fig.2.2 reports, the Belle collaboration observed the $X(3872)$ state in the $\pi\pi J/\psi$ invariant mass via the $B \to K\pi\pi J/\psi$ decays [17]. Subsequently, its existence was confirmed by both $p\bar{p}$ [62, 63] and e^+e^- [64] experiments.

[1] In 2022, the $Z_c(4430)$ neutral partner has not been observed.

Despite the CDF collaboration thinning its possible values [65], the spin-parity assignment for this state was determined to be 1^{++} by the LHCb collaboration [66]. This assignment hints that the $X(3872)$ state could be a good candidate for the standard charmonium state $\chi_{c1}(2^3P_1)$, despite the $X(3872)$ state mass being roughly 100 MeV/c^2 lower than the expected $\chi_{c1}(2^3P_1)$ one.

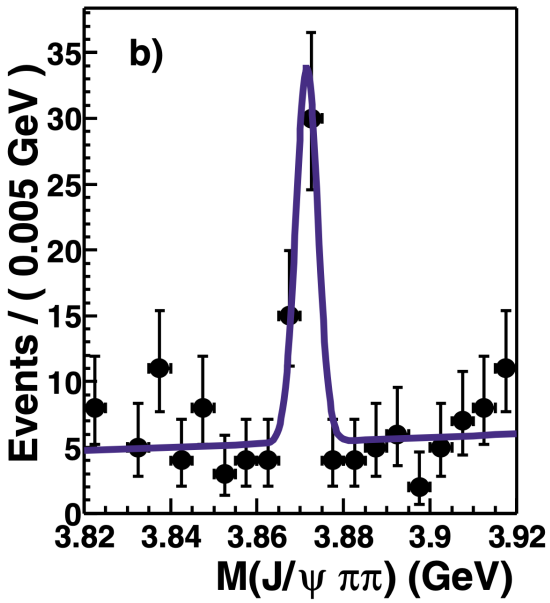

Figure 2.2: Reported finding of $X(3872)$ state as a clear peak in the $\pi\pi J/\psi$ by the Belle collaboration [17].

The mass of the $X(3872)$ state (3871.65 ± 0.06 MeV/c^2) [1], instead, lies interestingly near the $D^0\bar{D}^{*0}$ threshold (3871.69 ± 0.07 MeV/c^2), suggesting a possible molecular nature. Moreover, as a confirmation of this possible loosely bound molecular nature, Ref. [67] adduces the $X(3872)$ relatively small width ($\sim$1 MeV/c^2 [1]), which was the main reason that made the Belle collaboration suspect that the $X(3872)$ state is not standard charmonium.

On top of the mentioned and its prompt pp and $p\bar{p}$ production mechanisms, the $X(3872)$ state is also observed by the BESIII collaboration in the $e^+e^- \to \gamma X(3872)$ channel via the $\omega J/\psi$ transition [68], and via its $\pi\pi J/\psi$ decay in the $B \to K\pi X(3872)$ process by the Belle collaboration [69] and in the $\Lambda_b^0(\to pK^- X(3872))$ decay by LHCb [70].

Ref. [71] suggests that the BESIII collaboration's report of the evidence for the $Y(4260) \to \gamma X(3872)$ decay [72] is a suggestion of a common molecular nature between these two states.

The $\omega J/\psi$ transition was searched by the BESIII collaboration as it can shed some light on the nature of this state. Indeed, its $\omega J/\psi$ decay proves the isospin-violating nature of the $X(3872)$ as its decay towards the J/ψ is mediated by both 2π and 3π transitions. Again, the BESIII reported the observation of the $X(3872) \to \pi^0\chi_{c1}$ decay [73], which contradicts the interpretation of the $X(3872)$ being a conventional $c\bar{c}$ charmonium as the transition should be suppressed being isospin breaking.

Another comparison which can be discriminant on the nature of the $X(3872)$ structure regards its radiative decays towards the $\psi(nS)$ states. The transition towards the J/ψ resonance is well-established as the BaBar [74], the Belle [75], and the LHCb [76] collaborations report consistent values. Despite no consensus being reached on this point, Ref. [77] claims that a relatively large branching fraction for the $\gamma\psi(2S)$ transition is inconsistent with a pure $D^0\bar{D}^{*0}$ molecule (*i.e.*, the $X(3872)$ structure could be an admixture of a conventional $c\bar{c}$ charmonium and a $D^0\bar{D}^{*0}$ molecule). The BaBar [74] and LHCb [76] collaborations seem to second this hypothesis measuring the ratio (R) of the two radiative branching fractions to be (3.4±1.4) and (2.31±0.57), respectively. More studies are necessary to clear this picture, as the Belle collaboration measures an $R < 2.1$ (at 90% C.L.). Another measurement of the BaBar collaboration supports this hypothesis of a molecular component, in Ref. [78] the experiment estimates the upper limit on the partial width of the $X(3872) \to \pi^+\pi^- J/\psi$ decay to be ∼100 keV in accordance with Ref. [79].
Decays towards open-charm mesons are also observed; in particular, the Belle collaboration observed the $X(3872) \to D^0\bar{D}^0\pi^0$ [80] and $X(3872) \to D^0\bar{D}^{*0}$ [81] decays (the latter also found by the BaBar collaboration [82]).

To conclude, it is clear that from the experimental point of view, a lot of data is still needed. After all, as Ref. [83] discusses, the unseen $X(3872)$ branching fraction decays roughly amounts to 32%. Of particular interest is the LHCb collaboration *Run 3* data, as it will be crucial in estimating the $X(3872)$ state parameters with relatively high precision.

2.3 The Vectorial Y Resonances

The Y resonances are vector states. Though, conversely to the other vector conventional $c\bar{c}$ charmonia, the Y resonances show strong coupling to hidden-charm final states, indicating a possible different nature.
Y states have been historically studied using the ISR (Initial State Radiation) technique, which, as described in Chapter 1.4, allows probing the e^+e^- interaction at all energies below centre-of-mass energy. Another way to analyse and discover these states is to study the line shape cross-section of the e^+e^- annihilation to a given channel at different centre-of-mass energies and to check for any resonant behaviour which is not predicted by the Quark Model.

2.3.1 $Y(4260)$

While studying the $e^+e^- \to \pi^+\pi^- J/\psi$ process, to assess the $X(3872)$ quantum numbers, the BaBar collaboration observed a structure at about 4.26 GeV/c^2, dubbing it $Y(4260)$. The resonance was confirmed by the CLEO [84] and the Belle collaborations [85]. Improving their measurements, both the BaBar [86] and the Belle [87] collaborations confirmed the observation of a more complex structure instead of a single $Y(4260)$ resonance around 4.26 GeV/c^2 in the $e^+e^- \to \pi^+\pi^- J/\psi$ line shape.

With a different probing technique (*i.e.*, performing a cross-section scan instead of using the ISR) and with much more statistics, the BESIII collaboration was then able to distinguish two structures around 4.26 GeV/c^2 in the $e^+e^- \to \pi^+\pi^- J/\psi$ line shape. In the $Y(4260)$ asymmetric peak, the BESIII collaboration observed the "$Y(4260)$" as a dominant resonant structure around 4.23 GeV/c^2, dubbed $Y(4230)$ since, and new resonance with a mass of 4.32 GeV/c^2, called $Y(4320)$ [88]. This was performed under the assumption that the asymmetric structure is composed of two symmetric states, despite some references stating that in the molecular picture, a single resonance could generate asymmetric line shapes [71]. The BESIII collaboration also reported the same structure, and its two-resonance composition, by studying the $e^+e^- \to \pi^0\pi^0 J/\psi$ line shape [89].
The exotic nature of the $Y(4230)$ resonance might be inferred from the R-value measurement, where a dip in the cross-section is observed at around 4.26 GeV (c.f., PDG [1]), suggesting a non-standard $c\bar{c}$ structure.

The BESIII collaboration, switching the vector J/ψ state with its pseudovector counterpart (the $h_c(1^1P_1)$ resonance), studied the $e^+e^- \to \pi\pi h_c$ cross-section [24, 25, 90]. The line shape suggests the presence of two resonant structures around 4.3 GeV, with one being that of the $Y(4230)$ state. The same collaboration also probed the $e^+e^- \to \omega\chi_{cJ}$ cross-section [91–93], finding the $Y(4230)$ resonance in the $\omega\chi_{c0}$ invariant mass. Finally, the BESIII collaboration studied the $e^+e^- \to \pi^+D^0D^{*-}+c.c.$ process [94], finding two resonant structures in agreement with those observed in the $e^+e^- \to \pi^+\pi^-h_c$ cross-section. Considering the lower mass structure is compatible with the $Y(4230)$ resonance, this suggests the first observation of this state decaying to an open-charm final state.
Some of these studies are summarised in Ref. [95]; as Fig. 2.3 reports, despite the mass measurements of the $Y(4230)$ state being in agreement among the different channels, the differences of the widths estimates require more studies.

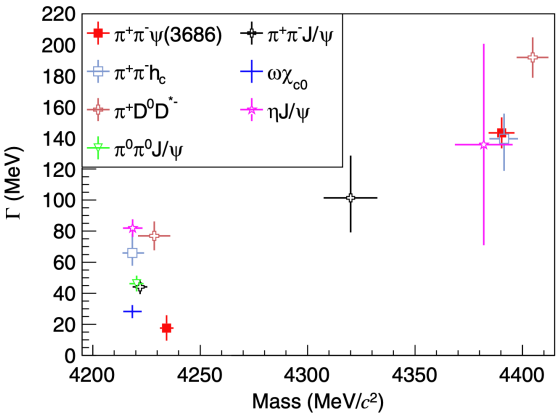

Figure 2.3: Masses versus widths of the $Y(4230)$ and $Y(4390)$ states obtained from different processes by the BESIII collaboration [25, 88, 93, 94, 96, 97]. From Ref. [95].

To sum up, lots of experimental studies lay ahead because, as reported below, many theoretical models [98–106] predict different natures for the $Y(4230)$ state and, at the same time, the experimental measurements cannot yet differentiate among the proposed framework. One more study needs to be pointed out, Ref. [107] suggests that the $Y(4320)$ might not exist and that the experimental data around the 4.26 GeV peak can be described by two standard charmonia ($\psi(4160)$ and the $\psi(4415)$ resonances) and another (non-$Y(4230)$) exotic Y state.

In the future, both the BESIII and the Belle-II collaborations will collect new data in this energy region to assess the nature of this resonance.

2.3.2 $Y(4660)$

While studying the $Y(4230) \to \pi^+\pi^-\psi(2S)$ spectrum, BaBar collaboration found a resonant structure around 4.32 GeV/c^2 [108] incompatible with the state found in the $\pi^+\pi^- J/\psi$ final state. The same process was studied by the Belle collaboration which was able to identify two structures, dubbed $Y(4360)$ and $Y(4660)$ [109]. Subsequently, both collaborations studied the same line shape with higher statistics to confirm the $Y(4360)$ and $Y(4660)$ resonances and measure their masses and widths [110,111]. The results from the BaBar collaboration are shown in Fig. 2.4(a). Historical considerations apart, both the collaborations interestingly report, for the $Y(4660)$ decay, a prompt $\pi^+\pi^-$ invariant mass distribution differing from the phase-space expectation, with an indication of a heap in the proximity of the $f_0(980)$ meson, as it is also shown in Fig. 2.4(b).
The BESIII collaboration measured as well the $e^+e^- \to \pi^+\pi^-\psi(2S)$ transition [95, 112]. At the time of Ref. [112], the BESIII experiment could only reach centre-of-mass energies up to 4.600 GeV, hence it only found that adding to the fit a resonance with the $Y(4660)$ parameters measured by the Belle collaboration measurement led to a better description of the cross-section. On the other hand, Ref. [95] reports the observation of the $Y(4660)$ resonance and its measured mass in agreement with the BaBar and Belle collaborations.

A state compatible with the $Y(4660)$ resonance, and dubbed $Y(4630)$, was observed by Belle collaboration in the $e^+e^- \to \Lambda_c^+\bar{\Lambda}_c^-$ process via the ISR technique. The compatibility between these two states led Refs. [113–115] to assume that they could be the same state and Refs. [116, 117] that they could be spin partners (essentially being an $f_0(980)c\bar{c}$ molecule).

The BESIII collaboration found two resonant structures corresponding to the $Y(4360)$ and $Y(4660)$ states while analysing $e^+e^- \to \pi^+\pi^-\psi_2(3823)$ line shape [118]. The observation of the $Y(4660)$ resonance in this channel challenges the $f_0(980)\psi(2S)$ molecule interpretation [116], the extended baryonium picture [119], and the compact tetraquark model [120]. All of these theoretical models predict a small (or absent) coupling to n = 1 states, which would be the quantum assignment to the $\psi_2(3823)$ state, *i.e.*, the $\psi_2(1^3D_2)$ charmonium resonance [1].

Our knowledge of this state is at best limited, if not contradictory, hence, steps

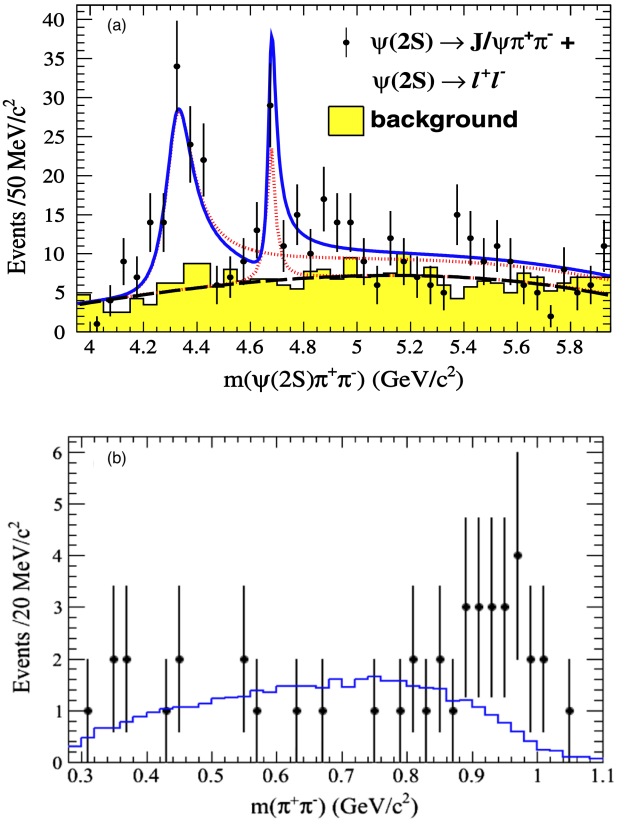

Figure 2.4: $e^+e^- \to \pi^+\pi^-\psi(2S)$ line shape analysis by the BaBar collaboration [110]. Fig. 2.4(a) shows the invariant $\pi^+\pi^-\psi(2S)$ mass spectrum with superimposed the fit. The solid curve shows the result of the fit. The dashed curve represents the background, while the dotted curves indicate the resonant contributions. In Fig. 2.4(b) one can appreciate the prompt $\pi^+\pi^-$ invariant mass distribution with its characteristic heap near the $f_0(980)$ meson mass.

forward are needed both theoretically and experimentally to better understand the nature of the $Y(4660)$ resonance.

2.4 The Z States

Quite the opposite of the states presented above, which could be interpreted as conventional $c\bar{c}$ resonances distorted by threshold or unitarisation effects [121], the charged structures hint at a completely exotic nature. The charged states require a minimum quark content of at least four and the isotriplets show strong couplings to

charm-hidden states in combination with a light meson. It is important to mention, though, that also for these state a non-exotic interpretation has been advanced; some authors (*e.g.*, Ref. [122]) states that they might be threshold cusps.

2.4.1 $Z_c(3900)$

To better understand the properties of the $Y(4230)$, the BESIII and the Belle collaborations started studying the process $e^+e^- \to Y(4230) \to \pi^+\pi^- J/\psi$ at centre-of-mass energies on and around the peak of the Y(4230) [87, 123]. In the $\pi^\pm J/\psi$ invariant mass both the collaborations observed a peak, which could not be generated by any of the $\pi\pi$ terms used to describe the complex $\pi\pi$ invariant mass structure. Fig. 2.5 reports a comparison between the $\pi^\pm J/\psi$ invariant mass distributions of the two collaborations, which measured mass and width values in agreement with each other allowing to dub this new structure $Z_c(3900)^\pm$. This state is recognised as exotic as it has a strong coupling to a $c\bar{c}$ resonance and it is charged.

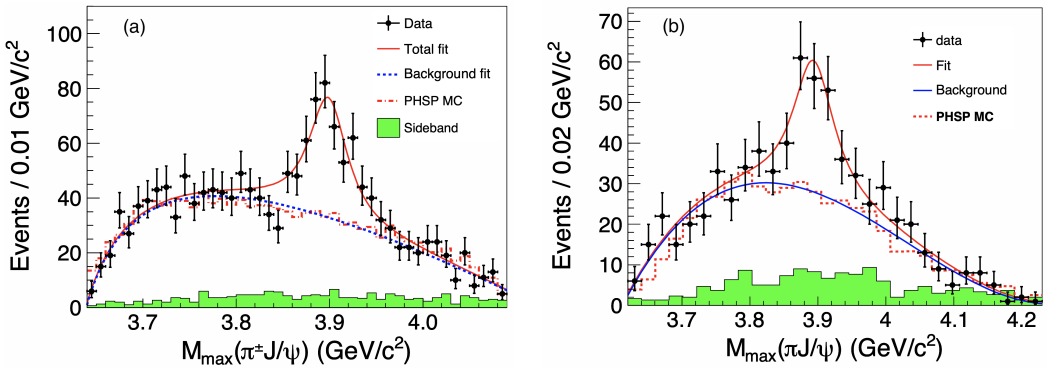

Figure 2.5: $\pi^\pm J/\psi$ invariant mass distributions from the BESIII [123], Fig. 2.5(a), and the Belle [87], Fig. 2.5(b), collaborations, the $Z_c(3900)$ state can be seen as an enhancement around 3.9 GeV/c^2. Dots with error bars are data, the solid curves are the fits, the dashed histograms represent the phase-space distribution, and the shaded histograms are the sideband events.

The CLEO-c collaboration confirmed [124] the existence of the $Z_c(3900)^\pm$ state and measured a mass and width in agreement with the previous measurements. In the same Ref. [124], studying the $e^+e^- \to \pi^0\pi^0 J/\psi$ process, CLEO-c found evidence for the $Z_c(3900)^\pm$ isospin neutral partner, the $Z_c(3900)^0$.

The BESIII collaboration confirmed the $Z_c(3900)^0$ state observation with mass and width in agreement with those of the $Z_c(3900)^{\pm}$ state and its production rate consistent with the expectation from isospin symmetry [89]. Hence, the BESIII collaboration confirmed that the $Z_c(3900)$ is an isovector state.

Considering its proximity to the $D\bar{D}^*$ mass threshold, the BESIII collaboration checked the $Z_c(3900) \to D\bar{D}^*$ coupling via $e^+e^- \to \pi^{\pm}(D\bar{D}^*)^{\mp}$. As expected, the BESIII collaboration observed in the $D\bar{D}^*$ invariant mass a structure compatible with the $Z_c(3900)$ state [125, 126]. The angular distribution of the $\pi - Z_c$ system is studied and the analysis favours a quantum number assignment of $J^P = 1^+$. Studying the neutral counterpart of the $e^+e^- \to \pi^{\pm}(D\bar{D}^*)^{\mp}$ process, the BESIII collaboration observed the $Z_c(3900)^0 \to D\bar{D}^*$ neutral decay with a production rate consistent with the isospin symmetry.
The BESIII collaboration was able to assess the $Z_c(3900)$ 1^+ spin-parity assignment with a partial wave analysis (PWA) [127] of the $e^+e^- \to \pi^+\pi^- J/\psi$ process [128].

The $Z_c(3900)$ state is also observed in $p\bar{p}$ collisions via bottom-flavoured hadronic decays, the D0 collaboration has seen evidence of the $Z_c(3900)^{\pm} \to \pi^{\pm} J/\psi$ decays. Interestingly, the $Z_c(3900)$ state is observed in the $\pi^{\pm} J/\psi$ invariant mass regions between 4.25 and 4.6 GeV (*i.e.*, in correspondence of the $Y(4230)$ resonance), and an enhancement is observed on the $Y(4230)$ invariant mass. It must be stressed that a similar enhancement in correspondence of the $Y(4230)$ resonance is also seen by the BESIII collaboration, in the $e^+e^- \to \pi\pi J/\psi$ process [96,123]. This might be an indication of a common exotic nature between these two states (and the $X(3872)$ as discussed above).

Finally, following Ref. [129] stating that the relative decay rate ($R_{Z_c(3900)}$) of the $Z_c(3900)$ state towards the $\rho\eta_c$ final state to the $\pi^0 J/\psi$ one is a good discriminant between compact tetraquark scenario and the molecular one, the BESIII collaboration studied the $e^+e^- \to \pi^+\pi^-\pi^0\eta_c$ process [130]. Finding a relative ratio $R_{Z_c(3900)}$ of 2.2±0.9, therefore favouring the compact tetraquark interpretation for the $Z_c(3900)$ state.

2.4.2 $Z_c(4430)$

Observed by the Belle collaboration [58] via the $B \to K\pi\psi(2S)$ decay channel, the $Z_c(4430)$ is the first multiquark candidate ever found. Shown in Fig. 2.6 as a heap in the $\psi(2S)\pi$ invariant mass, the state was searched by the BaBar collaboration [131].

Analysing the $\psi(2S)\pi$ invariant mass distribution, BaBar found that it could be described without additional structures. Updating its measurement [132], the Belle collaboration, while it confirmed its findings, found a mass and width which were at odds with the previous ones. In the same Ref. [132], the Belle collaboration favoured the $Z_c(4430)$ $J^P = 1^+$ spin-parity assignment.

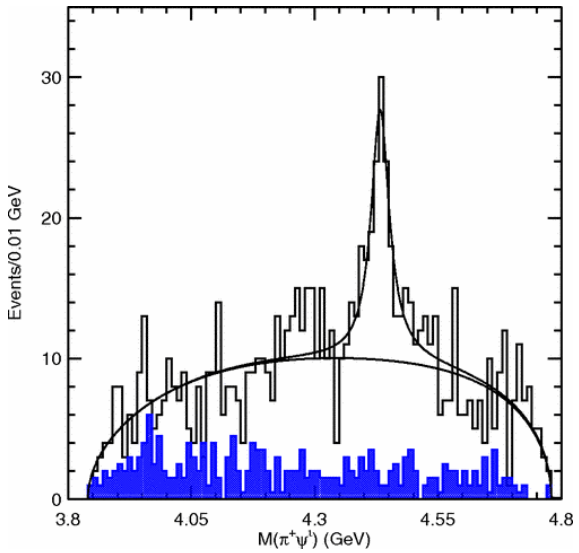

Figure 2.6: Reported finding of the $Z_c(4430)$ state as a clear peak in the $\psi(2S)\pi$ invariant mass by the Belle collaboration [58]. The solid curves show the results of the fit, while the shaded histogram shows the distribution from the sidebands.

Studying the $B \to K\pi\psi(2S)$ decay, the LHCb collaboration [59] confirmed the $Z_c(4430)$ state with a significance of 13.9σ, providing a mass and width more precise yet compatible with the Belle collaboration results. The LHCb collaboration performed a 4-dimensional amplitude fit and confirmed $J^P = 1^+$ spin-parity assignment. Finally, the LHCb collaboration produced an Argand plot of the $Z_c(4430)$ amplitude (taken from the 4-dimensional amplitude fit) as a function of different $\psi(2S)\pi$ squared invariant mass bins. Fig. 2.7 reports the resulting Argand plot, showing the characteristic behaviour of a change of the resonance phase when its magnitude approaches the maximum.

Exchanging the $\psi(2S)$ resonance with the J/ψ one, the Belle collaboration studied the $B \to K\pi J/\psi$ decay channel [133]. The collaboration found evidence of the $Z_c(4430)$ in the $\pi J/\psi$ invariant mass. The LHCb collaboration studied the same

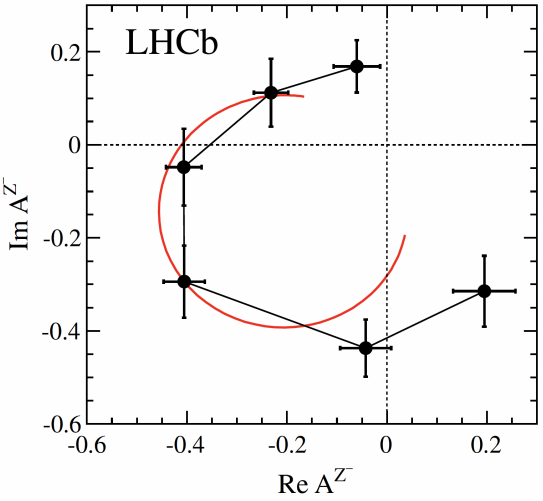

Figure 2.7: Fitted values of the $Z_c(4430)$ amplitude in six $\psi(2S)\pi$ squared invariant mass bins, shown in an Argand diagram by the LHCb collaboration [59]. The superimposed red curve is the prediction from the Breit-Wigner formula.

$B \to K\pi J/\psi$ decay channel [134], though the contribution from the $Z_c(4430)$ in the $\pi J/\psi$ invariant mass is not clear. This behaviour is somewhat expected; Ref. [135] argues that in the compact tetraquark hypothesis the $Z_c(4430)$ state would decay preferentially towards the $\psi(2S)$ resonance rather than the J/ψ one. A different proposal is advanced by Ref. [136], which suggests the $Z_c(4430)$ to be a hadroquarkonium structure.

With a mass $(4478^{+15}_{-18})\,\mathrm{MeV}/c^2$ and width of $(181\pm31)\,\mathrm{MeV}/c^2$, respectively, the elusive $Z_c(4430)$ resonance lacks more experimental observations. With the beginning of the Belle-II experiment, the *Run 3* at the LHCb detector, and the possibility for the BESIII collaboration to probe centre-of-mass energies up to 4.95 GeV, more data will be available to continue the search for this state. This thesis contributes to this effort by studying the $e^+e^- \to \pi^+\pi^-\psi(2S)$ process at centre-of-mass energies ranging from 4.612 GeV to 4.698 GeV.

2.4.3 $Z_{cs}(3985)$

On the wave of the Z_c discoveries, experimental collaborations started searching for their strange partners, the Z_{cs} states. Indeed, in the hadronic molecule framework, a Z_{cs} state was predicted to be a $J^{PC} = 1^{++}$ D_sD^* and have a mass of

(3.97±0.08) GeV/c^2 by Ref. [137].

The BESIII collaboration observed the first allegedly four-quark state with non-zero strangeness, the $Z_{cs}(3985)^-$, while studying the $e^+e^- \to K^+(D_s^- D^{*0} + D_s^{*-} D^0) + c.c.$ process [138]. Using five centre-of-mass energies from 4.628 GeV to 4.699 GeV, the BESIII collaboration measured a mass of $(3982.5^{+1.8}_{-2.6} \pm 2.1)$ MeV/c^2 for the $Z_{cs}(3985)^-$ state, strikingly in agreement with the prediction from Ref. [137]. Again, BESIII, searching for its neutral counterpart in the same energy region, found evidence of the $Z_{cs}(3985)^0$ state via the $e^+e^- \to K_S(D_s^+ D^{*-} + D_s^{*+} D^-) + c.c.$ process [139]. The mass of the neutral partner is established to be heavier than the charged $Z_{cs}(3985)$ state following the prediction from Ref. [140] (in either a molecular or compact tetraquark framework). Moreover, assuming isospin symmetry the Born cross-section of the neutral channel is consistent with that of the charged one, suggesting that indeed the $Z_{cs}(3985)^0$ state is the neutral partner of the $Z_{cs}(3985)^-$.

Finally, the LHCb collaboration reported via the study of the $B \to K^+ \phi J/\psi$ decay [141] in the $K^+ J/\psi$ final state a Z_{cs} candidate (dubbed $Z_{cs}(4000)$), the mass of which is consistent with the $Z_{cs}(3985)$. However, since the $Z_{cs}(3985)$ state width is 10 times smaller than the $Z_{cs}(4000)$ one, there is no evidence that the two states are the same one.

2.5 Theoretical Interpretations

In this section, for sake of completion, the theoretical interpretation will be briefly sketched. The efforts towards a theoretical understanding of the XYZ scenario can be synthesised into three big groups: the phenomenological approaches, the effective field theories, and the lattice QCD numerical computations.
The phenomenological approaches, which are treated here, provide a scheme for classifying exotic hadrons and offering physics insights for observables, though, they do not start from first principles. The more rigorous and systematic methods are not discussed in the subsections, as they go beyond the scope of this thesis. It is worth mentioning, though, that also effective field theories [56, 142–144] and lattice QCD [57, 145–147], despite being powerful tools, have drawbacks, such as the range of applicability and the computational cost, that can be reduced by requiring big (and sometimes unphysical) approximations.

2.5.1 Phenomenological Approaches

This subsection briefly depicts the main phenomenological frameworks commonly used in the literature to classify exotic states.

2.5.1.1 Hybrids

Due to its non-Abelian nature, QCD can also admit valence gluons. As already mentioned, the word "hybrid" refers to quark-antiquark mesons with additional constituent gluons, but also states with only gluonic degrees of freedom are admitted, and dubbed glueballs.

Typically, theoretical models differ in the procedure they treat and describe hybrids, though there are some cornerstones from which experimentalists can start. A constituent gluon contributes roughly 1 GeV/c^2 to the mass of the system, in such a way the ground-state mass for a charmed-hybrid structure would be $2m_c + 1$ GeV/c^2 [148, 149] (*i.e.*, roughly 4 GeV/c^2 for the lightest charmonium hybrid).

Extending the Quark Model to describe hybrids by modifying the potential term (c.f., Chapter 1.3.1) to allow constituent gluons to interact with the quarks and antiquarks, one can describe the hybrid system and its potential spin-parity assignments [60, 150]. Assuming hybrids with a $J^{PC} = 1^{+-}$ gluon and the quark-antiquark pair in an S-wave state spin-triplet state, the hybrid might have, among others, the exotic quantum numbers $J^{PC} = 1^{-+}$. Indeed, non-exotic quantum numbers are admitted as well.

Another signature of these exotic states stems from the fact that the quark-antiquark pair is dominantly in a colour-octet state and, hence, cannot annihilate into a photon making the leptonic width of hybrids small. Moreover, the quark-antiquark pair inside the hybrid either converts into a colour-singlet state by emitting a gluon or annihilates into gluons. Two scenarios are, then, possible; either (i) hidden-flavour states are accompanied by light mesons [151] or (ii) the complete annihilation guarantees that the final states do not contain heavy quarks [152].

2.5.1.2 Hadroquarkonia

In Ref. [153], it is proposed some exotic states could be described as a compact colour-singlet heavy-quarkonium core surrounded by a colour-singlet light-quark cloud, bound together by residual QCD forces (*i.e.*, Van-der-Waals-like). The hadroquarkonium framework can predict both decay patterns and spin-partner states, mainly due to two assumptions; states sharing the same light-quark cloud, but having different spin coupling in the heavy-quark core, are degenerate at leading order; and, the spin of heavy quarks is conserved (as spin interactions scale with the inverse of the heavy-quark mass), constraining the final states.

Typically, Y states are described as hadroquarkonia [136], even though some of these resonances decay into final states containing both triplet- and singlet-state charmonia, like the $Y(4230)$ resonance. Ref. [154] supposes that the $Y(4230)$ resonance might be a mixture of a $J^{PC} = 1^{--}$ charmonium core $J^{PC} = 0^{++}$-light-quark-cloud-surrounded hadrocharmonium and a $J^{PC} = 1^{+-}$ charmonium core $J^{PC} = 0^{-+}$-light-quark-cloud-surrounded one.

To conclude, a useful prediction [155] for hadrocharmonia sharing the same light-quark cloud with different spin coupling in the heavy-quark core is that the ratio of their production rates should be roughly similar[2] to that of their sub-lying continuum processes.

2.5.1.3 Hadronic Molecules

Vaguely similar to hadroquarkonia, hadronic molecules are colour-singlet open-flavour mesons loosely bound together [156]. Typically, the properties of these structures are derived in analogy from those of standard light nuclei (*i.e.*, protons and neutrons). Following this analogy, the one-pion exchange is considered central to molecular binding, which is studied as a function of the binding momentum, a quantity defining the size of the molecule and the typical momentum within the bound state.

In general, considering that a narrow and shallow hadronic molecule can be formed from narrow constituents [157] (< 100 MeV/c^2), in the open-charm sector, only the spin doublets $\{D, D^*\}$ and $\{D_1, D_2\}$ can be used to form hadronic

[2] Around the same invariant mass as the exotic resonances.

molecules [60], making this scheme not too applicable to many of XYZ states.

As mentioned above, the most prominent candidate for being a hadronic molecule is the $X(3872)$ state, claimed to be $D\bar{D}^*$ [158]. This would imply that the $X(3872)$ state is an equal admixture of an isospin-1 and -0 component. However, it decays with equal rates into $\rho J/\psi$ and $\omega J/\psi$ final states when the latter is kinematically suppressed. Some fine tunings are proposed [159] but still await experimental confirmations.

Also, the $Y(4230)$ resonance is suggested to be a hadronic molecule candidate, in particular, a $D_1\bar{D}$ molecular nature [71]. The reason behind this proposal is that this resonance has a two-hadron channel nearby (the $D_1\bar{D}$ one [1]). As already stated, a molecular nature for the $Y(4230)$ resonance would generate asymmetric line shapes in the $\pi\pi J/\psi$ channel. As seen by the BESIII collaboration [94], the $Y(4230)$ resonance would have a preferential decay towards its constituents. Finally, the $D_1 \to D^*$ decays [1] would explain the observation of the $Y(4230) \to \pi Z_c(3900)$ transition and the $Y(4230) \to \gamma X(3872)$ process [160].

2.5.1.4 Compact Tetraquarks

Probably the most intuitive generalisation to a 4-quark system, a compact tetraquark (also called *diquonium*) consists of a colour-antitriplet Qq diquark and a colour-triplet $\bar{Q}\bar{q}$ anti-diquark, bound together by the QCD colour force [161].

Assuming similar behaviour to the open-flavour mesons (*i.e.*, similar mass differences between excited states), it is hypothesised that spin-spin interaction is predominant inside the diquarks [120]. This hypothesis requires that the diquark and the antidiquark do not come too close, laying in a sort of double-well potential. The potential would act as a barrier between the diquarks and would influence the compact tetraquark decay, explaining the reason why some exotics are seen to preferentially decay into open-flavour mesons. Moreover, considering the diquarks' spins are not correlated with each other, the whole structure can naturally decay into both singlet- and triplet-states.

This framework can also explain some puzzling decay chains, as in the $Y(4230) \to \gamma X(3872)$ decay. Assuming this scheme, the two states would share the same heavy-

quark spin structure up to an electric dipole switch [162].

2.5.2 No New States

Some of the exotic candidates reside close to open-flavour thresholds or in environments which are already rich in other standard $c\bar{c}$ resonances. Indeed, the impact of these thresholds is not clear yet, as they might induce kinematic enhancements [163, 164]; some structures could be generated by non-analyticities of the production amplitudes emerging whenever a threshold related to a new channel is crossed [165]; the XYZ states could emerge as interference effects of various standard quarkonia [107].

2.5.3 Outlook

Just as sketched in this Chapter, the interpretative models match the number of analyses performed by the different experiments. As such, to clarify the situation in the XYZ sector there is a dire need for more data. With the start of the Belle-II experiment data taking [166], with the data coming from *Run 3* and LHC-HL at the LHCb detector [167], and with the newest upgrade for BECPII and the BESIII detector (c.f., Chapter 3), new studies and analyses will probe the nature of the XYZ states and search for new resonances. This Chapter highlighted the BESIII effort, as this collaboration has been at the forefront of the XYZ sector studies since the dawn of these discoveries and because this thesis' work is performed analysing the BESIII collaboration data.

This thesis wants to be a piece of the XYZ sector puzzle. Studying the $e^+e^- \to \pi^+\pi^-\psi(2S)$ process at centre-of-mass energies ranging from 4.612 GeV to 4.698 GeV allows both to probe the $Y(4660)$ nature and to search for the $Z_c(4430)$ state. Indeed, the BESIII collaboration has already seen the $Y(4660)$ in this channel, but measuring the $e^+e^- \to f_0(980)\psi(2S)$ component percentage to the whole $e^+e^- \to \pi^+\pi^-\psi(2S)$ process might give some insights over the $f_0(980)c\bar{c}$ molecule interpretation. Furthermore, the direct search for the $Z_c(4430)$ state at the BESIII experiment is fundamental as its discovery would be an important step ahead to understanding this resonance. Indeed, up to now, only the Belle and LHCb collaborations saw the $Z_c(4430)$ state and exclusively in B decays. Even a negative result (*i.e.*, an upper limit on the $Z_c(4430)$ state production rate) would allow theoretical models to be discriminated due to the $Z_c(4430)$ production mechanisms.

Chapter 3

BESIII Experiment

BESIII (Beijing Spectrometer III) is the third evolution of a high-energy physics experiment located at the accumulation ring BEPCII (Beijing Electron Positron Collider II) located at the Institute of High Energy Physics (IHEP) of the Chinese Academy of Science in Beijing, People's Republic of China.
The data taking for the physics programme began in 2009. The BESIII collaboration expects to keep collecting data beyond the 2030s [37].
In this Chapter, the BESIII experiment and its sub-detectors are presented and described. At the end of the Chapter, the future physics reach and the upgrade program will be discussed

3.1 BEPCII

BEPCII is a 237.5 meters long double-ring e^+e^- collider, running in the "τ-charm" region, with the centre of mass energy ($\sqrt{s}$) ranging from 2.0 to 4.95 GeV. The leptonic beams are provided to BEPCII by a 202 meters long linear injector. BECPII can reach an instantaneous luminosity of 1.05×10^{33} cm^{-2} s^{-1} at $\sqrt{s} = 3.77$ GeV[1].

Fig. 3.1 shows a schematic view of the layout of the machine. The symmetrical leptonic beams cross each other in two interaction points (IPs). The northern IP hosts the Beam Energy Monitor System [168], *i.e.*, the routine equipment for measuring the beams energy and spread, and monitoring their status. In the southern

[1]Reached on January the 7$^{\text{th}}$ 2023. This is the highest luminosity achieved for a leptonic accelerator in this energy region.

IP, the electron and positron beams intersect and collide with a horizontal crossing angle of 11 mrad. Here, the BESIII detector and all the machinery necessary for the colliding and detecting operations, such as focussing magnets, vacuum pumps, and cooling systems, are located.

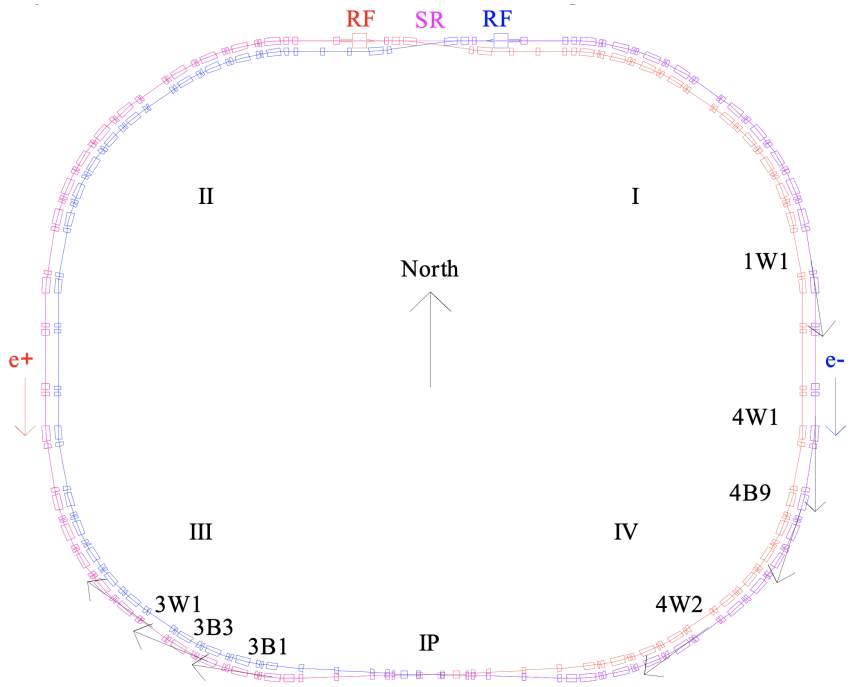

Figure 3.1: Layout of the BEPCII storage rings.

To match the physics requirements of higher luminosity (to probe rare charmonia decays) and higher energy (to pursue the XYZ exotic searches), an upgrade for BEPCII was envisioned and is under development [37, 169] to be ready for the 2025 data-taking. The upgraded BEPCII-U will reach 2.8 GeV per beam, tripling current the instantaneous luminosity at the beam energy of 2.35 GeV and bringing it to the same level as the one reached at $\sqrt{s} = 3.77$ GeV.

3.2 BESIII Detector

BESIII [170] is a multi-purpose detector designed to investigate a broad range of high-energy physics topics. In Fig. 3.2 a schematic view of the BESIII detector is presented. Moving from the IP outward, BESII is composed of the following sub-

detectors: a Multilayer Drift Chamber (MDC), a Time of Flight (ToF) detector, an ElectroMagnetic Calorimeter (EMC) (all surrounded by a 1 T superconducting solenoid), and, interleaved in the magnet flux return yoke, a Muon Counter (MUC) as the outermost sub-detector.
BESIII can be divided into a central part called *barrel* and two *endcaps*, which cover the forward and backward regions. It covers 93% of the solid angle with the polar angle ranging from 21° to 159°.
The reference frame used by the BESIII collaboration consists of a right-handed coordinate system with its origin at the IP in the centre of the detector. The cylindrical coordinates ($\hat{\theta}$, $\hat{\phi}$, $\hat{z}$) are defined so that $\hat{z}$ is parallel to the beamline, $\hat{\phi}$ sweeps the plane orthogonal to BECPII rings, and $\hat{\theta} = 180° \mapsto 0°$ corresponds to the $\hat{z} > 0$ beam axis.

3.2.1 The Multilayer Drift Chamber

The MDC is a drift chamber whose purpose is to track and measure the momentum, and the $\mathrm{d}E/\mathrm{d}x$ of charged particles with a momentum $\gtrsim 50$ MeV/c. It has a single wire spatial resolution of 120 μm (2 mm) in the ϕ plane (along the z-axis, limited by the small stereo angle), while the charged-particle momentum resolution at 1 GeV/c is $\mathrm{d}p/p \sim 0.5\%$. The MDC has a good $\mathrm{d}E/\mathrm{d}x$ measurement capability ($\sigma \sim 6\%$ for electrons from Bhabha scattering) and it is also employed as a level 1 trigger. Finally, the MDC allows the identification of secondary vertices of long lifetime neutral hadrons (such as K^0_S and Λ^0).

To minimize the multiple scattering and maintain a good dE/dx resolution a 60:40 helium-propane mixture (He-C_3H_8) was chosen to fill the MDC. With an inner radius of 59 mm and an outer radius of 810 mm, the MDC was designed to be divided into layers grouped in two: the inner chamber and the outer one with 8 and 34 layers, respectively. The inner chamber can be removed for upgrade due to the inevitable radiation damage it undergoes. The coverage of the MDC reaches 93% of the solid angle.

As Ref. [123] reports, the contribution from the MDC tracking efficiency uncertainty is relatively low and it is estimated to be 1% for each track.
Among the many analyses in which charged tracks are employed, and, hence, the MDC is essential, one can mention the latest R-value estimation [171]. For such

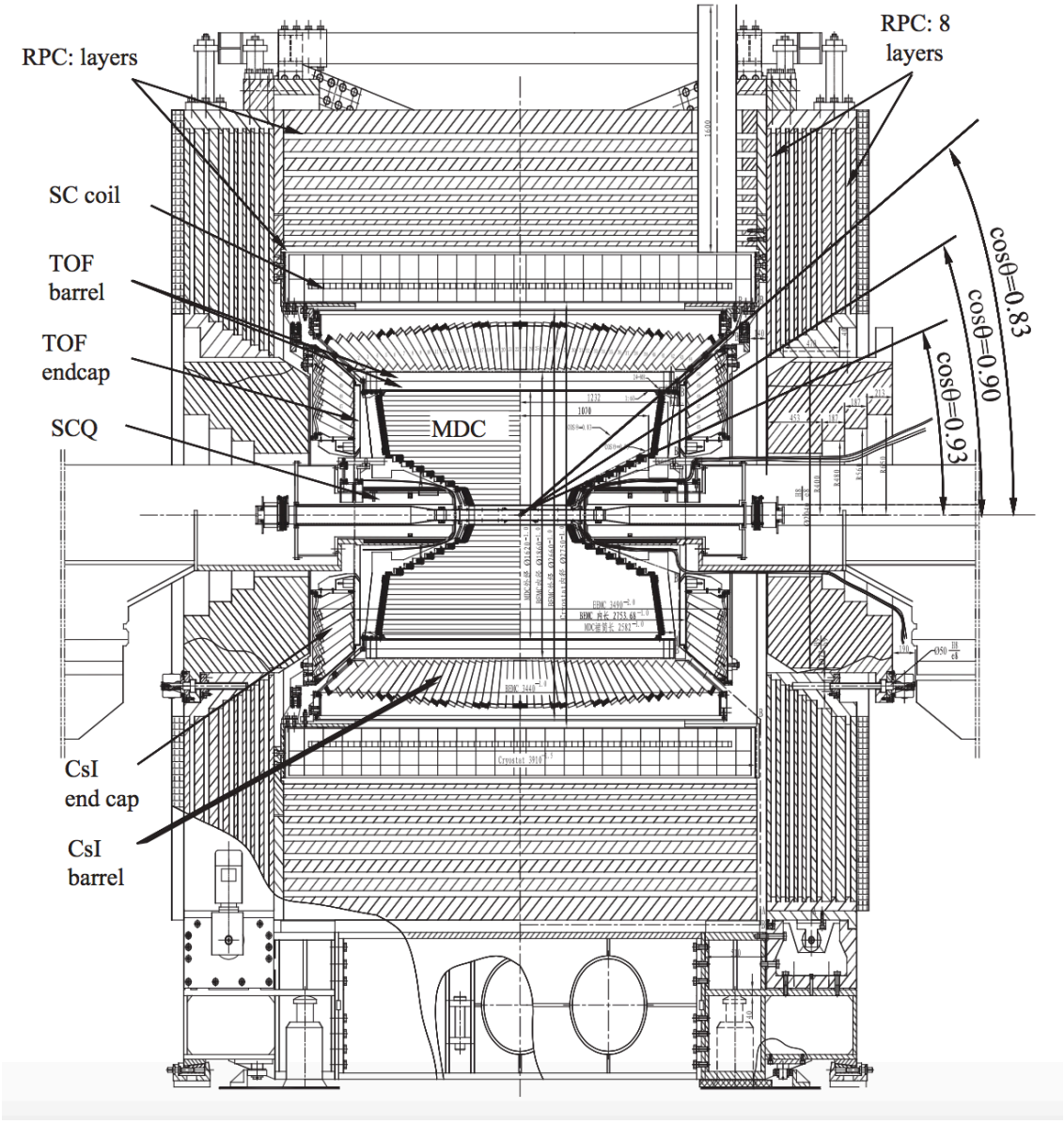

Figure 3.2: Schematic representation of BESIII detector. The different sub-detectors are also depicted; from the beam pipe (at the centre of the image): the multilayer drift chamber, the time of flight detector, the electromagnetic calorimeter, the 1 T superconducting solenoidal magnet, and the muon counter.

a measurement, good charged hadronic tracks are selected, while rejecting QED-related background. The trigger efficiency and the event selection are the least contributing uncertainties, thus, granting the most precise measurement of the R-

value for 14 energy points at $\sqrt{s}$ = [2.2324, 3.6710] GeV. Fig. 3.3 shows BESIII collaboration's results compared to QCD prediction [172] and other experiments (cf., Ref. [173]).

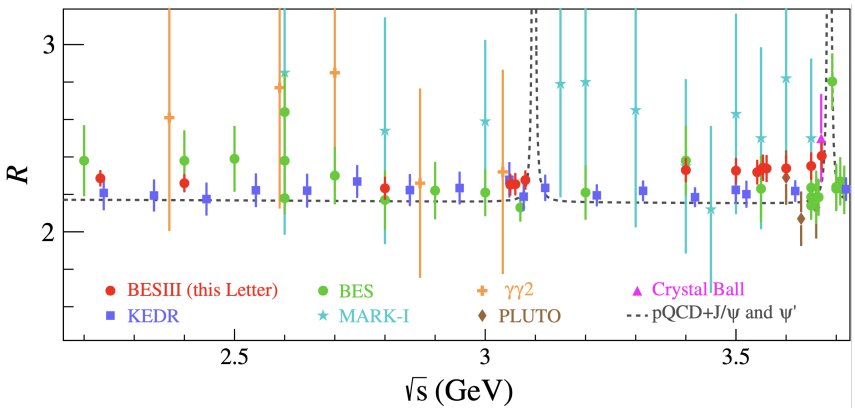

Figure 3.3: R-value measurements for 14 energy points at $\sqrt{s}$ = [2.2324, 3.6710] GeV [171]. The red dots denote the BESIII collaboration's results, the rectangles show the KEDR measurements [173], and the black dashed line represents the QCD prediction [172].

3.2.1.1 Aging of the MDC

Due to the high luminosity of the BEPCII collider, with a background rate of the order of the kHz/cm^2 [174], the inner chamber of the MDC has been showing ageing issues due to radiation damage. The ageing is associated with the polymerization on the cathode of the organic molecules used as a quencher in the MDC, this thin insulating layer then charges positively and causes secondary electron emission (Malter Effect). As shown in Fig. 3.4, BESIII inner tracker suffered a decrease in the gain of ∼4% per year, reaching a total gain loss of 51% in the innermost layer in 2022.

Considering BESIII is going to take data, with upgraded luminosity, up until the 2030s, at least, the inner MDC must be substituted. For this reason, the BESIII Italian teams proposed a tracking system based on a cylindrical Gas Electron Multiplier (cf. Sec. 3.4.3.2) [175].

3.2.2 The Time of Flight Detector

The ToF detector, present both in the barrel and two endcaps, participate in the particle identification by estimating the time elapsed between the collision and the

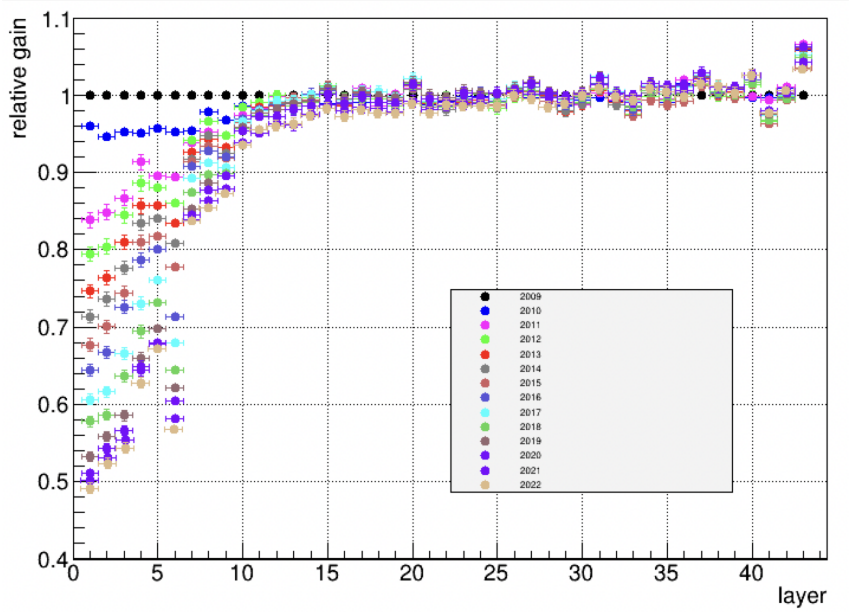

Figure 3.4: Gain loss of the MDC per year compared to its initial conditions.

particle's passage through the detector's layers. The barrel ToF has two layers of 88 scintillating bars directly coupled to PhotoMultiplier Tubes (PMTs) and mounted in a cylindrical geometry around the shell of the MDC. The endcap ToF system was upgraded in 2015 with a double layer of trapezoidal multigap resistive plate chambers [176].
Owing to 80 ps (65 ps) time resolution in the barrel (endcaps), combined with the aforementioned $\mathrm{d}E/\mathrm{d}x$ resolution, the ToF and MDC system provide a 3σ π/K separation up to momenta of 770 MeV/c. This good time resolution also makes the ToF a fast trigger for charged particles.

The ToF detector has been also particularly successful in probing the electromagnetic structure of the neutron, which was achieved by the BESIII collaboration via measuring its Sachs form factors [177]. The result was obtained by studying the $e^+e^- \to n\bar{n}$ process. The ToF is used in combination with the EMC to detect (anti-)neutrons, by searching for events with hadronic showers in the EMC and a corresponding knockoff proton in the ToF (either due to antineutron annihilation or neutron interaction). This allowed, as shown in Fig. 3.5, the observation for the first time of the oscillatory behaviour of the effective form factor for the neutron.

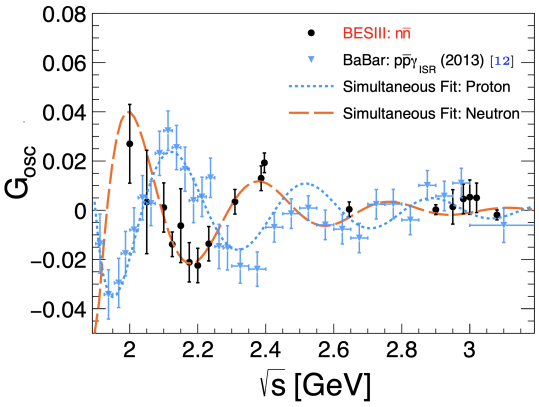

Figure 3.5: Fit to the deviation of the effective form factor |G| of the nucleon from the dipole law [177].

3.2.3 The ElectroMagnetic Calorimeters

The EMC is designed to measure the energies and the position of the leptons and photons with energy bigger than 20 MeV. It's also important for e-π discrimination at momenta larger than 200 MeV/c. The EMC consists of 6240 CsI(Tl) crystals placed in the barrel and the endcaps, each with a material budget equal to 15 radiation lengths.
With an acceptance of $\sim$ 93%, the designed energy resolution of electromagnetic showers is 2.5% (5%) in the barrel (endcaps) at 1 GeV and the position resolution is $\frac{0.6}{\sqrt{\text{E (GeV)}}}$ cm.

As already stated, the EMC is fundamental in those event signatures which do not contain charged tracks. Another example regarding this point comes from Ref. [23], in which the $h_c(1^1P_1)$ charmonium state is studied via the $\psi(2S) \to \pi^0 h_c \to \pi^0\gamma\eta_c$. In such a study, only three photons are used to describe the event, two of which to reconstruct the π^0 and one to tag the event. Owing to the EMC resolution, Ref. [23] was able to provide the second-ever measurement of the $h_c(1^1P_1)$ width, among the estimations of the branching fractions of the involved decays as reported in Fig. 1.3 of Chapter 1.

3.2.4 The Superconducting Solenoidal Magnet

The superconducting solenoidal magnet is designed to provide a uniform axial field of 1 T and to guarantee the MDC high momentum resolution for charged tracks

(0.5% for 1 GeV/c momentum). The steel flux return yoke used for hadron absorption allows muon-hadron separation and provides support to the whole BESIII structure. Made of carbon steel, the return yoke is divided into nine layers both in the barrel and on the endcaps.

3.2.5 The Muon Counter

The MUC is the outermost subsystem of the BESIII detector. It can distinguish muons (with momenta bigger than 400 MeV/c) from hadrons by their hit patterns. The muon-hadron separation is performed thanks to the instrumented steel flux return yoke of the solenoidal magnet.
The muon spectrometer is made of alternating layers of RPC (Resistive Plate Chamber) and steel absorber. The barrel is divided into octants, each of which is made of 9 layers of absorber and 9 layers of RPC, while the endcaps are instrumented with 8 active layers.
The 4 cm large readout strips can be found both in ϕ and θ covering $\sim 89\%$ of the solid angle.

A topical analysis for this subdetector is Ref. [178], in which the MUC allowed the estimation of the product $f_{D_s^+}|V_{cs}|$ [2]. Via the $D_s^+ \to \mu^+\nu_\mu$ decay, from the missing mass squared (presented in Fig. 3.6), Ref. [178] obtained the branching fraction of the searched channel. Combining this information with the μ^+ and D_s^+ masses and the meson lifetime, the BESIII collaboration measured the $f_{D_s^+}$ and $|V_{cs}|$ variables.

3.3 BESIII Physics Programme

Since 2009, BESIII has collected data samples of J/ψ, $\psi(2S)$, and $\psi(3770)$ states along with data sets to fully cover its rich programme that will be shortly presented in this section (cf., Table 4.1).
There exist many possible studies with the BESIII detector which are subdivided into the five main physics subgroups.

Light Hadron Spectroscopy The light hadron group concentrates its efforts on light (u, d, s) meson and baryon spectroscopy, along with form factors estimations

[2] Where $f_{D_s^+}$ is the D_s^+ decay constant and $|V_{cs}|$ is the CKM matrix element for the $c \to s$ quark mixing

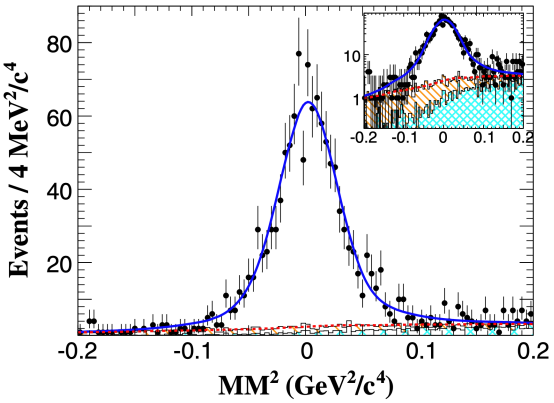

Figure 3.6: Fit to the missing mass squared of the $D_s^+ \to \mu^+\nu_\mu$ decay [178]. The inset plot shows the distribution in log scale. Dots with error bars are data. The blue solid curve is the fit result and the red dotted one represents the background fit. The histograms are the different background components.

and exotic states searches. The search for these states, after all, did begin in the light quark sector; and, with its 10 billion J/ψ, the BESIII collaboration can make use of this resonance's radiative decays (which are gluon-rich processes) to study light glueballs and hybrids.

Among many other results [179, 180], the latest and the most interesting one is shown in Refs. [181, 182]; in such an analysis, a new state, the $\eta_1(1855)$ resonance, is found. Due to its quantum numbers, $J^{PC} = 1^{-+}$, the $\eta_1(1855)$ is an *exotic* isoscalar state, whose parameters are consistent with Lattice QCD calculations for the 1^{-+} hybrid [183].

Moreover, one of the results in which the BESIII collaboration plays a crucial role in the light hadron spectroscopy sector is the analysis of the exotic state $X(1835)$, firstly observed by the BES collaboration [184] and six years later confirmed by the BESIII experiment [184]. The latest study on this exotic state is brought by Ref. [185], in which the $J/\psi \to e^+e^-X(1835)$ Dalitz transition is observed and its transition form factor measured for the first time.

Charmonium Physics The subgroup focuses on the studies of conventional charmonia and the searches for the XYZ states. On the one hand, it measures cross sections, transitions, and decays between the different charmonia, allowing us to probe the charmonium potential model and shedding light on our knowledge of these states. On the other hand, it allows the BESIII collaboration to be one of the

main protagonists in the XYZ studies, probing the transition among these states (and their connections to the conventional ones) and their cross-section at different energies.
Many of the analyses presented in Chapter 2 and this thesis itself lay within the charmonium subgroup. In the XYZ regime, the most recent study is Ref. [96];. This analysis found evidence of the $Z_{cs}(3985)^0$ state. Found near-threshold in the $e^+e^- \to K^0_S(D^+_s D^{*-} + D^{*+}_s D^-)$ reaction, its coupling to charmed mesons suggests a minimum quark content of $c\bar{c}s\bar{d}$, making the most plausible interpretation for it to be the isospin partner of the charged $Z_{cs}(3985)$ state [138, 140].
Regarding the conventional charmonium states, apart from the already discussed Ref. [23], the BESIII collaboration also investigates the $h_c(1^1P_1)$ states searching for its hadronic decays [186, 187] as it is not yet clear if this pseudovector hadronic width is of the same order of its radiative one.

Charm Physics The charm subgroup studies the other part of the charm quark systems, *i.e.*, the charmed mesons and baryons. The group contributes to the light quark *exotic* states searches, by probing their connections to the $D_{(s)}$ mesons. The charm division also takes care of the electroweak part of the Standard Model (SM) measuring the Cabibbo-Kobayashi-Maskawa (CKM) matrix entries [178, 188] and studying the D^0-mixing [189] and the CP-violating $D_{(s)}$ decays (such as Ref. [190]).
A flagship analysis for the charm group is presented in Ref. [188]. This analysis is analogous to the one of Ref. [178], presented earlier in this Chapter, with the difference that the $D^+_{(s)}$ is reconstructed in its $D^+_{(s)} \to \tau^+\nu_\tau$ decay, with τ^+ going to $e^+\nu_e\bar{\nu}_\tau$. The product $f_{D^+_s}|V_{cs}|$ is estimated with an improved precision with respect to Ref. [178]. Finally, the branching ratio measurement of the $D^+_{(s)} \to \tau^+\nu_\tau$ process is improved by a factor of 2 compared to the previous best measurement [190], allowing the estimation of the branching fractions ratio $\mathcal{B}_{D^+_{(s)}\to\tau^+\nu_\tau}/\mathcal{B}_{D^+_{(s)}\to\mu^+\nu_\mu} = 9.72 \pm 0.37$. The branching fractions ratio is found consistent with the SM prediction [1] of lepton flavour universality.

τ-QCD Physics The τ-QCD physics group is dedicated to the precise measurement of key parameters of the SM (such as the τ lepton mass and its decays) and of the perturbative regime of QCD (e.g., R-value estimation and form factors).
The long waited work of Ref [171] has already been presented above. With such an analysis, the BESIII collaboration provided the most precise up-to-date measurement of the R-value for 14 energy points at $\sqrt{s}$ = [2.2324, 3.6710] GeV. Reaching

an accuracy of 2.6% at $\sqrt{s} < 3.1$ GeV and 3.0% at $\sqrt{s} > 3.1$ GeV, the results are consistent with KEDR ones [173] and QCD predictions [172].
An example of how the BESIII collaboration can perform regarding the form factors is represented in Ref. [191]. In this study, the τ-QCD subgroup measured the Born cross-section of the $e^+e^- \to \Sigma^0\bar{\Sigma}^0$ reaction at 7 centre-of-mass energies ($\sqrt{s} =$ [2.3864, 3.0200] GeV), providing the 7 corresponding Σ^0 effective form factors [192]. The results are in agreement with the BaBar collaboration's ones [193], but with improved precision of a factor of 2. Moreover, following Ref. [194], an asymmetry in the effective form factors (G_{Eff}) of Σ-triplet is observed confirming that G_{Eff} is proportional to the squared sum of the valence quarks' charge.

New Physics The new physics subgroup focuses on all those studies beyond the SM (BSM) physics that can be performed in the low energy regime (*i.e.*, at $\sqrt{s} \ll m_Z$, where m_Z is Z-boson's mass). The focus in this sector revolves around a possible massive partner of the photon, whose mass should be of the order of the GeV/c^2 [195–197]. This new "dark photon" would behave as a portal between the SM and the dark sector, coupling to the photon and decaying both to the SM and BSM sector. In Ref. [198] the search for this extra boson is performed using the Initial State Radiation (ISR) to cover a mass range between 1.5 and 3.4 GeV/c^2. From the $e^+e^- \to \gamma_{ISR}\gamma' \to \gamma_{ISR}\ell^+\ell^-$ reaction, the dark photon (γ') would appear as an enhancement in the invariant mass distribution of the leptonic pairs ($\ell = e, \mu$). The BESIII collaboration also probes supersymmetric models [199, 200] via searching for J/ψ radiative invisible decays (*i.e.*, $J/\psi \to \gamma +$ invisible) [201];. In said scenarios, a light stable candidate of dark matter couples with SM via a light pseudoscalar Higgs boson, which can be produced in radiative decays of charmonium vector resonances (such as the J/ψ).
Finally, the BESIII collaboration can also perform searches on lepton/baryon number violating processes both with D mesons decays ($D^0 \to pe^- + c.c.$ [202] and $D^+ \to \bar{\Lambda}(\bar{\Sigma^0})e^- + c.c.$ [203]) or J/ψ transitions ($\to \Lambda_c e^- + c.c.$ [204]).

3.4 BESIII Upgrade Programme

As explained in the previous Chapters, despite the discovery of the charm quark almost 60 years ago, many questions about the charmed sector still remain unanswered. Moreover, the physics related to the XYZ states is still an object of theoretical debate and consensus seems far to be reached; indeed, many discoveries are

expected and needed to understand more about the nature of these exotic hadrons. Hence, an upgrade of the BEPCII collider and the BESIII detector is of the utmost importance to keep the collaboration competitive in these topics [174]. The upgrades will contribute not only to understanding the XYZ sector but will impact also the standard physics, investigating lepton flavour universality, the charmonium spectrum and decays, the unitarity of the CKM matrix, hadronic properties, and new physics.

3.4.1 Physics Reach

Increasing energy and luminosity will grant the BESIII collaboration to be competitive in the upcoming years. This is particularly true in the XYZ sector; a relatively high luminosity at high energy means new information, with the ability to perform finer and more precise scans for the Y states, to study Argand diagrams and Dalitz plots for understanding the Z resonances, and to investigate with more sensitivity the X structures CP values.
Despite the main aim being increasing the information regarding the XYZ sector, all of the five main physics subgroups will profit from the upgrades, especially considering the possible increase of the three $\psi(nS)$ data sets and the studies, not yet performed, with the current ones.
The light hadron group with J/ψ and $\psi(2S)$ events can and will perform more systematic studies on glueballs and investigate exotic hybrid nonets, probing a larger phase space and reaching higher masses without suffering from sensitivity constraints.
Thanks to higher statistics, the charmonium subgroup can search for new $h_c(1^1P_1)$ decay modes, and, more generally, investigate charmonia M1 transitions and with baryon final states, even performing partial-wave analyses to understand intermediate particles contributions to charmonia transitions.
The charm subgroup will profit from the increased $\psi(3770)$ data sample; with more $D_{(s)}D_{(s)}$ events double-tag technique can be employed to fully reconstruct $D_{(s)}$ decays, probing CP violation and measuring CKM matrix entries.
Finally, the τ-QCD physics and the new physics subgroups can increase their energy reach and sensitivity for transition and EM form factors, for probing Bell inequality, and search for states non-predicted by the SM.

3.4.2 Luminosity Upgrade

To keep the physics requirements attainable from both a statistical and an energetic point of view, an upgrade for BEPCII is under development [37,169]. The upgraded BEPCII-U will reach 2.8 GeV per beam, tripling current the instantaneous luminosity at $\sqrt{s} \approx 4.70$ GeV to reach 6×10^{33} cm^{-2} s^{-1}, the same luminosity of $\sqrt{s} =$ 3.77 GeV as shown in Fig. 3.7.

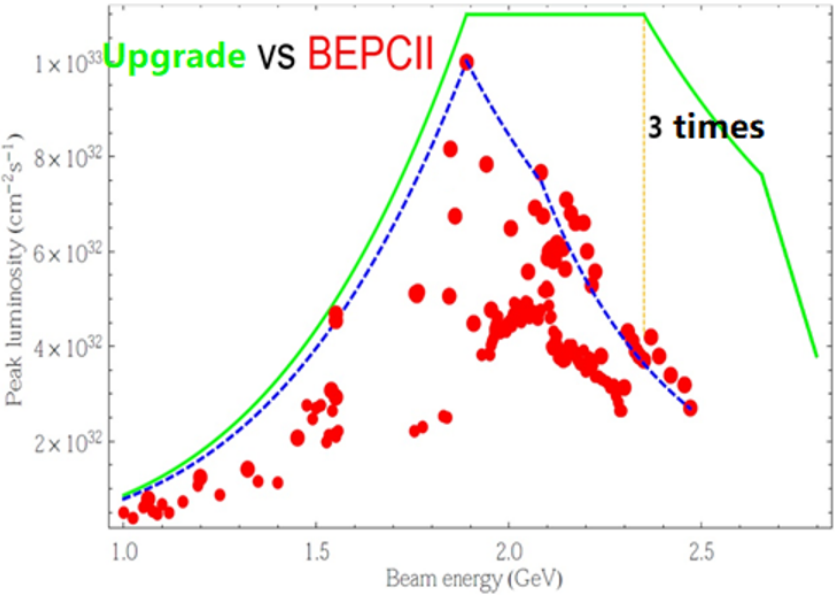

Figure 3.7: BEPCII-U expected luminosity compared to BEPCII performances. The green solid line represents the envisioned luminosity at the future upgrade of BEPCII. The red points and the dashed blue line are the achieved values and the trend line of the BEPCII luminosity. The expected upgrade will allow BEPCII-U to reach a peak luminosity of 6×10^{33} cm^{-2} s^{-1} within the $\sqrt{s}$ range [3.77, 4.70] GeV.

3.4.3 The CGEM-IT Project

As mentioned in Sec. 3.2.1.1, the inner MDC will be substituted by a tracking system based on a cylindrical Gas Electron Multiplier (CGEM) technology, proposed by the Italian collaboration. This project (BESIII-CGEM) is funded in part by European Commission.

GEMs are micropattern gaseous detectors first introduced in 1997 [205], and, since then, adopted by several high-energy physics experiments [206–208].

3.4.3.1 GEM Detectors

A GEM (Fig. 3.8) foil consists of a 50 μm Kapton film, coated on both sides by 5 μm of copper. This sandwich-like foil is then hole-etched, to create a 70 μm wide holes mesh [205]. A single GEM detector consists of a cathode, an anode (which serves as the readout plane), and a GEM foil, all separated by gaps of a few millimetres.

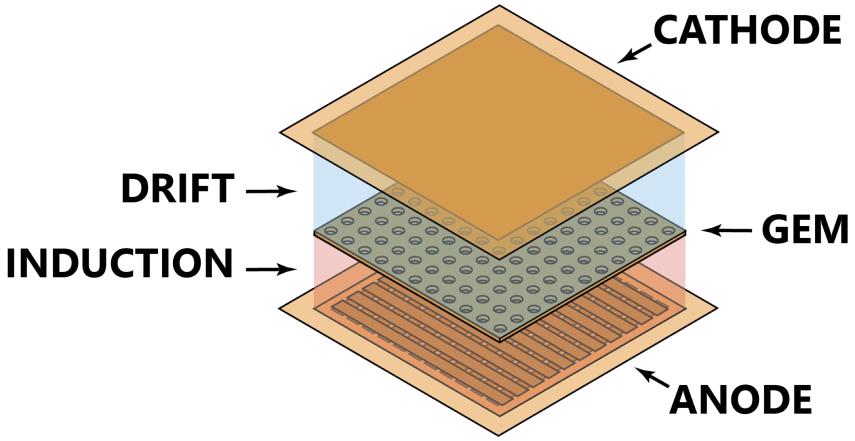

Figure 3.8: Schematic representation of a GEM foil. Courtesy of S. Gramigna.

Applying a high voltage between the two copper faces, it is possible to generate an electric field inside the holes in such a way that GEMs can provide electron multiplication [205,209]. The electrons, produced via primary ionization by charged particles interactions with the gas, are brought towards the GEM. Approaching the GEM holes the electrons are accelerated by an electric field of the order of 10^2 kV/cm, producing (by secondary ionization) the charge multiplication. The charge is then drifted to and collected by readout strips placed on the anode. To increase the charge collected it is possible to use a series of GEM layers, as in Fig. 3.9. This setup minimizes also discharges inside the GEM, allowing to diminish the electric field in the holes as shown in Fig. 3.10 and Ref. [210].

3.4.3.2 CGEM-IT

The CGEM-IT (Cylindrical GEM-Inner Tracker) project was proposed and approved with the main idea being that GEMs are less prone to ageing concerning wire chambers (c.f., Refs. [1,211]), they have a relatively low material budget, and that, as shown Ref. [175], the secondary vertex resolution will improve by a factor

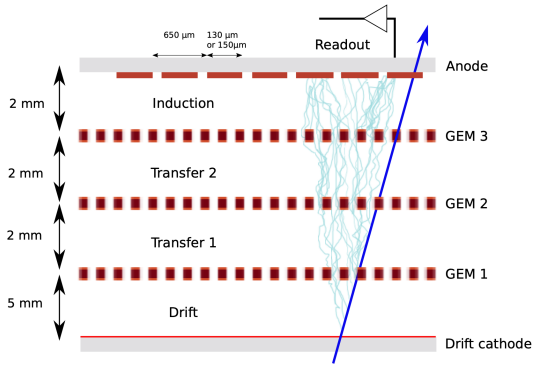

Figure 3.9: Schematic representation of a triple GEM detector.

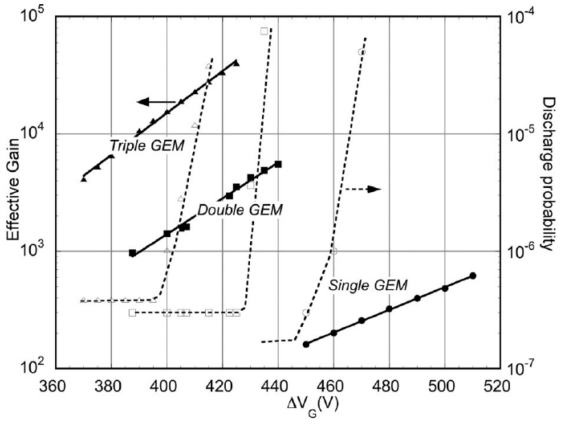

Figure 3.10: Gain as a function of the voltage difference applied on a GEM foil for different detector configurations [210].: single (SGEM), double (DGEM), and triple GEM (TGEM).

between 2 and 3 better with this new detector.

As shown in Fig. 3.11, the CGEM-IT consists of three independent cylindrical layers, each composed of a triple GEM (*i.e.*, with three multiplication stages). The cylindrical structure is needed to envelop the entire beam pipe. A 90:10 Ar-iC_4H_{10} gas mixture was chosen according to the results of validation analyses [212].

The CGEM Inner Tracker has been introduced by the KLOE-2 experiment at LNF [213]. Despite the similarities between the two aforementioned experiments, the CGEM-IT has stringent requirements that must be observed. It has to sustain a 1 T magnetic field maintaining a spatial resolution in the ϕ plane better than

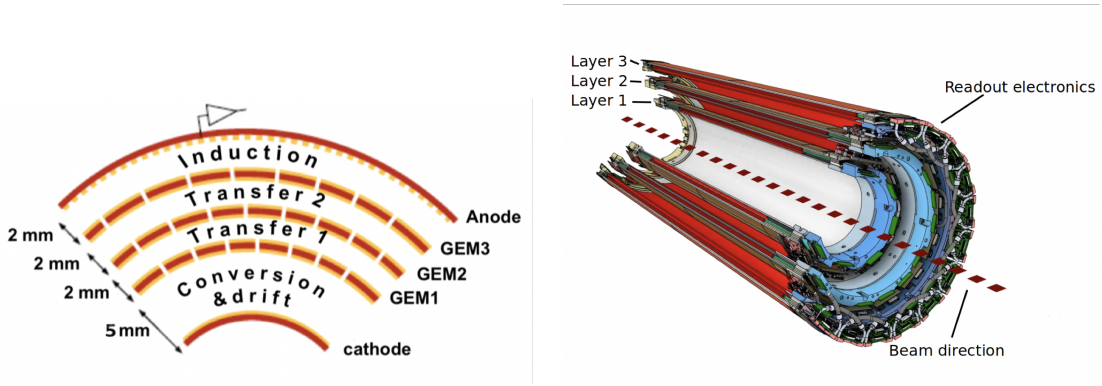

Figure 3.11: Schematic representations of the CGEM detector. Fig. 3.11(a) is a layout of a cylindrical triple-GEM detector, while Fig. 3.11(b) is a sketch of the whole CGEM detector.

130 μm [37, 214].

The two innermost layers have already been built, and are currently under validation at IHEP with cosmic-ray data acquisition. The third and outermost layer is under construction as it underwent mechanical review in 2021.

As I proceeded with my analysis work, I also contributed to the characterisation of the CGEM-IT by developing a Geant4 simulation to understand the behaviour of the supporting structure holding the first two CGEM layers. The supporting structure is the assembly machine for the layers and as of 2022 operates as a cosmic stand. The knowledge of its impact on cosmic rays is fundamental to understanding its contribution to tracking resolution. The simulation allows the collaboration to understand that the structure introduces a small deflection ($\sim$0.5 mrad) on the primary particles. The simulation also proves that secondary particles are produced in less than 10% of the events. The results allows continuing data analysis without the need to apply for corrections. Furthermore, I carried out quality assurance studies on the two CGEM-IT innermost layers and participated in beam tests at CERN for the validation of the custom electronics developed for the CGEM-IT.

Collected Events (fb^{-1})	Scan Type Motivation	Centre-of-mass Energy (GeV)	Year
2.9	$\psi(3770)$	3.773	2010 - 2011
0.5	$\psi(4040)$	4.009	2011
0.024	τ mass	3.554	2011
1.3 billions (*total*)	J/ψ	3.097	2009 - 2012
0.5 billions (*total*)	$\psi(2S)$	3.686	2009 - 2012
1.9	$Y(4260)$	Around 4.23, 4.26	2013
0.5	$Y(4360)$	Around 4.36	2013
0.5	$Y(4260)/Y(4360)$	Around 4.23, 4.26, 4.36	2013
0.8	R-value	[3.85, 4.59]	2014
0.04	Λ_c threshold	4.599	2014
0.5	R-value	[2.00, 3.08]	2015
0.1	$Y(2175)$	2.125	2015
3.1	$D_s^* D_s$ threshold	4.18	2016
5	Scan	[4.19, 4.30]	2017
10 billions (*total*)	J/ψ	3.097	2018 - 2019
4	Scan	4.13, 4.16 [4.29, 4.44]	2018 - 2019
3.8	Scan	[4.61, 4.70]	2020
2	Scan	[4.74, 4.946]	2021
3 billions (*total*)	$\psi(2S)$	3.686	2021
20	$\psi(3770)$	3.770	2022

Table 3.1: BESIII data samples collected since 2009. The first column reports the size of the data sample either in fb^{-1} or expressed in terms of number-of-events (for the J/ψ and $\psi(2S)$ resonances). The type of data sample collected and its corresponding year are presented in the second and last columns, respectively. The third column reports the centre-of-mass energy at or around which the data set was taken. Owing to its luminosity, BESIII has collected the biggest data samples in the world of J/ψ, $\psi(2S)$, and $\psi(3770)$ resonances.

Chapter 4

Study of the $e^+e^- \to \pi^+\pi^-\psi(2S)$ Reaction

Using six data samples with a total integrated luminosity of $\sim$5 fb^{-1} collected by the BESIII detector, the $e^+e^- \to \pi^+\pi^-\psi(2S)$ process is studied at centre-of-mass energies ranging from 4.6121 GeV to 4.6984 GeV both to probe the $Y(4660)$ structure nature and to search for the $Z_c(4430)^\pm$ state. First, $e^+e^- \to \pi^+\pi^-\psi(2S)$ cross-section is studied; then, the Dalitz plot of the $e^+e^- \to \pi^+\pi^-\psi(2S)$ process is analysed to investigate the $f_0(980)c\bar{c}$ molecule interpretation of the $Y(4660)$ resonance. Finally, a search for the charged $Z_c(4430)$ exotic hadron is performed; this search is motivated by Refs. [112, 123], where the $Z_c(3900)^\pm$ state is seen both in the $\pi J/\psi$ and $\pi\psi(2S)$ invariant masses and in relation with the $Y(4260)$ resonance. In analogy with these analyses, and drawing from the Ref. [123] finding of the production ratio $R = \sigma(e^+e^- \to \pi^\pm Z_c(3900)^\mp \to \pi^+\pi^- J/\psi)/\sigma(e^+e^- \to \pi^+\pi^- J/\psi) = (21.5 \pm 3.3 \pm 7.5)\%$, neglecting the change of phase space due to the J/ψ to $\psi(2S)$ switch, roughly 100 $Z_c(4430)^\pm$ events are expected around the $Y(4660)$ peak.

4.1 Analysis Strategy

The $e^+e^- \to \pi^+\pi^-\psi(2S)$ process is studied following the $\psi(2S) \to \pi^+\pi^- J/\psi$ transition with the J/ψ resonance decaying into a couple of leptons (ℓ), either electrons (e) or muons (μ). To estimate the $e^+e^- \to \pi^+\pi^-\psi(2S)$ cross-section, the $\psi(2S)$ invariant mass ($M(\psi(2S))$) is fitted and the number of events extracted and normalised as described below. As will be evident below, the analysis of the Dalitz plot shows the potential of studying the $e^+e^- \to f_0(980)\psi(2S)$, $f_0(980) \to \pi^+\pi^-$

sub-channel. The $e^+e^- \to f_0(980)\psi(2S)$ contribution to the total process is estimated from the $M(\pi^+\pi^-)$ spectrum. Finally, to search for the charged $Z_c(4430)$ exotic state, the $\pi\psi(2S)$ invariant mass distribution is studied. The last step uses together the 6 data sets (for an integrated luminosity $\sim$5 fb^{-1}) collected by the BESIII collaboration in 2020.

4.2 Monte Carlo and Data Samples

BESIII software group provides the entire data processing, and physics analysis packages consisting of generation, simulation, reconstruction and other useful analysis tools in a GAUDI [215] environment called BESIII Offline Software System (BOSS) [216]. This analysis was performed with BOSS version 7.0.6, which contains the full reconstruction of the 6 data sets collected in 2020.

4.2.1 Monte Carlo Samples

Simulated data samples, produced with a GEANT4-based [217] Monte Carlo (MC) package, which includes the geometric description of the BESIII detector and the detector response, are used to determine detection efficiencies and to estimate backgrounds. The centrally produced simulation models the beam energy spread and initial state radiation (ISR) in the e^+e^- annihilations with the generator KKMC [218, 219]. The inclusive MC sample used to study and estimate background components includes the production of open charm processes, the ISR production of vector charmonium(-like) states, and the continuum processes incorporated in KKMC. All particle decays are modelled with EVTGEN [220, 221] using branching fractions either taken from the Particle Data Group [1], when available or otherwise estimated with LUNDCHARM [222, 223]. Final state radiation (FSR) from charged final state particles is incorporated using the PHOTOS [224] package. For each energy point (*cf.*, second column of Table 4.1) and the hadronic and QED contributions, samples ten times the statistics, estimated considering the centre-of-mass energy and the integrated luminosity (*cf.*, third column of Table 4.1), are generated; for the simulation of open charm processes, samples of forty times the statistics are produced.

In the signal MC samples, both the non-resonant ($e^+e^- \to \pi^+\pi^-\psi(2S)$) and the exotic ($e^+e^- \to f_0(980)\psi(2S)/\pi^\pm Z_c(4430)^\mp$) processes are generated by EVTGEN.

The CONEXC generator [225] (*cf.*, Appendix A) is used to simulate the ISR process and estimate the vacuum polarisation [226] and the ISR correction factors. For each energy point and each data sample, 300000 events are generated.

4.2.2 Data Samples

This analysis data, collected by the BESIII collaboration in 2020, corresponds to an integrated luminosity of $\sim$5 fb^{-1}. Table 4.1 shows a summary of the 6 data sets with their centre-of-mass beam energy (E_{CoM}) and the associated luminosity ($\mathcal{L}$).

Sample	E_{CoM} (MeV)	$\mathcal{L}$ (pb^{-1})
4610	4611.86 $\pm$ 0.12 $\pm$ 0.30	103.65 $\pm$ 0.05 $\pm$ 0.55
4630	4628.00 $\pm$ 0.06 $\pm$ 0.32	521.53 $\pm$ 0.11 $\pm$ 2.76
4640	4640.91 $\pm$ 0.06 $\pm$ 0.38	551.65 $\pm$ 0.12 $\pm$ 2.92
4660	4661.24 $\pm$ 0.06 $\pm$ 0.29	529.43 $\pm$ 0.12 $\pm$ 2.81
4680	4681.92 $\pm$ 0.08 $\pm$ 0.29	1667.39 $\pm$ 0.21 $\pm$ 8.84
4700	4698.82 $\pm$ 0.10 $\pm$ 0.36	535.54 $\pm$ 0.12 $\pm$ 2.84

Table 4.1: BESIII analysis data samples collected in 2020 [227]. The first column reports how the data sample is dubbed. The centre-of-mass beam energy (E_{CoM}) of the data sample collected and its corresponding luminosity ($\mathcal{L}$) are presented in the second and last columns, respectively.

4.3 Event Selection

The procedure of selection consists of two main steps: good charged tracks selection and cuts to select the chosen process. The selection process was optimised on signal MC data sets and checked on the inclusive MC sample.

4.3.1 Charged Particle Selection

Good tracks reconstructed in the MDC must pass the following fiducial and production vertex cuts. Tracks are required to satisfy $|\cos\theta| < 0.93$, where θ is the angle of the momentum direction with respect to the beam axis. The distance of closest approach to the interaction point must be less than 10 cm along the beam axis (R_z), and less than 1 cm in the transverse plane (R_{xy}). A comparison of these three

distributions, for the 4680 data sample, among the non-resonant simulation, the $Z_c(4430)$ exclusive MC events, and the inclusive MC sample is reported in Fig. 4.1.

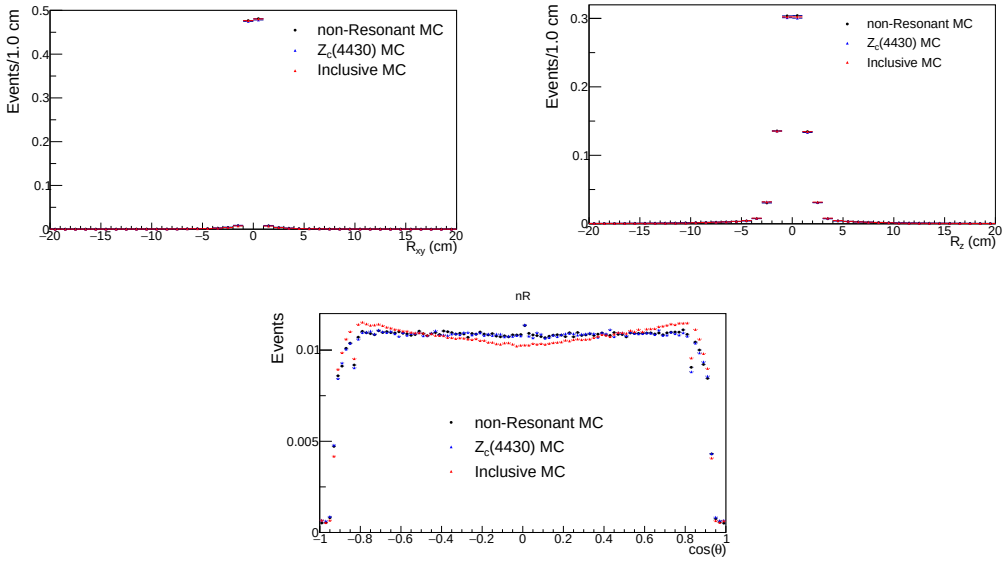

Figure 4.1: Charged tracks distributions for the 4680 energy point; black dots refer to non-resonant MC simulation, the blue triangles to the $Z_c(4430)$ exclusive MC sample, and the red triangles to the inclusive MC data set. The samples are normalised to their respective total. The top left represents the distance of closest approach in the transverse plane; the top right plot is the closest approach distance along the beam axis; the bottom histogram shows the cosine of the angle between the momentum and beam axis.

The final decay topology consists of 4 pions and 2 leptons, though, to increase the final selection efficiency, a missing pion (π_{Miss}) is allowed, and a 3 pions and 2 leptons final topology is also reconstructed. The six-track ($2\ell 4\pi$) and the five-track ($2\ell 3\pi$) events are reconstructed starting from the requirement of having exactly 6 or 5 good charged tracks, respectively. The number of (good) charged tracks for the 4680 data sample is reported in Fig. 4.2.

Leptons and pions are distinguished via their momenta, as leptons are those charged particles with momenta bigger than $1\,\text{GeV}/c$, while momenta less than $0.85\,\text{GeV}/c$ define pions. The last requirement is then optimised as described below. Further, electrons and muons are distinguished via the ratio of their deposited energy in the EMC to the momentum measured by the MDC (E_{EMC}/p_{MDC}); it is

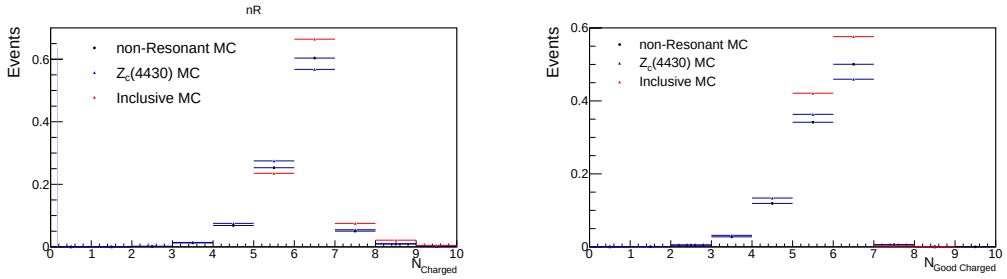

Figure 4.2: Number of charged tracks for the 4680 energy point; black dots refer to non-resonant MC simulation, the blue triangles to the $Z_c(4430)$ exclusive MC sample, and the red triangles to the inclusive MC data set. The samples are normalised to their respective total. The left plot shows the number of charged tracks for each event, while the number of good charged tracks is reported on the right. The number of good charged tracks for the inclusive MC data set si reported after all of the selection criteria.

required to be bigger than 0.7 for the electrons and smaller than 0.6 for the muons. The momentum and the E_{EMC}/p_{MDC} distributions are reported for the 4680 data sample in Fig. 4.3.

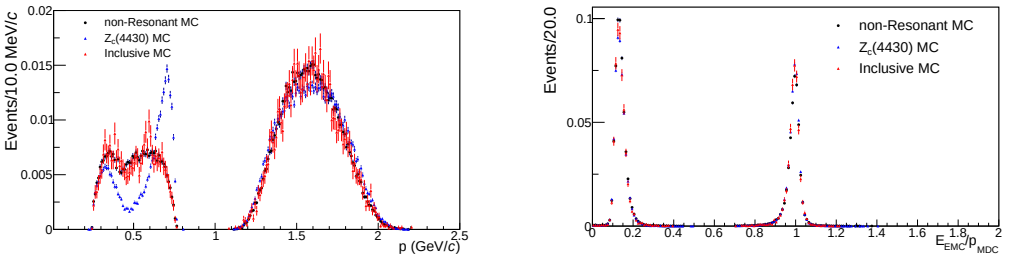

Figure 4.3: Charged tracks momentum and the E_{EMC}/p_{MDC} distributions for the 4680 energy point; black dots refer to non-resonant MC simulation, the blue triangles to the $Z_c(4430)$ exclusive MC sample, and the red triangles to the inclusive MC data set. The samples are normalised to their respective total. The left plot shows the charged tracks momentum spectrum, while the E_{EMC}/p_{MDC} distribution is reported on the right.

On the $Z_c(4430)$ signal MC dataset, the upper bound for the pion identification is optimised based on the figure of merit $\frac{S}{B}$, where S and B are the numbers of signal and background events estimated from the signal and inclusive MC samples, respectively. Starting from a momentum $p = 1\,\mathrm{GeV}/c$, the momentum spectrum of the pions is probed down to $0.60\,\mathrm{GeV}/c$ as shown in Fig. 4.4. Table 4.2 reports, for

each data set, the momentum value which optimised the figure of merit $\frac{\mathrm{S}}{\mathrm{B}}$ (p_{Best}).

Sample	p_{Best} (GeV/c)
4.610	0.72
4.630	0.73
4.640	0.74
4.660	0.75
4.680	0.77
4.700	0.78

Table 4.2: Optimised maximum momentum for pion identification. The upper bound for the pion identification is optimised based on the figure of merit $\frac{\mathrm{S}}{\mathrm{B}}$.

On the 6-track topology, a four-constraint kinematic fit is used to improve the event resolution fixing the total four-momentum; on the other hand, due to the missing pion track, a one-constraint kinematic fit is applied on the 5-track events by requiring the missing mass to be that of a pion. Moreover, on both the selected topologies, two constraints are added by fixing the masses of the $\psi(2S)$ and J/ψ resonances to their known values [1]. Candidates with a fit $\chi^2 > 200$ are rejected. In the six-track topology, the $\pi\pi$ couples are selected via the best χ^2. On the other hand, in the five-track events, the $\pi\pi$ and the $\pi\pi_{\mathrm{Miss}}$ couples are selected by finding the combination that reconstructs (before the six-constraint kinematic fit) the $\psi(2S)$ mass closest to its known value [1]. An additional requirement is posed on the energy of the missing pions; as it would be hard to kinematically constrain events with missing pions coming from the $Z_c(4430)^{\pm}$ decays, five-track topologies with $E(\pi_{\mathrm{Miss}}) > 0.50\,\mathrm{GeV}$ are discarded. The distribution of $E(\pi_{\mathrm{Miss}})$ with the 0.50 GeV cut overlaid is reported in Fig. 4.5 for the 4680 data sample.

Finally, additional cuts are required on the reconstructed masses of the $\psi(2S)$ and J/ψ resonances ($M_{\psi(nS)}$). These requirements are defined by studying the invariant $\pi^+\pi^-\ell^+\ell^-$ and $\ell^+\ell^-$ masses for the $\psi(2S)$ and J/ψ resonances, respectively, with the momenta of the particles taken before the six-constraint kinematic fit. The constraints are fixed by fitting the aforementioned distributions with either a double Gaussian or a sum of Gaussian and Crystal Ball [228] functions depending on the J/ψ decay channel; for the skewed electronic decay channel the asymmetric sum of Gaussian and Crystal Ball is used. The fits for the 4680 data set are reported in Figures 4.6 and 4.7, with the selection windows highlighted by the black solid

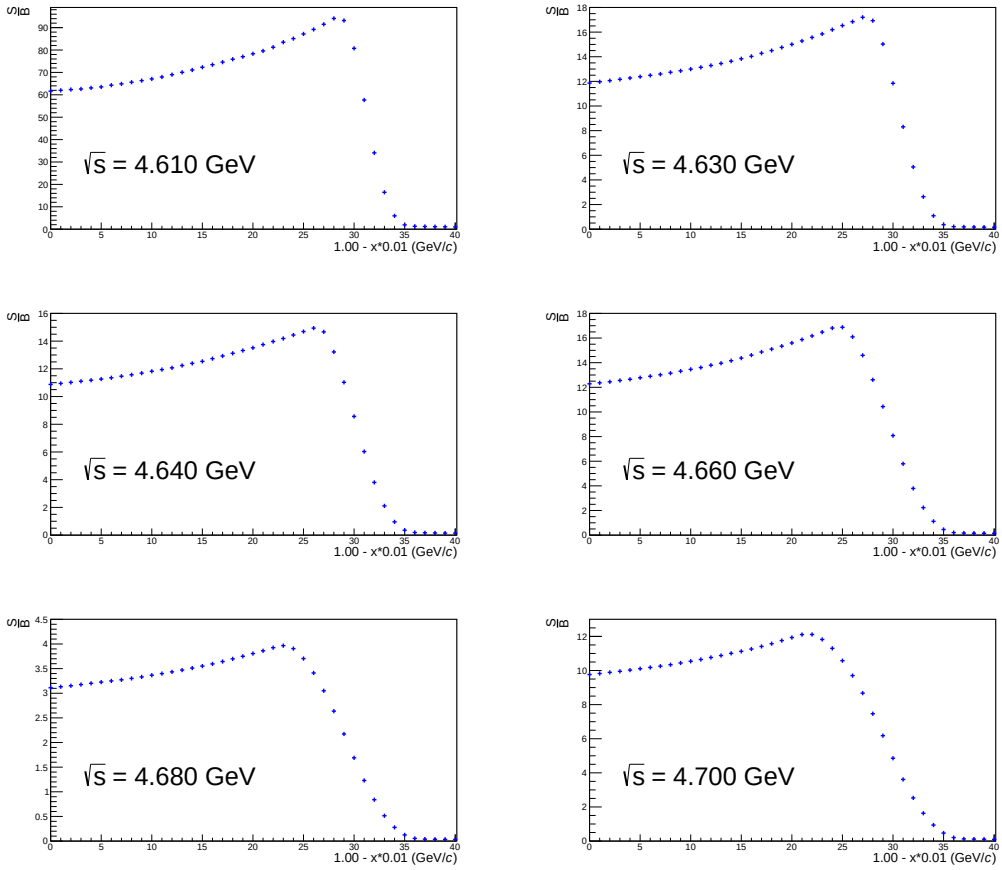

Figure 4.4: Charged particles momentum optimisation via the analysis of the $\frac{S}{B}$ figure of merit. For each centre-of-mass energy, the momentum spectrum of the pions is probed down to 0.60 GeV/c.

vertical lines. The widths (σ) of the final distributions, ranging from 19 MeV/c^2 to 25 MeV/c^2, are then taken and the events in the electron (muon) channel laying within $M_{\psi(nS)} - 5\sigma < M_{\psi(nS)} < M_{\psi(nS)} + 3\sigma$ ($M_{\psi(nS)} - 3\sigma < M_{\psi(nS)} < M_{\psi(nS)} + 3\sigma$) are then selected for further studies. For the invariant $\psi(2S)$ mass in the muon channel of the five-track topology, due to a more skewed distribution, a $M_{\psi(nS)} - 5\sigma < M_{\psi(nS)} < M_{\psi(nS)} + 3\sigma$ window is used.

Again for the five-track topology, the missing pion mass ($M_{\pi_{\text{Miss}}}$) is also constrained by fitting the $\pi\pi^+\pi^-\ell^+\ell^-$ recoil mass distribution with a sum of Gaussian and Crystal Ball functions and extracting its width (σ). The widths of the distributions are found to be in the [29, 37] MeV/c^2 range. The fit for the 4680 data set

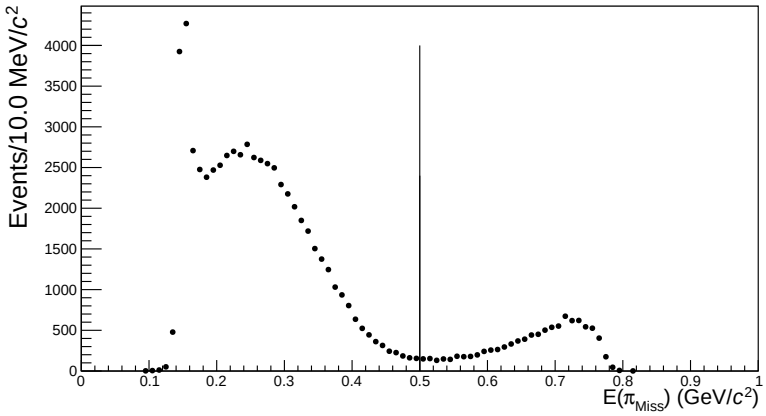

Figure 4.5: Missing energy $E(\pi_{\rm Miss})$ spectrum for the 4680 data sample. The black solid vertical line represents the selection criterion, above which the five-track topologies are discarded.

is reported in Fig. 4.8, with the selection windows highlighted by the black solid vertical lines. In this case, the events laying outside the $M_{\pi_{\rm Miss}} - 3\sigma < M_{\pi_{\rm Miss}} < M_{\pi_{\rm Miss}} + 5\sigma$ window are rejected.

4.4 Background evaluation

After the aforementioned cuts, in the real data samples, one expects to find mostly combinatorial background in addition to the searched non-resonant $e^+e^- \to \pi^+\pi^-\psi(2S)$ signal. To corroborate this hypothesis, the inclusive MC sample is studied. The inclusive MC sample includes the production of open charm processes, the ISR production of vector charmonium(-like) states, and the continuum processes. No $Z_c(4430)^\pm$ signal is generated within this sample. Via the study of this MC sample, two channels are found to survive after the selection cuts:

- the selected non-resonant $e^+e^- \to \pi^+\pi^-\psi(2S)$ channel;
- the $e^+e^- \to \pi^+\pi^-\pi^+\pi^-\pi^+\pi^-$ channel.

This study is performed with a tool from Ref. [229]; the inclusive MC sample is analysed with the MC truth of the final particles gathered to reconstruct their origin.

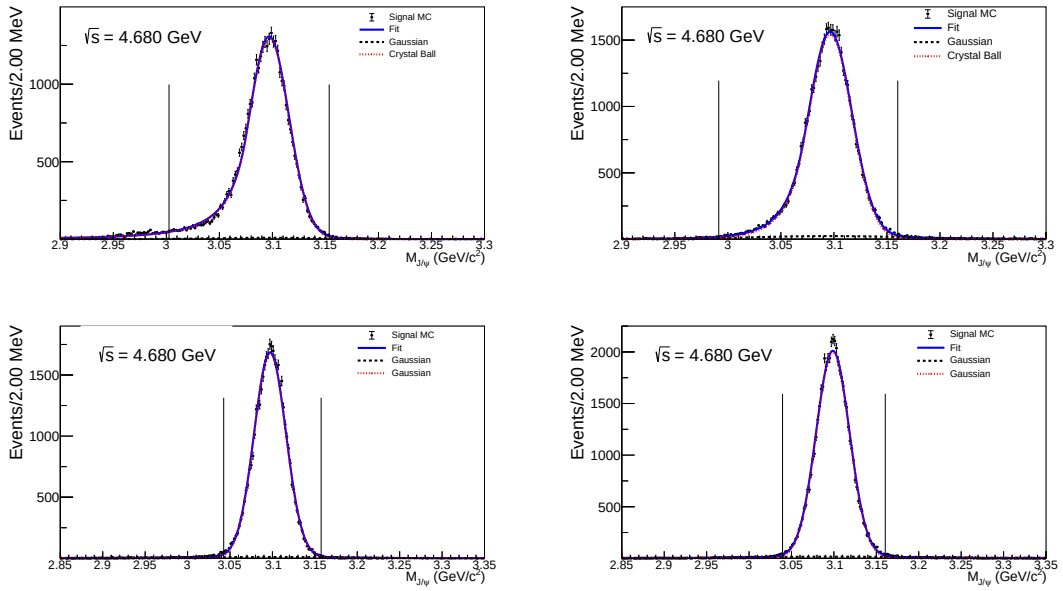

Figure 4.6: Fits to the invariant $\ell^+\ell^-$ masses to select the signal windows for the 4680 data set. The plots on the left represent the 5-track topologies, while the 6-track events are reported on the right. Top spectra refer to the $J/\psi \to e^+e^-$ decay, while the bottom two distributions are the J/ψ muonic transition. The solid blue lines refer to the fit, while the black dots with error bars are the data. The red dashed line represents the Crystal Ball (Gaussian) function, while the black dashed one is the Gaussian distribution. The selection windows are highlighted by the black solid vertical lines.

4.4.1 Background Rejection Efficiency

Starting from 1.3 billion inclusive MC events, less than 30000 survive the aforementioned selection criteria. The background events survival rate, estimated with the inclusive MC data set, oscillates between 9 to 28 parts per million among the different data sets. As summarized in Table 4.3, out of 28136 surviving inclusive MC events, more of the 90% of events are from the non-resonant $\pi^+\pi^-\psi(2S)$ signal and the multi-π transition, with the QED and the open charm processes removed from the sample.

4.5 Towards the Data Analysis

After applying the event selection criteria, one obtains the invariant $M(\pi^+\pi^-)$, $M(\pi^+\pi^-\ell^+\ell^-)$, and $M(\pi^+\psi(2S))$ distributions, shown in Fig. 4.9 for the 4.680 data

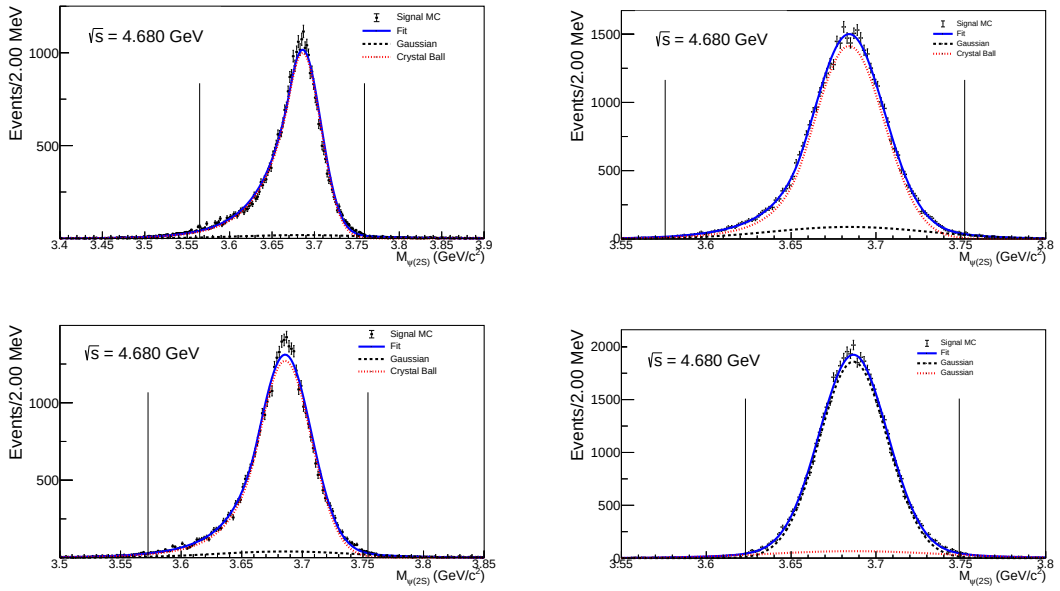

Figure 4.7: Fits to the invariant $\pi^+\pi^-\ell^+\ell^-$ masses to select the signal windows for the 4680 data set. The plots on the left represent the 5-track topologies, while the 6-track events are reported on the right. Top spectra refer to the $J/\psi \to e^+e^-$ decay, while the bottom two distributions are the J/ψ muonic transition. The solid blue lines refer to the fit, while the black dots with error bars are the data. The red dashed line represents the Crystal Ball (Gaussian) function, while the black dashed one is the Gaussian distribution. The selection windows are highlighted by the black solid vertical lines.

sample. The $\psi(2S)$ signal is visible.
With the distributions, one can proceed towards the three aforementioned objectives following three distinct lines of work, which will be treated in the next Chapters.

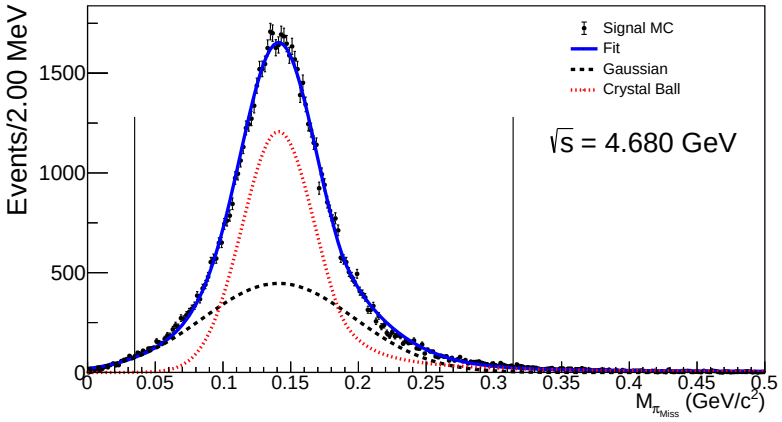

Figure 4.8: Fit to the $\pi\pi^+\pi^-\ell^+\ell^-$ recoil mass distribution to select the signal window for the 4680 data set. The solid blue lines refer to the fit, while the black dots with error bars are the data. The red dashed line represents the Crystal Ball function, while the black dashed one is the Gaussian distribution. The selection windows are highlighted by the black solid vertical lines.

Index (i)	Decay tree	N_{Evts}	$\sum_i^{\text{Tot}} N_{Evts}$
1	$e^+e^- \to \pi^+\pi^-\psi', \psi' \to \pi^+\pi^- J/\psi, J/\psi \to \mu^+\mu^-$	3389	3389
2	$e^+e^- \to \pi^+\pi^-\psi', \psi' \to \pi^+\pi^- J/\psi, J/\psi \to e^+e^-$	2983	6372
3	$e^+e^- \to \pi^+\pi^-\psi'\gamma^I, \psi' \to \pi^+\pi^- J/\psi, J/\psi \to \mu^+\mu^-$	2875	9247
4	$e^+e^- \to \pi^+\pi^-\psi', \psi' \to \pi^+\pi^- J/\psi, J/\psi \to \mu^+\mu^-$	2528	11775
5	$e^+e^- \to \pi^+\pi^-\psi'\gamma^I, \psi' \to \pi^+\pi^- J/\psi, J/\psi \to e^+e^-$	2499	14274
6	$e^+e^- \to \pi^+\pi^-\psi', \psi' \to \pi^+\pi^- J/\psi, J/\psi \to e^+e^-$	2313	16587
7	$e^+e^- \to \pi^+\pi^-\psi', \psi' \to \pi^+\pi^- J/\psi, J/\psi \to \mu^+\mu^-$	1346	17933
8	$e^+e^- \to \pi^+\pi^-\psi', \psi' \to \pi^+\pi^- J/\psi, J/\psi \to e^+e^-$	1249	19182
9	$e^+e^- \to \pi^+\pi^-\psi', \psi' \to \pi^+\pi^- J/\psi, J/\psi \to \mu^+\mu^-$	1037	20219
10	$e^+e^- \to \pi^+\pi^-\psi', \psi' \to \pi^+\pi^- J/\psi, J/\psi \to e^+e^-$	907	21126
11	$e^+e^- \to \pi^+\pi^-\psi', \psi' \to \pi^+\pi^- J/\psi, J/\psi \to \mu^+\mu^-$	307	21433
12	$e^+e^- \to \pi^+\pi^-\psi', \psi' \to \pi^+\pi^- J/\psi, J/\psi \to e^+e^-$	289	21722
13	$e^+e^- \to \pi^+\pi^-\psi', \psi' \to \pi^+\pi^- J/\psi, J/\psi \to \mu^+\mu^-$	276	21998
14	$e^+e^- \to \pi^+\pi^-\psi', \psi' \to \pi^+\pi^- J/\psi, J/\psi \to e^+e^-$	245	22243
15	$e^+e^- \to \pi^+\pi^-\psi', \psi' \to \pi^+\pi^- J/\psi, J/\psi \to \mu^+\mu^-$	240	22483
16	$e^+e^- \to \pi^+\pi^-\psi', \psi' \to \pi^+\pi^- J/\psi, J/\psi \to e^+e^-$	197	22680
17	$e^+e^- \to \pi^+\pi^-\psi', \psi' \to \pi^+\pi^- J/\psi, J/\psi \to \mu^+\mu^-$	188	22868
18	$e^+e^- \to \pi^+\pi^-\psi', \psi' \to \pi^+\pi^- J/\psi, J/\psi \to \mu^+\mu^-$	161	23029
19	$e^+e^- \to \pi^+\pi^-\psi', \psi' \to \pi^+\pi^- J/\psi, J/\psi \to e^+e^-$	156	23185
20	$e^+e^- \to \pi^+\pi^+\pi^+\pi^-\pi^-\pi^-$	144	23329
21	$e^+e^- \to \pi^+\pi^-\psi', \psi' \to \pi^+\pi^- J/\psi, J/\psi \to \mu^+\mu^-$	132	23461
22	$e^+e^- \to \pi^+\pi^-\psi', , \psi' \to \pi^+\pi^- J/\psi, J/\psi \to e^+e^-$	109	23570
23	$e^+e^- \to \pi^+\pi^-\psi', \psi' \to \pi^+\pi^- J/\psi, J/\psi \to \mu^+\mu^-$	104	23674
24	$e^+e^- \to \pi^+\pi^+\pi^+\pi^-\pi^-\pi^-\gamma^I$	103	23777
25	$e^+e^- \to \pi^+\pi^-\psi', \psi' \to \pi^+\pi^- J/\psi, J/\psi \to \mu^+\mu^-$	96	23873
26	...	...	...

Table 4.3: Topology table of the first 25 Inclusive MC decays. All of the decay which amounts to at least 100 events are listed. Only two decays channels appear, the $e^+e^- \to \pi^+\pi^-\psi(2S)$ and the $e^+e^- \to \pi^+\pi^-\pi^+\pi^-\pi^+\pi^-$. Despite the main decay tree being identical to many channels, J/ψ leptonic decays differ, as the pionic and muonic transitions, and the ISR photon (γ^I) can be present. For sake of brevity, the $\psi(2S)$ is dubbed ψ' and the list is not continued, but the subsequent decay trees contain variations of the two aforementioned topologies.

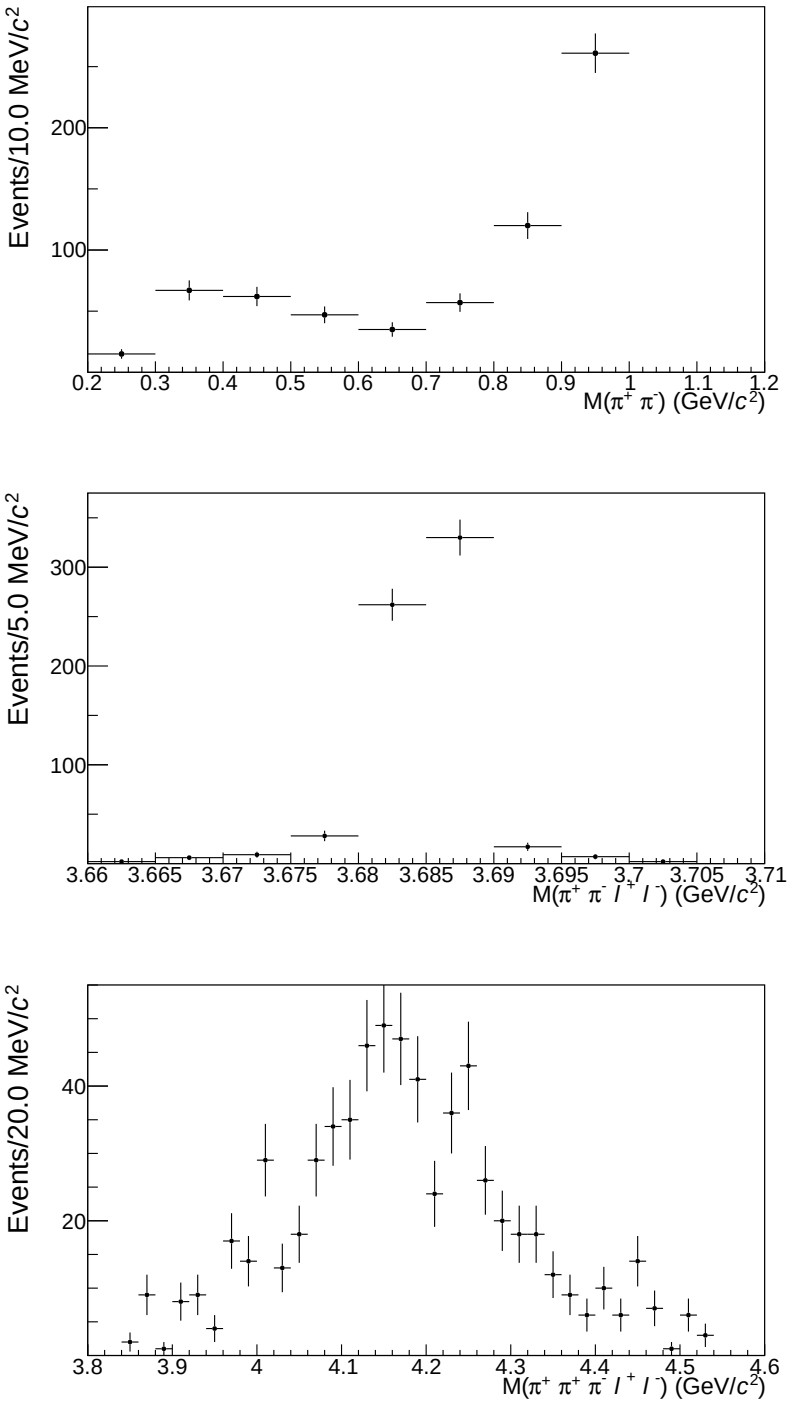

Figure 4.9: Invariant $M(\pi^+\pi^-)$, $M(\pi^+\pi^-\ell^+\ell^-)$, and $M(\pi^+\psi(2S))$ distributions for the 4.680 data sample.

Chapter 5

The $e^+e^- \to \pi^+\pi^-\psi(2S)$ Cross-section

Owing to the selection criteria described in the precedent Chapter, it is now possible to analyse the data and estimate the $e^+e^- \to \pi^+\pi^-\psi(2S)$ cross-section by studying the invariant $M(\pi^+\pi^-\ell^+\ell^-)$ distributions.
For each centre-of-mass energy, the Born cross-section ($\sigma_{\rm Born}$) of the $e^+e^- \to \pi^+\pi^-\psi(2S)$ process is estimated via the equation

$$\sigma_{\rm Born} = \frac{\sigma_{\rm Obs}}{(1+\delta)\frac{1}{|1-\Pi^2|}} = \frac{N_{\rm Obs}}{\mathcal{L}\ \epsilon\ \mathcal{B}\ (1+\delta)\frac{1}{|1-\Pi^2|}}, \tag{5.1}$$

where $\sigma_{\rm Obs}$ is the observed cross-section ($= N_{\rm Obs}/(\mathcal{L}\ \epsilon\ \mathcal{B})$), $N_{\rm Obs}$ is the observed signal yield, $\mathcal{L}$ is the integrated luminosity, $\mathcal{B}$ is the product of the branching fractions of the $\psi(2S) \to \pi^+\pi^- J/\psi$ and $J/\psi \to \ell^+\ell^-$ decays, estimated to be 4.00% from Ref. [1], ϵ is the signal detection efficiency estimated by the MC simulation and discussed in the subsection below, $(1+\delta)$ is the ISR correction factor and $\frac{1}{|1-\Pi^2|}$ is the vacuum polarisation factor from QED calculations [226] obtained from the CONEXC generator.

The cross-section for each centre-of-mass energy is obtained by performing a binned maximum likelihood fit to the $M(\pi^+\pi^-\ell^+\ell^-)$ spectrum. Based on MC, the signal shape is modelled with a sum of Gaussian and Crystal Ball functions; both contribute to symmetric smearing, while the latter also includes the low-energy tail. The background shape is a straight line. The signal function, shown in Fig. 5.1, is extracted from the signal MC sample.

5.1 Efficiency Studies

The signal detection efficiencies ϵ are estimated for each centre-of-mass energy, based on six signal MC samples of 300000 events each. The same samples are used to extrapolate the signal shape, which is modelled as a sum of Gaussian and Crystal Ball functions.

Since the cross-section σ_{Born} is used as input to estimate the vacuum polarisation factor $\frac{1}{|1-\Pi^2|}$ and the ISR correction $(1+\delta)$, an iterative procedure is performed based on the relation $\sigma_{\text{Born}} = \frac{\sigma_{\text{Obs}}}{\frac{1}{|1-\Pi^2|}(1+\delta)}$, where σ_{Obs} is the observed cross-section. The final σ_{Born} is obtained when the iteration converges. The convergence is defined when the $(1+\delta)\epsilon$ product is consistent with a previous iteration within 0.5% for each centre-of-mass energy. Following this criterion, 5 iterations are necessary.

The signal detection efficiencies and the signal shapes' parameters are updated for each iteration. The fifth column of Table 5.1 shows the final signal detection efficiencies for each centre-of-mass energy, while in Fig. 5.1 the functions used to model the signal are shown.

5.2 Fits and Cross-section results

The fits to the $M(\pi^+\pi^-\ell^+\ell^-)$ spectra used to estimate the $e^+e^- \to \pi^+\pi^-\psi(2S)$ process yields are shown in Fig. 5.2 for the six data samples, while the cross-section results and signal yields are summarised in Table 5.1.

A comparison shown in Fig. 5.3 validates the consistency of this thesis's cross-section results and the ones published in Ref. [95]. An enhancement in the $e^+e^- \to \pi^+\pi^-\psi(2S)$ cross-section can be seen around the 4.660 GeV, which was identified by Ref. [95] as the $Y(4660)$ state. Due to the difference in the uncertainties of the reported results in Fig. 5.3, it is appropriate to describe the procedural differences with respect to Ref. [95]. First, in Ref. [95], the four-constraint kinematic fit imposes the energy-momentum conservation is implemented only on the six-track topology, while, in the five-track events, a one-constraint kinematic fit constrains the missing mass to the pion mass; to both the topologies an additional one-constraint is imposed on the J/ψ mass. Hence, with respect to this thesis procedure, in Ref. [95]

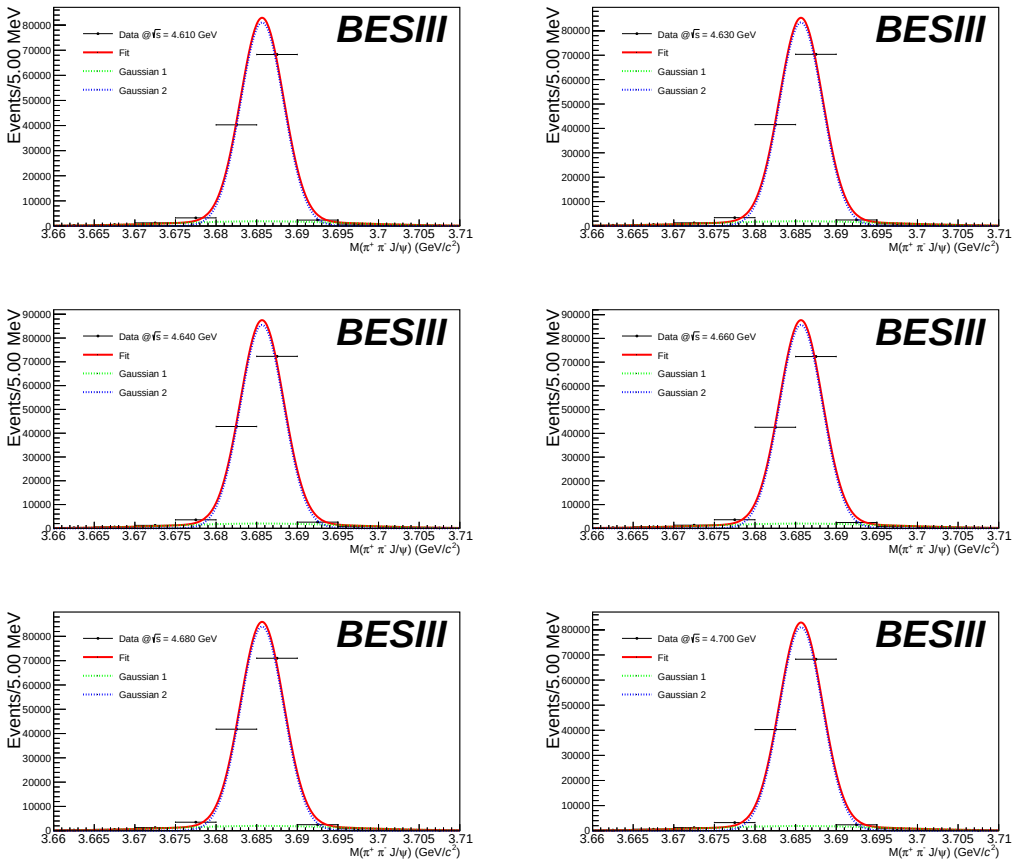

Figure 5.1: Fits to the signal MC $M(\pi^+\pi^-\ell^+\ell^-)$ spectra. The solid red line refers to the fit, while the black dots with error bars are the data. The blue dashed line represents the Crystal Ball function, while the green dashed one is the Gaussian distribution.

one has a five-constraint (two-constraint) kinematic fit in the six-track (five-track) topology. In addition to this, the signal description is performed differently, this thesis uses a MC motivated double Gaussian, while a signal MC shape is used in Ref. [95]. Despite affecting both the efficiencies and final statistical uncertainties, these procedural differences do not invalidate the results as reported in Fig. 5.3.
It is worth to mention that Fig. 5.3 refers only to the charged $\psi(2S)$ decays, but Ref. [95] also reconstructs the neutral $\psi(2S)$ to J/ψ transitions, involving π^0 and η mesons, as well as the cascade decay $\psi(2S) \to \gamma\chi_{cJ} \to \gamma\gamma J/\psi$.

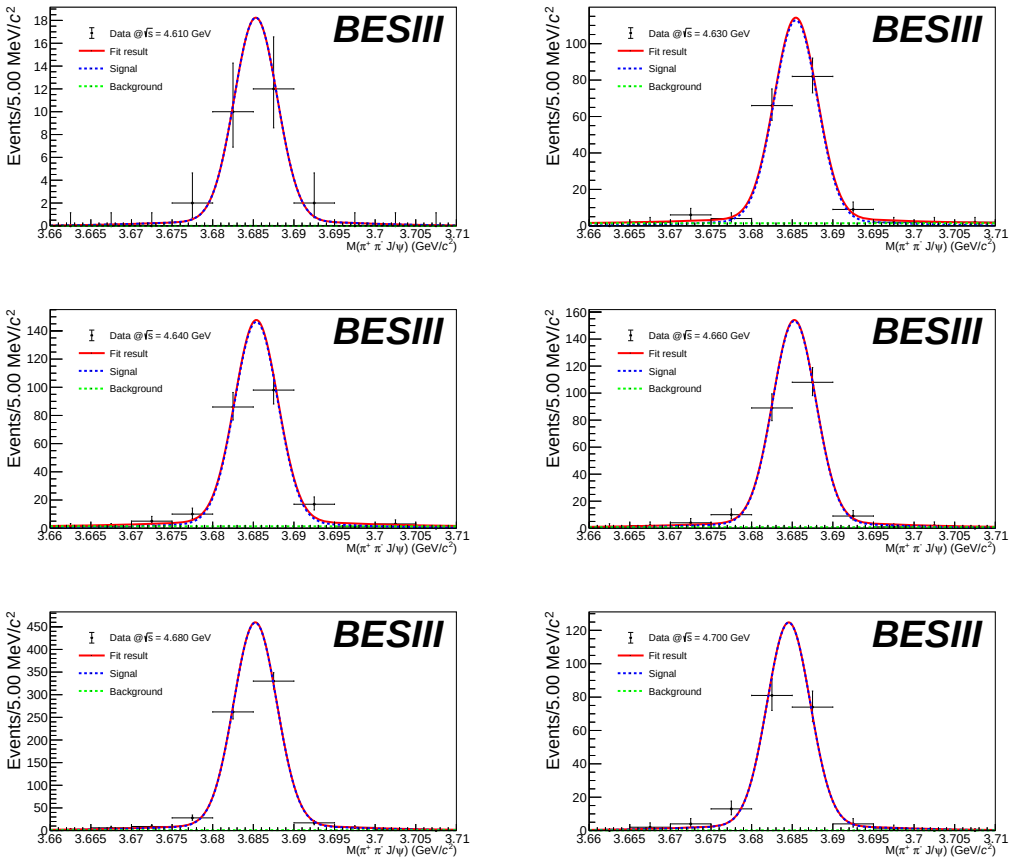

Figure 5.2: Fits to the $M(\pi^+\pi^-\ell^+\ell^-)$ spectra. The solid red line refers to the fit, while the black dots with error bars are the data. The blue dashed line represents the $\pi^+\pi^-\ell^+\ell^-$ signal component, while the green dashed one is the combinatorial and multi-pion background. The signal is modelled by a sum of Gaussian and Crystal Ball functions. The background shape is a straight line.

E_{CoM} (MeV)	$\mathcal{L}$ (pb^{-1})	N_{Obs}	ϵ (%)	σ_{Observed} (pb)	$(1+\delta)$	$\frac{1}{\lvert 1-\Pi\rvert^2}$	σ_{Born} (pb)
4611.86	103.83	24^{+2}_{-5}	38.90 ± 0.11	$16.28^{+0.14}_{-2.98}$	0.898	1.05453	$17.19^{+0.15}_{-3.14}$
4628.00	521.52	155^{+18}_{-18}	40.45 ± 0.12	$19.46^{+1.69}_{-1.57}$	0.877	1.05444	$21.04^{+1.83}_{-1.70}$
4640.91	552.41	193^{+27}_{-29}	41.59 ± 0.12	$23.20^{+1.44}_{-1.66}$	0.854	1.05442	$25.77^{+1.60}_{-1.85}$
4661.24	529.63	202^{+20}_{-20}	41.54 ± 0.12	$25.15^{+0.80}_{-1.72}$	0.867	1.05441	$27.52^{+0.88}_{-1.89}$
4681.92	1669.31	563^{+46}_{-46}	40.72 ± 0.12	$24.60^{+0.34}_{-1.02}$	0.897	1.05448	$26.00^{+0.36}_{-1.07}$
4698.82	536.45	162^{+16}_{-16}	39.16 ± 0.11	$21.59^{+1.58}_{-1.70}$	0.949	1.05453	$21.57^{+1.58}_{-1.70}$

Table 5.1: $e^+e^- \to \pi^+\pi^-\psi(2S)$ Born cross-section for each energy point. The signal yields (N_{Obs}) and the efficiencies (ϵ) are reported too for each energy point. For sake of completion, the observed cross-section (σ_{Observed}) is reported too. The uncertainties on the signal yields and the cross-sections are statistical only. The table shows the ISR correction $(1+\delta)$, the vacuum polarisation factor $\frac{1}{\lvert 1-\Pi\rvert^2}$, and the integrated luminosity $\mathcal{L}$ as well. The uncertainties on E_{CoM} and $\mathcal{L}$ are reported in Table 4.1.

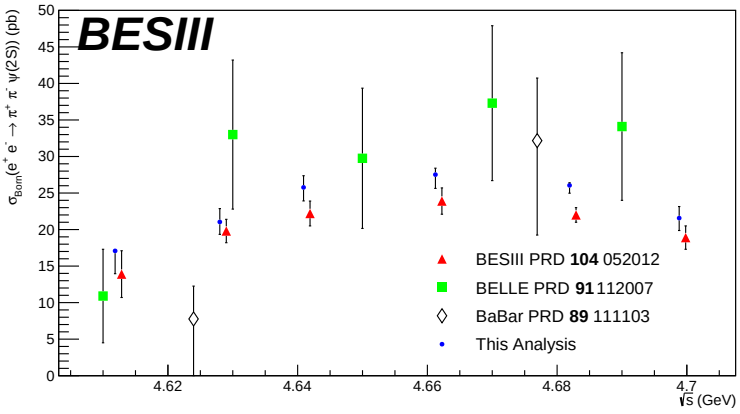

Figure 5.3: Born cross-section of the $e^+e^- \to \pi^+\pi^-\psi(2S)$ process. The blue dots with error bars refer to this thesis' results, while the red triangles with error bars refer to the charged channel Born cross-section from Ref. [95]. In the graphic, the results from BELLE [111] and BaBar [110] are reported too, as green squares and white diamonds, respectively. The comparison validates the consistency of the two results. Data points are slightly shifted along the x-axis for sake of readability.

Chapter 6

Study of the Dalitz Plots of the $e^+e^- \to \pi^+\pi^-\psi(2S)$ Reaction

To better understand the contribution of the $Y(4660)$ state to the $e^+e^- \to \pi^+\pi^-\psi(2S)$ channel and motivated by the results of Ref. [95], stating that a rapid check with a simplified Partial Wave Analysis performed on the data sets highlighted $f_0(500)$ and $f_0(980)$ contributions, the $M^2(\pi^+\pi^-)$ vs $M^2(\pi^+\psi(2S))$ and the $M^2(\pi^-\psi(2S))$vs $M^2(\pi^+\psi(2S))$ Dalitz plots are analysed. For this study, the six data samples are merged together to have more statistical significance. The signal MC data set is a weighted sum of the single data samples, where the weights are the product of the integrated luminosity $\mathcal{L}$ and the production cross-section of the $e^+e^- \to \pi^+\pi^-\psi(2S)$ process at each centre-of-mass energy. The study of these plots, reported in Fig. 6.1, points towards a clear $f_0(980)$ contribution. The inclusive MC simulations (top plots of Fig. 6.1) show a flat behaviour for both the $M^2(\pi^+\pi^-)$ vs $M^2(\pi^+\psi(2S))$ distribution and the $M^2(\pi^-\psi(2S))$vs $M^2(\pi^+\psi(2S))$ one. On the contrary, a heap in the $M^2(\pi^+\pi^-)$ vs $M^2(\pi^+\psi(2S))$ data (central left plot of Fig. 6.1) at $0.8 < M^2(\pi^+\pi^-) < 1.0$ GeV$^2/c^4$ can be seen and related to the one in the $f_0(980)$ signal MC sample (bottom left plot of Fig. 6.1). Moreover, the $M^2(\pi^-\psi(2S))$vs $M^2(\pi^+\psi(2S))$ Dalitz plots shows distinct band which is reproduced by the $f_0(980)$ signal MC sample.

Hence, with these conclusions and with the intention to probe the $f_0(980)\psi(2S)$ molecule interpretation of the $Y(4660)$ state [116], the cross-section of the $e^+e^- \to f_0(980)\psi(2S)$ transition is studied.

Similarly to what it is done for the $e^+e^- \to \pi^+\pi^-\psi(2S)$ process, for each

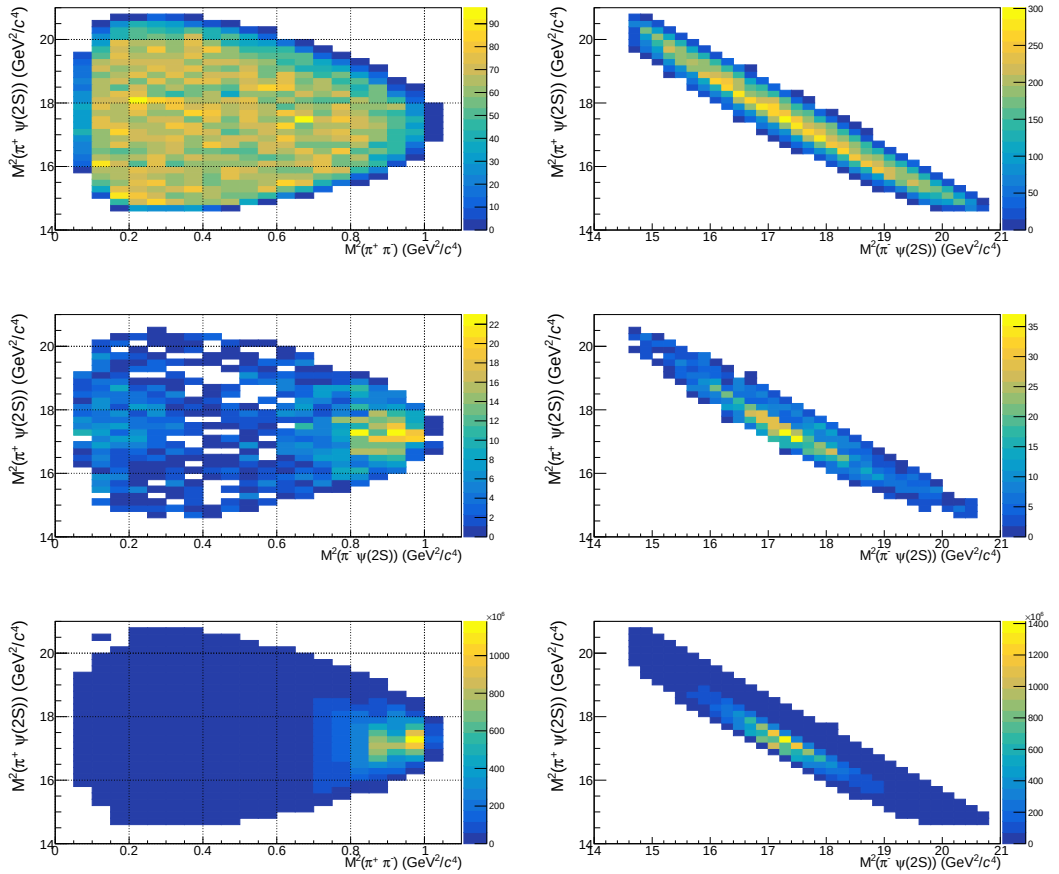

Figure 6.1: Dalitz plots of the $e^+e^- \to \pi^+\pi^-\psi(2S)$ process compared to those of the $e^+e^- \to f_0(980)\psi(2S)$ sub-channel. The two plots at the top are from inclusive MC, the middle ones are the real data, and the $f_0(980)$ simulation is reported at the bottom. A clear heap in the data $M^2(\pi^+\pi^-)$ vs $M^2(\pi^+\psi(2S))$ at $0.8 < M^2(\pi^+\pi^-) < 1.0$ GeV$^2/c^4$ can be confronted to the one in the $f_0(980)$ signal MC sample. Furthermore, the $M^2(\pi^-\psi(2S))$vs $M^2(\pi^+\psi(2S))$ Dalitz plots shows distinct band which is reproduced by the $f_0(980)$ signal MC sample. The inclusive MC simulations, instead, report flat distributions for both the $M^2(\pi^+\pi^-)$ vs $M^2(\pi^+\psi(2S))$ and the $M^2(\pi^-\psi(2S))$vs $M^2(\pi^+\psi(2S))$ spectra.

centre-of-mass energy, the product of the $f_0(980) \to \pi^+\pi^-$ branching fraction[1] ($\mathcal{B}(f_0(980) \to \pi^+\pi^-)$) and the Born cross-section of the $e^+e^- \to f_0(980)\psi(2S)$

[1]Ref. [1] does not provide any value. So, instead of making additional assumptions, the Born cross-section is left unnormalized.

transition is estimated via the equation

$$\mathcal{B}(f_0(980) \to \pi^+\pi^-) \times \sigma_{\text{Born}}^{f_0(980)} = \mathcal{B}(f_0(980) \to \pi^+\pi^-) \times \left(\frac{N_{\text{Obs}}^{f_0(980)}}{\mathcal{L}(1+\delta)\frac{1}{|1-\Pi^2|}\epsilon^{f_0(980)}\mathcal{B}} \right), \tag{6.1}$$

where $N_{\text{Obs}}^{f_0(980)}$ is the observed $f_0(980)$ yield, $\mathcal{L}$ is the integrated luminosity, $(1+\delta)$ is the ISR correction factor and $\frac{1}{|1-\Pi^2|}$ is the vacuum polarisation factor from QED calculations [226] obtained from the CONEXC generator, $\mathcal{B}$ is the product of the branching fractions of the $\psi(2S) \to \pi^+\pi^- J/\psi$ and $J/\psi \to \ell^+\ell^-$ decays, estimated to be 4.00% from Ref. [1], and $\epsilon^{f_0(980)}$ is the $e^+e^- \to f_0(980)\psi(2S)$ transition detection efficiency estimated by the MC simulation and discussed in the subsection below.

The cross-section for each centre-of-mass energy is obtained by performing a binned maximum likelihood fit to the $M(\pi^+\pi^-)$ spectrum.
For each centre-of-mass energy, the $f_0(980)$ signal shape is modelled with a Flatté function [230], the parameters of which are fixed to the ones obtained by Ref. [231], multiplied to a threshold function simulating the closure of the phase space. Both the Flatté and the threshold functions are spread via convolution with a Gaussian distribution with no bias and a width equal to the bin width and the bin width divided by $\sqrt{12}$, respectively. On the other hand, the $f_0(500)$ contribution is estimated using a MC signal shape, extrapolated from a $f_0(500)$ signal MC sample of 300000 events.

6.1 Efficiency Studies

As it is done for the $e^+e^- \to \pi^+\pi^-\psi(2S)$ channel, the $f_0(980)$ detection efficiencies $\epsilon^{f_0(980)}$ are estimated for each centre-of-mass energy, based on six signal MC samples of 300000 events each.

Also in this sub-cannel, the cross-section $\sigma_{\text{Born}}^{f_0(980)}$ is used as input to estimate the vacuum polarisation factor $\frac{1}{|1-\Pi^2|}$ and the ISR correction $(1+\delta)$ and an iterative procedure is performed. The final $\sigma_{\text{Born}}^{f_0(980)}$ is obtained when the iteration converges. Due to the large statistical error on the cross-section values, the convergence is deemed reached when $(1+\delta)$ is consistent with a previous iteration within 0.5% for

each centre-of-mass energy. Following this criterion, 5 iterations are necessary.

For each iteration, the signal detection efficiencies are updated. The third column of Table 6.1 shows the final signal detection efficiencies for each centre-of-mass energy.

6.2 Fits and Cross-section results

The fits to the $M(\pi^+\pi^-)$ distributions used to estimate the $e^+e^- \to f_0(980)\psi(2S)$ process yields are shown in Fig. 6.2 for the six data samples, while the cross-section results and signal yields are summarised in Table 6.1.

E_{CoM} (MeV)	$N_{\rm Obs}^{f_0(980)}$	$\epsilon^{f_0(980)}$ (%)	$(1+\delta)$	$\frac{1}{\lvert 1-\Pi\rvert^2}$	$\sigma \times \mathcal{B}$ (pb)
4611.86	14 ± 5	49.57 ± 0.13	0.690	1.05453	9.46 ± 3.38
4628.00	125 ± 22	48.99 ± 0.13	0.686	1.05444	17.25 ± 3.04
4640.91	149 ± 21	48.30 ± 0.13	0.757	1.05442	17.83 ± 2.52
4661.24	131 ± 15	45.76 ± 0.12	0.823	1.05441	15.74 ± 1.81
4681.92	424 ± 32	44.86 ± 0.12	0.809	1.05448	16.91 ± 1.29
4698.82	115 ± 16	44.83 ± 0.12	0.797	1.05453	14.49 ± 2.02

Table 6.1: $e^+e^- \to f_0(980)\psi(2S)$ Born cross-section multiplied by the $f_0(980) \to \pi^+\pi^-$ branching fraction, here called $\sigma \times \mathcal{B}$ for brevity sake, for each energy point. The signal yields ($N_{\rm Obs}^{f_0(980)}$) and the efficiencies ($\epsilon^{f_0(980)}$) are reported too for each data sample. The uncertainties on the signal yields and the Born cross-section are statistical only. The table shows the ISR correction $(1+\delta)$ and the vacuum polarisation factor $\frac{1}{\lvert 1-\Pi\rvert^2}$ as well. The uncertainties on E_{CoM} and $\mathcal{L}$ are reported in Table 4.1.

Fig. 6.3 shows the cross-section results. No particular structures can be recognised as the statistical uncertainty prevents any conclusion to be possible. This result represents the first measurement of this final state.

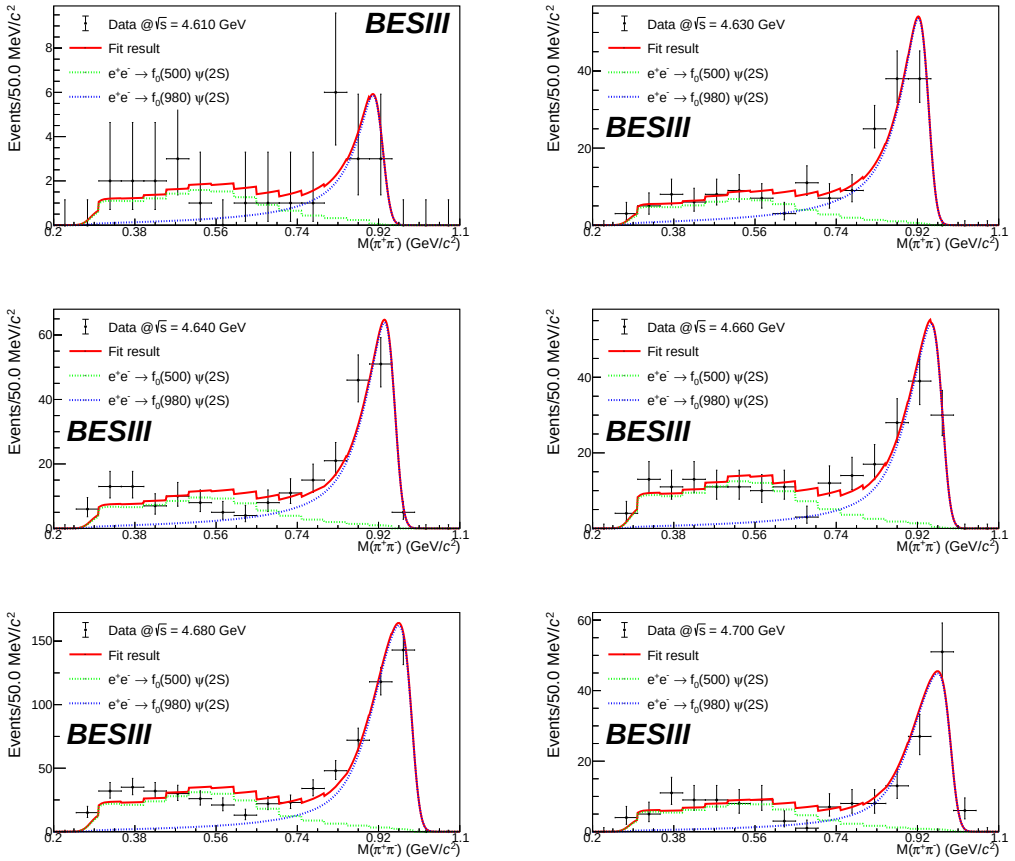

Figure 6.2: to the $M(\pi^+\pi^-)$ spectra to estimate the $e^+e^- \to f_0(980)\psi(2S)$ process yields. The solid red line refers to the fit, while the black dots with error bars are the data. The blue dashed line represents the $f_0(980)$ signal component, while the green dashed one is the $f_0(500)$ contribution. The $f_0(980)$ signal is modelled by a smeared Flatté function multiplied by a threshold function. The $f_0(500)$ background shape is described by a signal MC-shape. Insets at the bottom of each figure show the $f_0(500)$-subtracted data with the $f_0(980)$ signal overlaid.

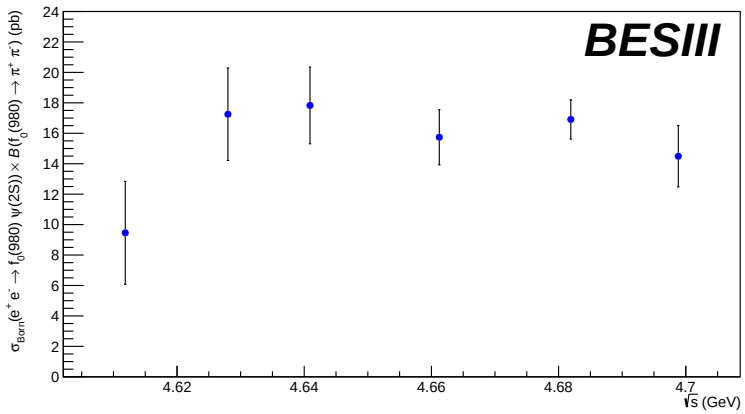

Figure 6.3: Born cross-section of the $e^+e^- \to f_0(980)\psi(2S)$ sub-process multiplied by the $f_0(980) \to \pi^+\pi^-$ branching fraction. No particular structures can be recognised and the statistical uncertainty prevents any conclusion.

Chapter 7

Analysis of the $\pi^{\pm}\psi(2S)$ Invariant Mass

Finally, to search for the $Z_c(4430)^{\pm}$ exotic state, the invariant mass $M(\pi^{\pm}\psi(2S))$ is analysed by summing all of the six data sets together. Following the same reasoning for the $e^+e^- \to f_0(980)\psi(2S)$ cross-section, the $M(\pi^{\pm}\psi(2S))$ spectrum is modelled considering only $f_0(500)$ and $f_0(980)$ contributions, in addition to a possible $Z_c(4430)^{\pm}$ resonance. The distributions are modelled using a MC signal shape for each of them. The signal shape is a weighted sum of the single centre-of-mass energies shapes, where the weights are the product of the integrated luminosity $\mathcal{L}$ and the production cross-section of the $e^+e^- \to \pi^+\pi^-\psi(2S)$ process. The $f_0(500)/f_0(980)$ fraction, the $Z_c(4430)^{\pm}$ signal and f_0 background yields are left floating.

7.1 Efficiency Studies

The $Z_c(4430)^{\pm}$ detection efficiencies are estimated for each centre-of-mass energy, based on six signal MC samples of 300000 events each. In this case, though, the MC samples are generated with a flat cross-section to not make any specific assumption, without ISR or vacuum polarisation corrections which depend on the $Z_c(4430)^{\pm}$ cross-section production. The average detection efficiency for the summed data set, $\epsilon^{Z_c(4430)} = (54.24 \pm 0.13)\%$, is calculated by performing a weighted average of the single centre-of-mass energies efficiencies, where the weights are the product of the integrated luminosity $\mathcal{L}$ and the production cross-section of the $e^+e^- \to \pi^+\pi^-\psi(2S)$ process.

7.2 Resolution Studies

For each centre-of-mass energy, the detector resolution contribution to the $Z_c(4430)^{\pm}$ state is obtained from a signal MC dataset of 300000 events where the $Z_c(4430)^{\pm}$ width is set to 0. As shown in Fig. 7.1, the resolution contributions are estimated to be within 2 MeV/c^2 and can be neglected as the $Z_c(4430)^{\pm}$ resonance width is estimated to be ∼200 MeV [1].

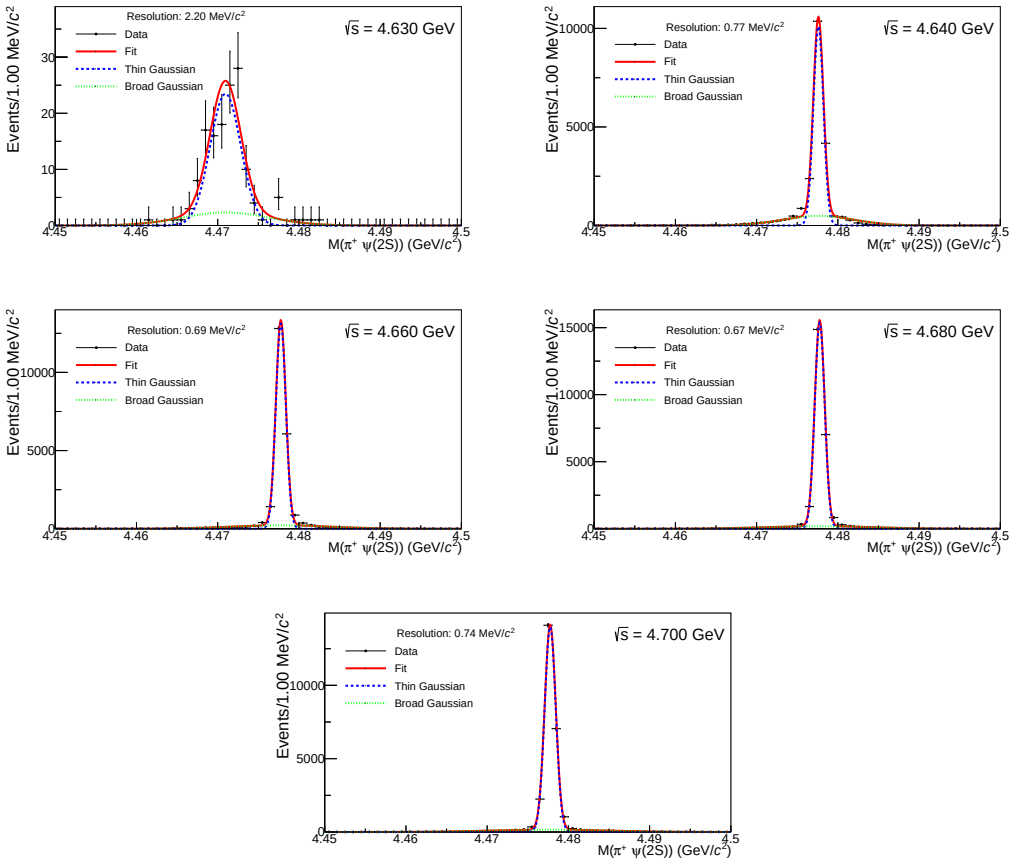

Figure 7.1: Fits to the signal MC $M(\pi^{+}\psi(2S))$ spectra for the resolution estimation. The solid red line refers to the fit, while the black dots with error bars are the data. The blue and the green dashed lines represent the two Gaussian components of the fit function Ball function. No 4610 data sample is shown as the phase space would not allow producing a $Z_c(4430)^{\pm}$ with 0 width at that energy point.

7.3 Fit and Upper Limit

Finally, a fit is performed on the $M(\pi^{\pm}\psi(2S))$ distributions combined data set with a total integrated luminosity of $\sim$5 fb^{-1}. The f_0 distributions are modelled using a MC signal shape for each of them. The signal shape, reported in Fig. 7.2, is a weighted sum of the single centre-of-mass energies shapes, and the weights are the product of the integrated luminosity $\mathcal{L}$ and the production cross-section of the $e^+e^- \to \pi^+\pi^-\psi(2S)$ process. This signal model takes also into account the reflection of the $Z_c(4430)^{\pm}$ at low mass. The $f_0(500)/f_0(980)$ fraction, the $Z_c(4430)^{\pm}$ signal and f_0 background yields are left floating.

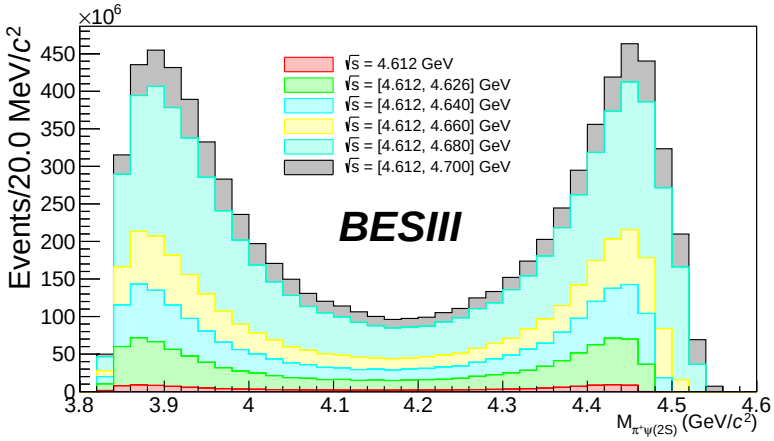

Figure 7.2: Signal MC shape of the $M(\pi^+\psi(2S))$ spectrum. The signal shape is a weighted sum of the single centre-of-mass energies shapes, and the weights are the product of the integrated luminosity $\mathcal{L}$ and the production cross-section of the $e^+e^- \to \pi^+\pi^-\psi(2S)$ process. The model takes also into account the reflection of the $Z_c(4430)^+$ at low mass, as it can be seen from the peak at 3.88 GeV/c^2. The figure reports the stacked weighted sum of the single centre-of-mass energies shapes, the final shape is represented by the grey-filled histogram.

Fig. 7.3 shows the result of the fit, where no evident signal is found (the number of $Z_c(4430)^{\pm}$ events is estimated to be 0 ± 4). A Bayesian upper limit (U.L.) with a uniform prior is defined at a 90% confidence level (C.L.). The U.L. on the charged $Z_c(4430)$ expected number of events is found to be 16 leading to a production ratio $R = \sigma(e^+e^- \to \pi^{\pm}Z_c(4430)^{\mp} \to \pi^+\pi^-\psi(2S))/\sigma(e^+e^- \to \pi^+\pi^-\psi(2S))$ less than 1.0% at 90% C.L.. Comparing this result with that of Ref. [123], which was used as the initial motivation for this search, one sees that the $Z_c(4430)^{\pm}$ hadron production

in the $e^+e^- \to \pi^+\pi^-\psi(2S)$ channel is suppressed by at least 20 times with respect of that of the $Z_c(3900)^{\pm}$ state in the $e^+e^- \to \pi^+\pi^- J/\psi$ transition.

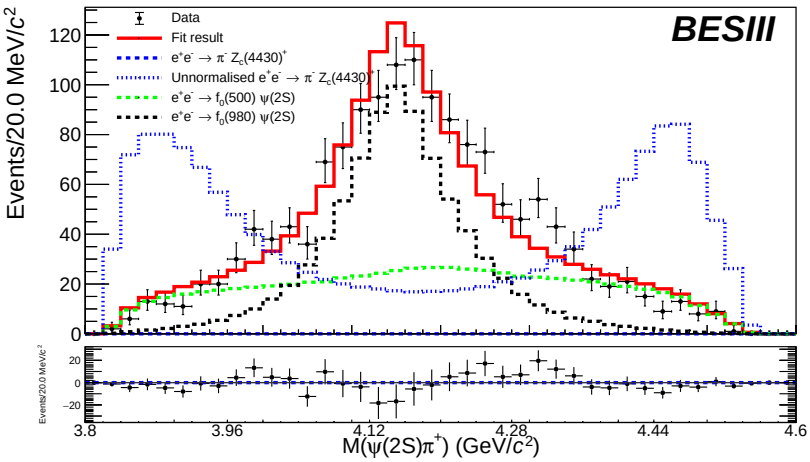

Figure 7.3: Fit to the $M(\pi^{\pm}\psi(2S))$ spectrum. The solid red line refers to the fit, while the black dots with error bars are the data. The blue dashed line represents the $Z_c(4430)^+$ signal component, while the black and green dashed ones are the $f_0(980)$ and the $f_0(500)$ backgrounds, respectively. Signal MC-shapes are used to model the f_0 contributions and the $Z_c(4430)^+$ component; the $f_0(500)/f_0(980)$ fraction, the $Z_c(4430)^+$ signal and f_0 background yields are left floating. The blue dashed line represents the unnormalised $Z_c(4430)^+$ signal shape component. The inset at the bottom shows the background-subtracted data with the normalised signal overlaid.

Chapter 8

Systematic Uncertainties and Outlook

Several sources of systematic uncertainties are considered in the estimation of the Born cross-sections of the $e^+e^- \to \pi^+\pi^-\psi(2S)$ and $e^+e^- \to f_0(980)\psi(2S)$ processes. These uncertainties come from the integrated luminosity, the vacuum polarisation, the ISR radiative corrections, the tracking efficiency, and residual sources. The uncertainty of the integrated luminosity is estimated to be 1% as obtained by analysing the large-angle Bhabha scattering events [95, 227]. The uncertainty of the vacuum polarisation factor is taken as 0.5% from Ref. [232]. As already mentioned, the ISR radiative corrections depend on the input line shape of the cross-section. Hence, an iterative process is employed. The difference in the $(1 + \delta)$ values between the last two iterations is taken as systematic uncertainty related to the ISR correction. The tracking efficiency uncertainty is 1.0% per lepton or pion track [123]. Therefore, the two leptons in the final state result contribute to a 2.0% of uncertainty, while the pions contribute on average (5-track and 6-track topologies) to a 3.5%. Other sources, such as lepton separation, trigger efficiency, and FSR, are estimated to be 1.0% [95]. The intermediate states branching fractions uncertainties are taken from the PDG [1]. Other sources, coming from the J/ψ, $\psi(2S)$, and π_{Miss} mass veto windows and from the kinematic fits, are considered as well but found negligible. The contributions from each source are shown in Table 8.1 and Table 8.2 for the $\pi^+\pi^-\psi(2S)$ cross-section and the $f_0(980)\psi(2S)$ cross-section, respectively. For each measurement, the total systematic uncertainty corresponds to a quadrature sum of all individual sources, which are discussed in detail next.

Finally, for sake of completion, Table 8.3 shows the results of the Born $\pi^+\pi^-\psi(2S)$

Source	4.610 (pb)	4.630 (pb)	4.640 (pb)	4.660 (pb)	4.680 (pb)	4.700 (pb)
Luminosity	0.17	0.21	0.26	0.28	0.26	0.22
Vacuum polarisation	0.09	0.11	0.13	0.14	0.13	0.11
ISR corrections	0.07	0.07	0.00	0.03	0.03	0.02
Tracking efficiency	0.60	0.74	0.90	0.96	0.91	0.75
Intermediate states branching fractions	0.16	0.20	0.25	0.26	0.25	0.21
Other sources	0.17	0.21	0.26	0.28	0.26	0.22
Total systematic uncertainty	0.68	0.83	1.01	1.08	1.02	0.85

Table 8.1: Summary of the systematic uncertainties on the Born $\pi^+\pi^-\psi(2S)$ cross-section for each centre-of-mass energy. For each measurement, the total systematic uncertainty corresponds to a quadrature sum of all individual contributions.

cross-section and of the $e^+e^- \to f_0(980)\psi(2S)$ Born cross-section multiplied by the $f_0(980) \to \pi^+\pi^-$ branching fraction for each centre-of-mass energy with both the statistical and systematic uncertainties reported. From Table 8.3, it can be appreciated that the measurements are statistically limited and that our knowledge will profit from more data collected in this energy region.

The systematic sources on the U.L. of the $Z_c(4430)^\pm$ events number come from the fitting procedure and choices, such as the binning, the signal range, and the parametrisation of the signal and background. In the U.L. of the production ratio $R = \sigma(e^+e^- \to \pi^\pm Z_c(4430)^\mp \to \pi^+\pi^-\psi(2S))/\sigma(e^+e^- \to \pi^+\pi^-\psi(2S))$ estimation, additional systematic uncertainties come from the number of $e^+e^- \to \pi^+\pi^-\psi(2S)$ events and its relative efficiency. Technically, the $e^+e^- \to \pi^\pm Z_c(4430)^\mp \to \pi^+\pi^-\psi(2S)$ cross-section is also affected by the same systematic sources as the Born $\pi^+\pi^-\psi(2S)$ cross-section, but, in the production ratio R, they cancel out. Moreover, the parametrisation of the signal and background is left to be studied after PWA-motivated signal MC data sets are produced and analysed (see Sec. 8.1). Hence,

Source	4.610 (pb)	4.630 (pb)	4.640 (pb)	4.660 (pb)	4.680 (pb)	4.700 (pb)
Luminosity	0.09	0.17	0.18	0.16	0.17	0.14
Vacuum polarisation	0.05	0.09	0.09	0.08	0.08	0.07
ISR corrections	0.00	0.00	0.00	0.01	0.01	0.00
Tracking efficiency	0.33	0.60	0.62	0.55	0.59	0.51
Intermediate states branching fractions	0.09	0.16	0.17	0.15	0.16	0.14
Other sources	0.09	0.17	0.18	0.16	0.17	0.14
Total systematic uncertainty	0.37	0.68	0.70	0.62	0.67	0.57

Table 8.2: Summary of the systematic uncertainties on the $e^+e^- \to f_0(980)\psi(2S)$ Born cross-section multiplied by the $f_0(980) \to \pi^+\pi^-$ branching fraction for each centre-of-mass energy. For each measurement, the total systematic uncertainty corresponds to a quadrature sum of all individual contributions.

Sample	$\sigma_{\rm Born}(\pi^+\pi^-\psi(2S))$ (pb)	$\sigma_{\rm Born}(f_0(980)\psi(2S))\times$ $\mathcal{B}(f_0(980) \to \pi^+\pi^-)$ (pb)
4.610	$17.19^{+0.15}_{-3.14} \pm 0.68$	$6.88^{+2.46}_{-2.46} \pm 0.37$
4.630	$21.04^{+1.83}_{-1.70} \pm 0.83$	$12.48^{+2.20}_{-2.20} \pm 0.68$
4.640	$25.77^{+1.60}_{-1.85} \pm 1.01$	$14.24^{+2.01}_{-2.01} \pm 0.70$
4.660	$27.52^{+0.88}_{-1.89} \pm 1.08$	$13.66^{+1.56}_{-1.56} \pm 0.62$
4.680	$26.00^{+0.36}_{-1.07} \pm 1.02$	$14.48^{+1.09}_{-1.09} \pm 0.67$
4.700	$21.57^{+1.58}_{-1.70} \pm 0.85$	$12.18^{+1.69}_{-1.69} \pm 0.57$

Table 8.3: Results of the Born $e^+e^- \to \pi^+\pi^-\psi(2S)$ cross-section and the $e^+e^- \to f_0(980)\psi(2S)$ Born cross-section multiplied by the $f_0(980) \to \pi^+\pi^-$ branching fraction. The first uncertainties are statistical, while the second ones are systematic.

the U.L. on the number of $Z_c(4430)^\pm$ events is studied as a function of the binning

and the signal range. These two sources of systematic uncertainties are found to be negligible. Finally, considering the uncertainties coming from the number of the $e^+e^- \to \pi^+\pi^-\psi(2S)$ events and the efficiencies of the two channels, the production ratio R is found to be less than 1.1% at 90% C.L..

8.1 Outlook

The results found in this analysis confirm previous results and for the first time highlight the f_0 contributions to the $\pi^+\pi^-\psi(2S)$ cross-section. Also, the first U.L. on the production of the charged $Z_c(4430)$ hadron is found, which can be used as insight for further theoretical studies on the nature of $Z_c(4430)^{\pm}$ state. Despite this, some work is still needed to finalise the analysis. An analytical shape has to be employed to describe the $f_0(500)$ contribution to the $M(\pi^+\pi^-)$ spectra, to better estimate the $e^+e^- \to f_0(980)\psi(2S)$ cross-section. For the charged $Z_c(4430)$ studies, a better model can be chosen following a PWA-motivated generated signal MC sample. In general, a possible interference between the two f_0 states needs to be accounted for, and the case with and without interference must be taken as a systematic source.

Summary and Conclusions

As the first two Chapters of this thesis discussed, Quantum ChromoDynamics and the Quark Model are still the blueprints to understanding strong interaction and its bound states. Beyond the so-called standard baryons and mesons, a new family of states, allowed by both Gell-Mann and Zweig's first papers, is being discovered. Indeed, a large number of XYZ states have been reported from different collaborations, the properties of which are at odds with the Quark Model, suggesting new kinds of hadrons.
Many of these XYZ structures can be easily identified as exotics, but many others still miss a definitive label. The specific nature of the unambiguous exotic is still a matter of experimental investigation and theoretical debate. The observation of a specific feature can discriminate among the several models proposed. As such, more data are needed to understand and study the XYZ sector. With the beginning of the Belle-II experiment data taking, the data from Run-3 and LHC-HL at the LHCb detector, with the newest upgrades for the BECPII collider and the BESIII detector, and with the future facilities, like PANDA at GSI, new studies are to be expected.

The BESIII collaboration plays a leading role in the search for these exotic states, owing to its luminosity, leptonic collider, and detector performances.

This thesis aims to help in understanding the XYZ sector. Studying the $e^+e^- \to \pi^+\pi^-\psi(2S)$ process at centre-of-mass energies ranging from 4.612 GeV to 4.698 GeV allows both to probe the $Y(4660)$ nature and to search for the $Z_c(4430)$ state. Indeed, up to now, only the Belle and LHCb collaborations saw the $Z_c(4430)$ state and exclusively in B decays. On the other hand, measuring the $e^+e^- \to f_0(980)\psi(2S)$ component percentage to the whole $e^+e^- \to \pi^+\pi^-\psi(2S)$ process might give some insights over the $f_0(980)c\bar{c}$ molecule interpretation.

Using six data samples with a total integrated luminosity of $\sim$5 fb^{-1} collected by the BESIII detector, the $e^+e^- \to \pi^+\pi^-\psi(2S)$ process is studied at centre-of-mass energies ranging from 4.6121 GeV to 4.6984 GeV. The measured cross-section of the $e^+e^- \to \pi^+\pi^-\psi(2S)$ reaction is consistent with the results of Ref. [95] and an enhancement in the $e^+e^- \to \pi^+\pi^-\psi(2S)$ cross-section can be seen around the 4.660 GeV, identified by Ref. [95] as the $Y(4660)$ state. This represents a kind of independent check of the previous BESIII results, fortifying the observation. The $e^+e^- \to \pi^+\pi^-\psi(2S)$ process is then studied via the $\pi^+\pi^-$ invariant mass ($M(\pi^+\pi^-)$) to probe and search for the $e^+e^- \to f_0(980)\psi(2S)$ interaction. The contribution of the $e^+e^- \to f_0(980)\psi(2S)$ process is found for the first time and its cross section is measured. In the $e^+e^- \to f_0(980)\psi(2S)$ cross-section no particular structures can be recognised as the statistical uncertainty prevents any conclusion. The results naturally pose a constraint on the $Y(4660)$ state contribution to the $e^+e^- \to \pi^+\pi^-\psi(2S)$ cross-section, since it is evident that the $f_0(980)$ contribution largely dominates the total production cross-section. More data is needed to see whether the $Y(4660)$ resonance appears also in $e^+e^- \to f_0(980)\psi(2S)$ data to further investigate its nature. Finally, a search for the charged $Z_c(4430)$ exotic state is performed, but no significant signal is found; a Bayesian upper limit at the 90% confidence level (C.L.) is set on the $e^+e^- \to \pi^\pm Z_c(4430)^\mp$ process' number of events to be 16, leading to a production ratio $R = \sigma(e^+e^- \to \pi^\pm Z_c(4430)^\mp \to \pi^+\pi^-\psi(2S))/\sigma(e^+e^- \to \pi^+\pi^-\psi(2S))$ of 1.1%.

While no observation is reported, the found upper limit will provide insights towards a better understanding of $Z_c(4430)^\pm$ resonance, a surely exotic charged four-quark state. With the data recently collected by the BESIII detector, this analysis will be extended to the centre-of-mass energies above 4.7 GeV to increase the sensitivity to a possible $Z_c(4430)^\pm$ state. Moreover, owing to the data that will be collected with the upgraded BESIII detector and BEPCII accelerator in the next future, improved precision and techniques will be expected to further probe the charged $Z_c(4430)$ nature and its underlying structure.

Appendix A

CONEXC: An event generator for Initial State Radiation Corrections

In e^+e^- colliders, before the e^+e^- collision, a leptonic beam can emit photon radiation. This phenomenon, called Initial State Radiation (ISR), can effectively reduce the beam energy. CONEXC is an event simulator integrated into the BesEvtGen software specifically created for the e^+e^- experiments to calculate ISR corrections up to the second order. The model of said generator takes as input the measured Born cross-section (σ_{exp}) and estimates the ISR-corrected cross-section ($\sigma_{e^+e^-\to\gamma X}$) via the following theoretical calculation:

$$\sigma_{e^+e^-\to\gamma X}(s) = \int dm \frac{2m}{s} W(s,x) \frac{\sigma_{\text{exp}}(m)}{[1+\Pi(m)]^2}, \tag{A.1}$$

where $W(s,x)$ is the radiator function, which encapsulates the probability of the $\sigma_{e^+e^-\to X}$ transition to occur at lower centre-of-mass energy with respect to the initial one ($\sqrt{s}$), $m = \sqrt{s(1-x)}$ is the invariant mass of the final γX state, with $x = 2E_\gamma/\sqrt{s}$ being the fractional energy taken away by the ISR photon radiated by a leptonic beam, and $\Pi(m)$ is the vacuum polarisation also provided by the generator.

Neglecting the vacuum polarisation, from the theoretical model the ISR correction factor $(1+\delta)$ calculated by CONEXC is defined as

$$1 + \delta = \int dx \frac{\sigma_{e^+e^-\to\gamma X}(s)}{\sigma_{\text{exp}}} W(s,x). \tag{A.2}$$

The experimental efficiency is also affected by the ISR, as the detector behaviour is different for different centre-of-mass energies, and it typically has a decreasing

trend as x increases. The effective efficiency ($\epsilon_{\text{effective}}$), the one measured by the operator, is

$$\epsilon_{\text{effective}} = \frac{N_{\text{Rec}}}{N_{\text{Gen}}} = \frac{\int dx\ \epsilon(x)\ \sigma_{e^+e^-\to\gamma X}(s)\ W(s,x)}{\int dx\ \sigma_{e^+e^-\to\gamma X}(s)\ W(s,x)}, \tag{A.3}$$

where $\epsilon(x)$ is the efficiency at the centre-of-mass m, and N_{Rec} and N_{Gen} are the number of reconstructed and generated events, respectively.

Finally, with the number of events (N) estimated from the data by the operator and the luminosity ($\mathcal{L}$) at a given centre-of-mass energy, the experimental measurements can be provided as:

$$\sigma_{\text{exp}} = \frac{N}{\mathcal{L}\ \epsilon_{\text{effective}}\ (1+\delta)}. \tag{A.4}$$

Operatively, the user iteratively feeds the experimental Born cross-sections to the generator, starting from a flat cross-section hypothesis and repeating the generation until the final σ_{Born} converges. The convergence is defined when $(1+\delta)\epsilon_{\text{effective}}$ is consistent with a previous iteration within a given percentage. An example of said iteration is presented in Fig. A.1, where it can be visually appreciated the convergence of the $(1+\delta)\epsilon_{\text{effective}}$ product of the $\sigma_{\text{Born}}(e^+e^- \to \pi^+\pi^-\psi(2S))$ for each centre-of-mass energy.

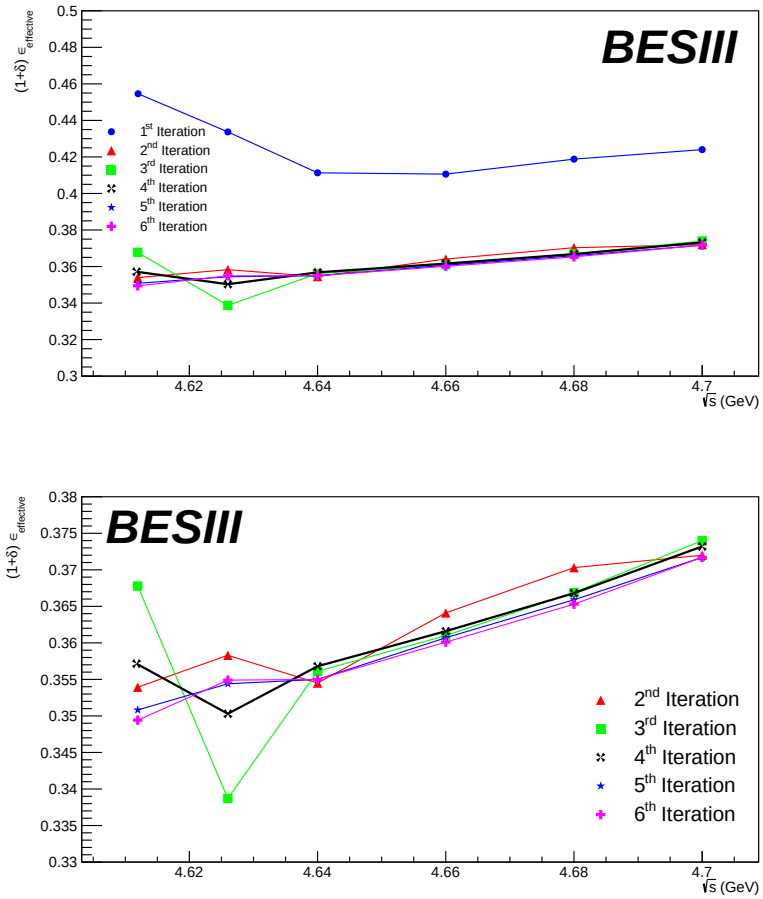

Figure A.1: $(1+\delta)\epsilon_{\text{effective}}$ convergence plots. For each CONEXC iteration of the $e^+e^- \to \pi^+\pi^-\psi(2S)$ process, the $(1+\delta)\epsilon_{\text{effective}}$ product at each centre-of-mass energy is plotted. For sake of readability, the plot on the bottom is a zoomed-in version of the one above, with the first iteration removed.

Bibliography

[1] P. Zyla *et al.*, "Review of Particle Physics," *PTEP*, vol. 2020, no. 8, p. 083C01, 2020.

[2] M. Gell-Mann, "A Schematic Model of Baryons and Mesons," *Phys. Lett.*, vol. 8, pp. 214–215, 1964.

[3] G. Zweig, "An SU(3) model for strong interaction symmetry and its breaking. Version 1," 1 1964.

[4] J. J. Aubert *et al.*, "Experimental Observation of a Heavy Particle J," *Phys. Rev. Lett.*, vol. 33, pp. 1404–1406, 1974.

[5] J. E. Augustin *et al.*, "Discovery of a Narrow Resonance in e^+e^- Annihilation," *Phys. Rev. Lett.*, vol. 33, pp. 1406–1408, 1974.

[6] G. S. Abrams *et al.*, "The Discovery of a Second Narrow Resonance in e^+e^- Annihilation," *Phys. Rev. Lett.*, vol. 33, pp. 1453–1455, 1974.

[7] M. E. Peskin and D. V. Schroeder, *An Introduction to quantum field theory*. Reading, USA: Addison-Wesley, 1995.

[8] J. D. Bjorken, "Asymptotic Sum Rules at Infinite Momentum," *Phys. Rev.*, vol. 179, pp. 1547–1553, 1969.

[9] R. P. Feynman, "Very high-energy collisions of hadrons," *Phys. Rev. Lett.*, vol. 23, pp. 1415–1417, 1969.

[10] T. Appelquist and H. D. Politzer, "Heavy Quarks and e+ e- Annihilation," 1975.

[11] A. De Rujula and S. L. Glashow, "Is Bound Charm Found?," *Phys. Rev. Lett.*, vol. 34, pp. 46–49, 1975.

[12] T. Appelquist, A. De Rujula, H. D. Politzer, and S. L. Glashow, "Charmonium Spectroscopy," *Phys. Rev. Lett.*, vol. 34, p. 365, 1975.

[13] E. Eichten, K. Gottfried, T. Kinoshita, J. B. Kogut, K. D. Lane, and T.-M. Yan, "The Spectrum of Charmonium," *Phys. Rev. Lett.*, vol. 34, pp. 369–372, 1975. [Erratum: Phys.Rev.Lett. 36, 1276 (1976)].

[14] S. L. Glashow, J. Iliopoulos, and L. Maiani, "Weak Interactions with Lepton-Hadron Symmetry," *Phys. Rev. D*, vol. 2, pp. 1285–1292, 1970.

[15] N. Cabibbo, "Unitary Symmetry and Leptonic Decays," *Phys. Rev. Lett.*, vol. 10, pp. 531–533, 1963.

[16] G. Mezzadri and S. Spataro, "XYZ states: An experimental point-of-view," *Rev. Phys.*, vol. 8, p. 100070, 2022.

[17] Choi, S.-K. and others, "Observation of a Narrow Charmoniumlike State in Exclusive $B^{\pm} \to K^{\pm}\pi^{+}\pi^{-}J/\psi$ Decays," *Phys. Rev. Lett.*, vol. 91, p. 262001, Dec 2003.

[18] W. Kwong, J. L. Rosner, and C. Quigg, "Heavy-quark systems," *Ann. Rev. Nucl. Part. Sci.*, vol. 37, pp. 325–382, 1987.

[19] M. Ablikim *et al.*, "Measurements of $h_c(^1p_1)$ in $\psi^{'}$ decays," *Phys. Rev. Lett.*, vol. 104, p. 132002, Mar 2010.

[20] M. Ablikim *et al.*, "Study of $\psi(3686) \to \pi^0 h_c$, $h_c \to \gamma\eta_c$ via η_c exclusive decays," *Phys. Rev. D*, vol. 86, p. 092009, Nov 2012.

[21] S. Dobbs *et al.*, "Precision measurement of the mass of the $h_c(^1p_1)$ state of charmonium," *Phys. Rev. Lett.*, vol. 101, p. 182003, Oct 2008.

[22] Andreotti, M. and others, "Results of a search for the $h_c(^1P_1)$ state of charmonium in the $\eta_c\gamma$ and $J/\psi\pi^0$ decay modes," *Phys. Rev. D*, vol. 72, p. 032001, Aug 2005.

[23] Ablikim, M. and others, "Study of the $h_c(1^1P_1)$ meson via $\psi(2S) \to \pi^0 h_c$ decays at BESIII," *Phys. Rev. D*, vol. 106, p. 072007, Oct 2022.

[24] M. Ablikim *et al.*, "Observation of a charged charmoniumlike structure $Z_c(4020)$ and search for the $Z_c(3900)$ in $e^+e^- \to \pi^+\pi^- h_c$," *Phys. Rev. Lett.*, vol. 111, p. 242001, Dec 2013.

[25] M. Ablikim *et al.*, "Evidence of two resonant structures in $e^+e^- \to \pi^+\pi^- h_c$," *Phys. Rev. Lett.*, vol. 118, p. 092002, Mar 2017.

[26] Rapidis, P. A. and others, "Observation of a Resonance in e^+e^- Annihilation Just above Charm Threshold," *Phys. Rev. Lett.*, vol. 39, pp. 526–529, Aug 1977.

[27] Ferretti, J. and Galatà, G. and Santopinto, E., "Interpretation of the $X(3872)$ as a charmonium state plus an extra component due to the coupling to the meson-meson continuum," *Phys. Rev. C*, vol. 88, p. 015207, Jul 2013.

[28] S. R. Wagner, "Recent results from the MARK-II experiment.," in *1991 SLAC Summer Institute on Particle Physics: Lepton Hadron Scattering (School: Aug 5-13, Topical Conf: Aug 14-16) (SSI 91)*, pp. 327–335, 1991.

[29] D. Hitlin, "A third generation detector for SPEAR," *Phys. Scripta*, vol. 23, pp. 634–641, 1981.

[30] H. Aihara *et al.*, "Charmonium Production in Photon-photon Collisions," *Phys. Rev. Lett.*, vol. 60, p. 2355, 1988.

[31] E. D. Bloom *et al.*, "A Proposal for a Large Solid Angle Neutral Detector for SPEAR-II: The Crystal Ball," 2 1975.

[32] R. Brandelik *et al.*, "Results from DASP on e^+e^- Annihilation between 3.1 GeV and 5.2 GeV," *Z. Phys. C*, vol. 1, pp. 233–256, 1979.

[33] V. Hepp, "Pluto results on jets and QCD," *AIP Conf. Proc.*, vol. 68, pp. 622–626, 1980.

[34] "Progress Report on Results From the CLEO Detector," 7 1980.

[35] C. M. Tarbert, "Recent charmonium results from CLEO-c," *Nuovo Cim. C*, vol. 033N5, pp. 229–236, 2010.

[36] C.-Z. Yuan and S. L. Olsen, "The BESIII physics programme," *Nature Rev. Phys.*, vol. 1, no. 8, pp. 480–494, 2019.

[37] M. Ablikim *et al.*, "Future Physics Programme of BESIII," *Chin. Phys. C*, vol. 44, no. 4, p. 040001, 2020.

[38] D. Boutigny *et al.*, "Letter of Intent for the Study of CP Violation and Heavy Flavor Physics at PEP-II," in *The B Factory: Extending the Luminosity Frontier*, 6 1994.

[39] S. L. Olsen, "The BELLE experiment at KEKB," in *1994 Meeting of the American Physical Society, Division of Particles and Fields (DPF 94)*, pp. 1908–1913, 8 1994.

[40] D. Websdale, "LHC-B: A Dedicated b physics detector for the LHC," *Nucl. Phys. B Proc. Suppl.*, vol. 50, pp. 333–342, 1996.

[41] P. Dalpiaz, "Charmonium and other onia at minimum energy," *Conf. Proc. C*, vol. 7903192, pp. 111–124, 1979.

[42] C. M. Ginsburg, "Fermilab E760 and E835 charmonium formation in $\bar{p}p$ annihilation," *AIP Conf. Proc.*, vol. 349, pp. 251–269, 1996.

[43] A. Dbeyssi, "The PANDA Experiment at FAIR," *Moscow Univ. Phys. Bull.*, vol. 77, no. 2, pp. 193–194, 2022.

[44] T. Lyubushkina, "ATLAS results on charmonium production and Bc+ meson production and decays," *Rev. Mex. Fis. Suppl.*, vol. 3, no. 3, p. 0308054, 2022.

[45] A. Abdulsalam, "Charmonium production in pp, p+Pb and Pb+Pb collisions with CMS experiment," *J. Phys. Conf. Ser.*, vol. 1258, no. 1, p. 1, 2019.

[46] T. Tork, "Charmonium production as a function of charged-particle multiplicity in pp and p–Pb collisions with ALICE at the LHC," in *29th International Workshop on Deep-Inelastic Scattering and Related Subjects*, 7 2022.

[47] A. B. Meyer, "Charmonium production at HERA," *Int. J. Mod. Phys. A*, vol. 22, pp. 455–463, 2007.

[48] R. Abdul Khalek *et al.*, "Science Requirements and Detector Concepts for the Electron-Ion Collider: EIC Yellow Report," *Nucl. Phys. A*, vol. 1026, p. 122447, 2022.

[49] D. Bettoni and R. Calabrese, "Charmonium spectroscopy," *Prog. Part. Nucl. Phys.*, vol. 54, pp. 615–651, 2005.

[50] Czyż", Henryk and Kühn, Johann H. and Tracz, Szymon, "χ_{c1} and χ_{c2} production at e^+e^- colliders," *Phys. Rev. D*, vol. 94, p. 034033, Aug 2016.

[51] M. Ablikim *et al.*, "First Observation of the Direct Production of the χ_{c1} in e^+e^- Annihilation," *Phys. Rev. Lett.*, vol. 129, p. 122001, Sep 2022.

[52] S.-K. Choi *et al.*, "Observation of the $\eta_c(2S)$ in Exclusive $B \to KK_SK^-\pi^+$ Decays," *Phys. Rev. Lett.*, vol. 89, p. 102001, Aug 2002.

[53] K. Abe *et al.*, "Observation of Double $c\bar{c}$ Production in e^+e^- Annihilation at $\sqrt{s} \approx 10.6$ GeV," *Phys. Rev. Lett.*, vol. 89, p. 142001, Sep 2002.

[54] Bodwin, Geoffrey T. and Braaten, Eric and Lepage, G. Peter, "Rigorous QCD analysis of inclusive annihilation and production of heavy quarkonium," *Phys. Rev. D*, vol. 51, pp. 1125–1171, Feb 1995.

[55] Bodwin, Geoffrey T. and Lee, Jungil and Braaten, Eric, "Exclusive double-charmonium production from e^+e^- annihilation into two virtual photons," *Phys. Rev. D*, vol. 67, p. 054023, Mar 2003.

[56] E. Eichten and B. R. Hill, "An Effective Field Theory for the Calculation of Matrix Elements Involving Heavy Quarks," *Phys. Lett. B*, vol. 234, pp. 511–516, 1990.

[57] Thacker, B. A. and Lepage, G. Peter, "Heavy-quark bound states in lattice QCD," *Phys. Rev. D*, vol. 43, pp. 196–208, Jan 1991.

[58] S.-K. Choi *et al.*, "Observation of a Resonancelike Structure in the $\pi^{+-}\psi'$ Mass Distribution in Exclusive $B \to K\pi^{+-}\psi'$ Decays," *Phys. Rev. Lett.*, vol. 100, p. 142001, Apr 2008.

[59] R. Aaij *et al.*, "Observation of the Resonant Character of the $Z(4430)^-$ State," *Phys. Rev. Lett.*, vol. 112, p. 222002, Jun 2014.

[60] Brambilla, N. and others, "The xyz states: Experimental and theoretical status and perspectives," *Physics Reports*, vol. 873, pp. 1–154, 2020. The XYZ states: experimental and theoretical status and perspectives.

[61] T. Gershon, "Exotic hadron naming convention," 6 2022.

[62] D. Acosta *et al.*, "Observation of the Narrow State $X(3872) \to J/\psi\pi^+\pi^-$ in $\overline{p}p$ Collisions at $\sqrt{s} = 1.96$ TeV," *Phys. Rev. Lett.*, vol. 93, p. 072001, Aug 2004.

[63] V. M. Abazov *et al.*, "Observation and Properties of the $X(3872)$ Decaying to $J/\psi\pi^+\pi^-$ in $p\overline{p}$ Collisions at $\sqrt{s} = 1.96$ TeV," *Phys. Rev. Lett.*, vol. 93, p. 162002, Oct 2004.

[64] B. Aubert *et al.*, "Study of the $B^- \to J/\psi K^-\pi^+\pi^-$ decay and measurement of the $B^- \to X(3872)K^-$ branching fraction," *Phys. Rev. D*, vol. 71, p. 071103, Apr 2005.

[65] A. Abulencia *et al.*, "Analysis of the Quantum Numbers J^{PC} of the X(3872) Particle," *Phys. Rev. Lett.*, vol. 98, p. 132002, Mar 2007.

[66] R. Aaij *et al.*, "Quantum numbers of the $X(3872)$ state and orbital angular momentum in its $\rho^0 J/\psi$ decay," *Phys. Rev. D*, vol. 92, p. 011102, Jul 2015.

[67] N. A. Tornqvist, "Isospin breaking of the narrow charmonium state of Belle at 3872 MeV as a deuson," *Phys. Lett. B*, vol. 590, pp. 209–215, 2004.

[68] M. Ablikim *et al.*, "Study of $e^+e^- \to \gamma\omega J/\psi$ and Observation of $X(3872) \to \omega J/\psi$," *Phys. Rev. Lett.*, vol. 122, p. 232002, Jun 2019.

[69] A. Bala *et al.*, "Observation of $X(3872)$ in $B \to X(3872)K\pi$ decays," *Phys. Rev. D*, vol. 91, p. 051101, Mar 2015.

[70] R. Aaij *et al.*, "Observation of the $\Lambda_b^0 \to \chi_{c1}(3872)pK^-$ decay," *JHEP*, vol. 09, p. 028, 2019.

[71] Cleven, Martin and Wang, Qian and Guo, Feng-Kun and Hanhart, Christoph and Meißner, Ulf-G. and Zhao, Qiang, "$Y(4260)$ as the first S-wave open charm vector molecular state?," *Phys. Rev. D*, vol. 90, p. 074039, Oct 2014.

[72] M. Ablikim *et al.*, "Observation of $e^+e^- \to \gamma X(3872)$ at BESIII," *Phys. Rev. Lett.*, vol. 112, p. 092001, Mar 2014.

[73] M. Ablikim *et al.*, "Observation of the Decay $X(3872) \to \pi^0\chi_{c1}(1P)$," *Phys. Rev. Lett.*, vol. 122, p. 202001, May 2019.

[74] B. Aubert *et al.*, "Evidence for $X(3872) \to \psi(2S)\gamma$ in $B^{\pm} \to X(3872)K^{\pm}$ Decays and a Study of $B \to c\bar{c}\gamma K$," *Phys. Rev. Lett.*, vol. 102, p. 132001, Mar 2009.

[75] V. Bhardwaj *et al.*, "Observation of $X(3872) \to J/\psi\gamma$ and Search for $X(3872) \to \psi'\gamma$ in B Decays," *Phys. Rev. Lett.*, vol. 107, p. 091803, Aug 2011.

[76] R. Aaij *et al.*, "Evidence for the decay $X(3872) \to \psi(2S)\gamma$," *Nucl. Phys. B*, vol. 886, pp. 665–680, 2014.

[77] E. S. Swanson, "Diagnostic decays of the $X(3872)$," *Phys. Lett. B*, vol. 598, pp. 197–202, 2004.

[78] J. P. Lees *et al.*, "Measurements of the Absolute Branching Fractions of $B^{\pm} \to K^{\pm}X_{c\bar{c}}$," *Phys. Rev. Lett.*, vol. 124, p. 152001, Apr 2020.

[79] Braaten, Eric and Kusunoki, Masaoki, "Decays of the $X(3872)$ into J/ψ and light hadrons," *Phys. Rev. D*, vol. 72, p. 054022, Sep 2005.

[80] G. Gokhroo *et al.*, "Observation of a Near-Threshold $D^0\overline{D}^0\pi^0$ Enhancement in $B \to D^0\overline{D}^0\pi^0 K$ Decay," *Phys. Rev. Lett.*, vol. 97, p. 162002, Oct 2006.

[81] T. Aushev *et al.*, "Study of the $B \to X(3872)(\to D^{*0}\overline{D}^0)K$ decay," *Phys. Rev. D*, vol. 81, p. 031103, Feb 2010.

[82] B. Aubert *et al.*, "Study of resonances in exclusive B decays to $\overline{D}^{(*)}D^{(*)}K$," *Phys. Rev. D*, vol. 77, p. 011102, Jan 2008.

[83] Li, C. and Yuan, C.-Z., "Determination of the absolute branching fractions of $X(3872)$ decays," *Phys. Rev. D*, vol. 100, p. 094003, Nov 2019.

[84] T. E. Coan *et al.*, "Charmonium Decays of $Y(4260)$, $\psi(4160)$, and $\psi(4040)$," *Phys. Rev. Lett.*, vol. 96, p. 162003, Apr 2006.

[85] C. Z. Yuan *et al.*, "Measurement of the $e^+e^- \to \pi^+\pi^- J/\psi$ Cross Section Via Initial-State Radiation at Belle," *Phys. Rev. Lett.*, vol. 99, p. 182004, Nov 2007.

[86] J. P. Lees *et al.*, "Study of the reaction $e^+e^- \to J/\psi\pi^+\pi^-$ via initial-state radiation at BABAR," *Phys. Rev. D*, vol. 86, p. 051102, Sep 2012.

[87] Z. Q. Liu *et al.*, "Study of $e^+e^- \to \pi^+\pi^- J/\psi$ and Observation of a Charged Charmoniumlike State at Belle," *Phys. Rev. Lett.*, vol. 110, p. 252002, Jun 2013.

[88] M. Ablikim *et al.*, "Precise Measurement of the $e^+e^- \to \pi^+\pi^- J/\psi$ Cross Section at Center-of-Mass Energies from 3.77 to 4.60 GeV," *Phys. Rev. Lett.*, vol. 118, p. 092001, Mar 2017.

[89] M. Ablikim *et al.*, "Observation of $Z_c(3900)^0$ in $e^+e^- \to \pi^0\pi^0 J/\psi$," *Phys. Rev. Lett.*, vol. 115, p. 112003, Sep 2015.

[90] M. Ablikim *et al.*, "Observation of $e^+e^- \to \pi^0\pi^0 h_c$ and a Neutral Charmoniumlike Structure $Z_c(4020)^0$," *Phys. Rev. Lett.*, vol. 113, p. 212002, Nov 2014.

[91] M. Ablikim *et al.*, "Study of $e^+e^- \to \omega\chi_{cJ}$ at Center of Mass Energies from 4.21 to 4.42 GeV," *Phys. Rev. Lett.*, vol. 114, p. 092003, Mar 2015.

[92] M. Ablikim *et al.*, "Observation of $e^+e^- \to \omega\chi_{c1,2}$ near $\sqrt{s} = 4.42$ and 4.6 GeV," *Phys. Rev. D*, vol. 93, p. 011102, Jan 2016.

[93] M. Ablikim *et al.*, "Cross section measurements of $e^+e^- \to \omega\chi_{c0}$ from $\sqrt{s} =$ 4.178 to 4.278 GeV," *Phys. Rev. D*, vol. 99, p. 091103, May 2019.

[94] M. Ablikim *et al.*, "Evidence of a Resonant Structure in the $e^+e^- \to \pi^+ D^0 D^{*-}$ Cross Section between 4.05 and 4.60 GeV," *Phys. Rev. Lett.*, vol. 122, p. 102002, Mar 2019.

[95] M. Ablikim *et al.*, "Cross section measurement of $e^+e^- \to \pi^+\pi^-\psi(3686)$ from $\sqrt{s} = 4.0076$ GeV to 4.6984 GeV," *Phys. Rev. D*, vol. 104, p. 052012, Sep 2021.

[96] M. Ablikim *et al.*, "Study of the process $e^+e^- \to \pi^0\pi^0 J/\psi$ and neutral charmoniumlike state $Z_c(3900)^0$," *Phys. Rev. D*, vol. 102, p. 012009, Jul 2020.

[97] M. Ablikim *et al.*, "Observation of the $Y(4220)$ and $Y(4390)$ in the process $e^+e^- \to \eta J/\psi$," *Phys. Rev. D*, vol. 102, p. 031101, Aug 2020.

[98] Chen, Dian-Yong and Pang, Cheng-Qun and He, Jun and Zhou, Zhi-Yong, "D-wave charmonia," *Phys. Rev. D*, vol. 100, p. 074016, Oct 2019.

[99] T. Bhavsar, M. Shah, and P. C. Vinodkumar, "Status of quarkonia-like negative and positive parity states in a relativistic confinement scheme," *Eur. Phys. J. C*, vol. 78, no. 3, p. 227, 2018.

[100] Z.-G. Wang, "Analysis of the vector tetraquark states with P-waves between the diquarks and antidiquarks via the QCD sum rules," *Eur. Phys. J. C*, vol. 79, no. 1, p. 29, 2019.

[101] Z.-G. Wang, "Vector tetraquark state candidates: $Y(4260/4220)$, $Y(4360/4320)$, $Y(4390)$ and $Y(4660/4630)$," *Eur. Phys. J. C*, vol. 78, no. 6, p. 518, 2018.

[102] J. Ferretti, "η_c- and J/ψ-isoscalar meson bound states in the hadro-charmonium picture," *Phys. Lett. B*, vol. 782, pp. 702–706, 2018.

[103] Wang, Qian and Cleven, Martin and Guo, Feng-Kun and Hanhart, Christoph and Meißner, Ulf-G. and Wu, Xiao-Gang and Zhao, Qiang, "$Y(4260)$: Hadronic molecule versus hadro-charmonium interpretation," *Phys. Rev. D*, vol. 89, p. 034001, Feb 2014.

[104] Chen, Dian-Yong and Xiao, Cheng-Jian and He, Jun, "Hidden-charm decays of $Y(4390)$ in a hadronic molecular scenario," *Phys. Rev. D*, vol. 96, p. 054017, Sep 2017.

[105] J. He and D.-Y. Chen, "Interpretation of $Y(4390)$ as an isoscalar partner of $Z(4430)$ from $D^*(2010)\bar{D}_1(2420)$ interaction," *Eur. Phys. J. C*, vol. 77, no. 6, p. 398, 2017.

[106] Lebed, Richard F., "Spectroscopy of exotic hadrons formed from dynamical diquarks," *Phys. Rev. D*, vol. 96, p. 116003, Dec 2017.

[107] D.-Y. Chen, X. Liu, and T. Matsuki, "Interference effect as resonance killer of newly observed charmoniumlike states $Y(4320)$ and $Y(4390)$," *Eur. Phys. J. C*, vol. 78, no. 2, p. 136, 2018.

[108] B. Aubert *et al.*, "Evidence of a Broad Structure at an Invariant Mass of 4.32 GeV/c^2 in the Reaction $e^+e^- \to \pi^+\pi^-\psi(2S)$ Measured at BABAR," *Phys. Rev. Lett.*, vol. 98, p. 212001, May 2007.

[109] X. L. Wang *et al.*, "Observation of Two Resonant Structures in $e^+e^- \to \pi^+\pi^-\psi(2S)$ via Initial-State Radiation at Belle," *Phys. Rev. Lett.*, vol. 99, p. 142002, Oct 2007.

[110] J. P. Lees *et al.*, "Study of the reaction $e^+e^- \to \psi(2S)\pi^+\pi^-$ via initial-state radiation at BaBar," *Phys. Rev. D*, vol. 89, p. 111103, Jun 2014.

[111] X. L. Wang *et al.*, "Measurement of $e^+e^- \to \pi^+\pi^-\psi(2S)$ via initial state radiation at Belle," *Phys. Rev. D*, vol. 91, p. 112007, Jun 2015.

[112] M. Ablikim *et al.*, "Measurement of $e^+e^- \to \pi^+\pi^-\psi(3686)$ from 4.008 to 4.600 GeV and observation of a charged structure in the $\pi^\pm\psi(3686)$ mass spectrum," *Phys. Rev. D*, vol. 96, p. 032004, Aug 2017.

[113] D. V. Bugg, "An Alternative fit to Belle mass spectra for $D\bar{D}$, $D^*\bar{D}^*$ and $\Lambda_c\bar{\Lambda}_c$," *J. Phys. G*, vol. 36, p. 075002, 2009.

[114] Cotugno, G. and Faccini, R. and Polosa, A. D. and Sabelli, C., "Charmed Baryonium," *Phys. Rev. Lett.*, vol. 104, p. 132005, Apr 2010.

[115] Guo, Feng-Kun and Haidenbauer, Johann and Hanhart, Christoph and Meißner, Ulf-G., "Reconciling the $X(4630)$ with the $Y(4660)$," *Phys. Rev. D*, vol. 82, p. 094008, Nov 2010.

[116] F.-K. Guo, C. Hanhart, and U.-G. Meissner, "Evidence that the Y(4660) is a $f_0(980)\psi'$ bound state," *Phys. Lett. B*, vol. 665, pp. 26–29, 2008.

[117] Guo, Feng-Kun and Hanhart, Christoph and Meißner, Ulf-G., "Implications of Heavy-Quark Spin Symmetry on Heavy-Meson Hadronic Molecules," *Phys. Rev. Lett.*, vol. 102, p. 242004, Jun 2009.

[118] M. Ablikim *et al.*, "Observation of Resonance Structures in $e^+e^- \to \pi^+\pi^-\psi_2(3823)$ and Mass Measurement of $\psi_2(3823)$," *Phys. Rev. Lett.*, vol. 129, p. 102003, Sep 2022.

[119] C.-F. Qiao, "A Uniform description of the states recently observed at B-factories," *J. Phys. G*, vol. 35, p. 075008, 2008.

[120] Maiani, L. and Piccinini, F. and Polosa, A. D. and Riquer, V., "$Z(4430)$ and a new paradigm for spin interactions in tetraquarks," *Phys. Rev. D*, vol. 89, p. 114010, Jun 2014.

[121] I. K. Hammer, C. Hanhart, and A. V. Nefediev, "Remarks on meson loop effects on quark models," *Eur. Phys. J. A*, vol. 52, no. 11, p. 330, 2016.

[122] Swanson, E. S., "Z_b and Z_c exotic states as coupled channel cusps," *Phys. Rev. D*, vol. 91, p. 034009, Feb 2015.

[123] M. Ablikim *et al.*, "Observation of a Charged Charmoniumlike Structure in $e^+e^- \to \pi^+\pi^- J/\psi$ at $\sqrt{s}$=4.26 GeV," *Phys. Rev. Lett.*, vol. 110, p. 252001, Jun 2013.

[124] T. Xiao, S. Dobbs, A. Tomaradze, and K. K. Seth, "Observation of the Charged Hadron $Z_c^{\pm}(3900)$ and Evidence for the Neutral $Z_c^0(3900)$ in $e^+e^- \to \pi\pi J/\psi$ at $\sqrt{s} = 4170$ MeV," *Phys. Lett. B*, vol. 727, pp. 366–370, 2013.

[125] M. Ablikim *et al.*, "Observation of a Charged $(D\overline{D}^*)^{\pm}$ Mass Peak in $e^+e^- \to \pi D\overline{D}^*$ at $\sqrt{s} = 4.26$ GeV," *Phys. Rev. Lett.*, vol. 112, p. 022001, Jan 2014.

[126] M. Ablikim *et al.*, "Confirmation of a charged charmoniumlike state $Z_c(3885)^{\mp}$ in $e^+e^- \to \pi^{\pm}(D\overline{D}^*)^{\mp}$ with double D tag," *Phys. Rev. D*, vol. 92, p. 092006, Nov 2015.

[127] Chung, Suh-Urk and Friedrich, Jan Michael, "Covariant helicity-coupling amplitudes: A new formulation," *Phys. Rev. D*, vol. 78, p. 074027, Oct 2008.

[128] M. Ablikim *et al.*, "Determination of the Spin and Parity of the $Z_c(3900)$," *Phys. Rev. Lett.*, vol. 119, p. 072001, Aug 2017.

[129] A. Esposito, A. L. Guerrieri, and A. Pilloni, "Probing the nature of $Z_c^{(\prime)}$ states via the $\eta_c\rho$ decay," *Phys. Lett. B*, vol. 746, pp. 194–201, 2015.

[130] M. Ablikim *et al.*, "Study of $e^+e^- \to \pi^+\pi^-\pi^0\eta_c$ and evidence for $Z_c(3900)^{\pm}$ decaying into $\rho^{\pm}\eta_c$," *Phys. Rev. D*, vol. 100, p. 111102, Dec 2019.

[131] B. Aubert *et al.*, "Search for the $Z(4430)^-$ at BABAR," *Phys. Rev. D*, vol. 79, p. 112001, Jun 2009.

[132] K. Chilikin *et al.*, "Experimental constraints on the spin and parity of the $Z(4430)^+$," *Phys. Rev. D*, vol. 88, p. 074026, Oct 2013.

[133] K. Chilikin *et al.*, "Observation of a new charged charmoniumlike state in $\overline{B}^0 \to J/\psi K^-\pi^+$ decays," *Phys. Rev. D*, vol. 90, p. 112009, Dec 2014.

[134] R. Aaij *et al.*, "Model-Independent Observation of Exotic Contributions to $B^0 \to J/\psi K^+\pi^-$ Decays," *Phys. Rev. Lett.*, vol. 122, p. 152002, Apr 2019.

[135] Brodsky, Stanley J. and Hwang, Dae Sung and Lebed, Richard F., "Dynamical Picture for the Formation and Decay of the Exotic XYZ Mesons," *Phys. Rev. Lett.*, vol. 113, p. 112001, Sep 2014.

[136] S. Dubynskiy and M. B. Voloshin, "Hadro-Charmonium," *Phys. Lett. B*, vol. 666, pp. 344–346, 2008.

[137] S. H. Lee, M. Nielsen, and U. Wiedner, "D(s)D* molecule as an axial meson," *J. Korean Phys. Soc.*, vol. 55, p. 424, 2009.

[138] M. Ablikim *et al.*, "Observation of a Near-Threshold Structure in the K^+ Recoil-Mass Spectra in $e^+e^- \to K^+(D_s^- D^{*0} + D_s^{*-} D^0)$," *Phys. Rev. Lett.*, vol. 126, no. 10, p. 102001, 2021.

[139] M. Ablikim *et al.*, "Evidence for a Neutral Near-Threshold Structure in the K_S^0 Recoil-Mass Spectra in $e^+e^- \to K_S^0 D_s^+ D^{*-}$ and $e^+e^- \to K_S^0 D_s^{*+} D^-$," *Phys. Rev. Lett.*, vol. 129, p. 112003, Sep 2022.

[140] B.-D. Wan and C.-F. Qiao, "About the exotic structure of Z_{cs}," *Nucl. Phys. B*, vol. 968, p. 115450, 2021.

[141] R. Aaij *et al.*, "Observation of New Resonances Decaying to $J/\psi K^+$ and $J/\psi\phi$," *Phys. Rev. Lett.*, vol. 127, p. 082001, Aug 2021.

[142] Steven Weinberg, "Phenomenological Lagrangians," *Physica A: Statistical Mechanics and its Applications*, vol. 96, no. 1, pp. 327–340, 1979.

[143] H. Leutwyler, "On the foundations of chiral perturbation theory," *Annals Phys.*, vol. 235, pp. 165–203, 1994.

[144] Brambilla, Nora and Krein, Gastão and Tarrús Castellà, Jaume and Vairo, Antonio, "Born-Oppenheimer approximation in an effective field theory language," *Phys. Rev. D*, vol. 97, p. 016016, Jan 2018.

[145] Burch, T. and DeTar, C. and Di Pierro, M. and El-Khadra, A. X. and Freeland, E. D. and Gottlieb, Steven and Kronfeld, A. S. and Levkova, L. and Mackenzie, P. B. and Simone, J. N., "Quarkonium mass splittings in three-flavor lattice QCD," *Phys. Rev. D*, vol. 81, p. 034508, Feb 2010.

[146] Namekawa, Y. and Aoki, S. and Ishikawa, K. -I. and Ishizuka, N. and Izubuchi, T. and Kanaya, K. and Kuramashi, Y. and Okawa, M. and Taniguchi, Y. and Ukawa, A. and Ukita, N. and Yoshié, T., "Charm quark system at the physical point of 2+1 flavor lattice QCD," *Phys. Rev. D*, vol. 84, p. 074505, Oct 2011.

[147] Donald, G. C. and Davies, C. T. H. and Dowdall, R. J. and Follana, E. and Hornbostel, K. and Koponen, J. and Lepage, G. P. and McNeile, C., "Precision tests of the J/ψ from full lattice QCD: Mass, leptonic width, and radiative decay rate to η_c," *Phys. Rev. D*, vol. 86, p. 094501, Nov 2012.

[148] Berwein, Matthias and Brambilla, Nora and Tarrús Castellà, Jaume and Vairo, Antonio, "Quarkonium hybrids with nonrelativistic effective field theories," *Phys. Rev. D*, vol. 92, p. 114019, Dec 2015.

[149] Barnes, T. and Close, F. E. and Swanson, E. S., "Hybrid and conventional mesons in the flux tube model: Numerical studies and their phenomenological implications," *Phys. Rev. D*, vol. 52, pp. 5242–5256, Nov 1995.

[150] Kalashnikova, Yu. S. and Nefediev, A. V., "QCD string in excited heavy-light mesons and heavy-quark hybrids," *Phys. Rev. D*, vol. 94, p. 114007, Dec 2016.

[151] F.E. Close, "New metastable charmonium and the ψ' anomaly at CDF," *Physics Letters B*, vol. 342, no. 1, pp. 369–374, 1995.

[152] Dunietz, Isard and Incandela, Joseph and Snider, Frederick D. and Yamamoto, Hitoshi, "Large charmless yield inB decays and inclusiveB decay puzzles," *The European Physical Journal C*, vol. 1, no. 1, pp. 211–219, 1998.

[153] M. B. Voloshin, "Charmonium," *Prog. Part. Nucl. Phys.*, vol. 61, pp. 455–511, 2008.

[154] X. Li and M. B. Voloshin, "$Y(4260)$ and $Y(4360)$ as mixed hadrocharmonium," *Mod. Phys. Lett. A*, vol. 29, no. 12, p. 1450060, 2014.

[155] Voloshin, M. B., "$Z_c(4100)$ and $Z_c(4200)$ as hadrocharmonium," *Phys. Rev. D*, vol. 98, p. 094028, Nov 2018.

[156] Guo, Feng-Kun and Hanhart, Christoph and Meißner, Ulf-G. and Wang, Qian and Zhao, Qiang and Zou, Bing-Song, "Hadronic molecules," *Rev. Mod. Phys.*, vol. 90, p. 015004, Feb 2018.

[157] Filin, A. A. and Romanov, A. and Baru, V. and Hanhart, C. and Kalashnikova, Yu. S. and Kudryavtsev, A. E. and Meißner, U.-G. and Nefediev, A. V., "Comment on *Possibility of Deeply Bound Hadronic Molecules from Single Pion Exchange*," *Phys. Rev. Lett.*, vol. 105, p. 019101, Jul 2010.

[158] Braaten, Eric and Kusunoki, Masaoki and Nussinov, Shmuel, "Production of the $X(3872)$ in B-Meson Decay by the Coalescence of Charm Mesons," *Phys. Rev. Lett.*, vol. 93, p. 162001, Oct 2004.

[159] Zhou, Zhi-Yong and Xiao, Zhiguang, "Comprehending isospin breaking effects of $X(3872)$ in a Friedrichs-model-like scheme," *Phys. Rev. D*, vol. 97, p. 034011, Feb 2018.

[160] Wang, Qian and Hanhart, Christoph and Zhao, Qiang, "Decoding the Riddle of $Y(4260)$ and $Z_c(3900)$," *Phys. Rev. Lett.*, vol. 111, p. 132003, Sep 2013.

[161] Richard, Jean-Marc and Valcarce, Alfredo and Vijande, Javier, "Few-body quark dynamics for doubly heavy baryons and tetraquarks," *Phys. Rev. C*, vol. 97, p. 035211, Mar 2018.

[162] A. Ali, L. Maiani, A. V. Borisov, I. Ahmed, M. J. Aslam, A. Y. Parkhomenko, A. D. Polosa, and A. Rehman, "A new look at the Y tetraquarks and Ω_c baryons in the diquark model," *The European Physical Journal C*, vol. 78, no. 1, p. 29, 2018.

[163] D. V. Bugg, "Reinterpreting several narrow 'resonances' as threshold cusps," *Phys. Lett. B*, vol. 598, pp. 8–14, 2004.

[164] E. S. Swanson, "Cusps and Exotic Charmonia," *Int. J. Mod. Phys. E*, vol. 25, no. 07, p. 1642010, 2016.

[165] Adam P. Szczepaniak, "Triangle singularities and XYZ quarkonium peaks," *Physics Letters B*, vol. 747, pp. 410–416, 2015.

[166] L. Aggarwal *et al.*, "Snowmass White Paper: Belle II physics reach and plans for the next decade and beyond," 7 2022.

[167] R. Aaij *et al.*, "Physics case for an LHCb Upgrade II - Opportunities in flavour physics, and beyond, in the HL-LHC era," 8 2018.

[168] Lu, Jiada and Xiao, Yanjia and Ji, Xiaobin, "Online monitoring of the center-of-mass energy from real data at BESIII," *Radiation Detection Technology and Methods*, vol. 4, no. 3, pp. 337–344, 2020.

[169] H. Geng, W. Liu, J. Qiu, J. Xing, C. Yu, and Y. Zhang, "Lattice Design for BEPCII Upgrade," *JACoW*, vol. IPAC2021, pp. 3756–3758, 2021.

[170] M. Ablikim *et al.*, "Design and construction of the besiii detector," *Nucl. Instrum. Methods Phys. Res., Sect. A*, vol. 614, no. 3, pp. 345 – 399, 2010.

[171] M. Ablikim *et al.*, "Measurement of the Cross Section for $e^+e^- \to$ Hadrons at Energies from 2.2324 to 3.6710 GeV," *Phys. Rev. Lett.*, vol. 128, p. 062004, Feb 2022.

[172] P. A. Baikov, K. G. Chetyrkin, J. H. Kuhn, and J. Rittinger, "Adler Function, Sum Rules and Crewther Relation of Order $\mathcal{O}(\alpha_s^4)$: the Singlet Case," *Phys. Lett. B*, vol. 714, pp. 62–65, 2012.

[173] V. V. Anashin *et al.*, "Precise measurement of $R_{\rm uds}$ and R between 1.84 and 3.72 GeV at the KEDR detector," *Phys. Lett. B*, vol. 788, pp. 42–51, 2019.

[174] M. Ablikim *et al.*, "White Paper on the Future Physics Programme of BESIII," *Chin. Phys. C*, vol. 44, p. 040001, apr 2020.

[175] M. Ablikim *et al.*, "Conceptual design report besiii cylindrical gem inner tracker," 2014.

[176] Z. Wu, "The Upgrade of Endcap TOF in BESIII," *Int. J. Mod. Phys. Conf. Ser.*, vol. 46, p. 1860078, 2018.

[177] M. Ablikim *et al.*, "Oscillating features in the electromagnetic structure of the neutron," *Nature Physics*, vol. 17, no. 11, pp. 1200–1204, 2021.

[178] M. Ablikim *et al.*, "Determination of the Pseudoscalar Decay Constant $f_{D_s^+}$ via $D_s^+ \to \mu^+\nu_\mu$," *Phys. Rev. Lett.*, vol. 122, p. 071802, Feb 2019.

[179] M. Ablikim *et al.*, "Observation of a State $X(2600)$ in the $\pi^+\pi^-\eta'$ System in the Process $J/\psi \to \gamma\pi^+\pi^-\eta'$," *Phys. Rev. Lett.*, vol. 129, p. 042001, Jul 2022.

[180] M. Ablikim *et al.*, "Partial wave analysis of $J/\psi \to \gamma\eta'\eta'$," *Phys. Rev. D*, vol. 105, p. 072002, Apr 2022.

[181] M. Ablikim *et al.*, "Observation of an Isoscalar Resonance with Exotic $J^{PC} = 1^{-+}$ Quantum Numbers in $J/\psi \to \gamma\eta\eta^{'}$," *Phys. Rev. Lett.*, vol. 129, p. 192002, Oct 2022.

[182] M. Ablikim *et al.*, "Partial wave analysis of $J/\psi \to \gamma\eta\eta^{'}$," *Phys. Rev. D*, vol. 106, p. 072012, Oct 2022.

[183] Dudek, Jozef J. and Edwards, Robert G. and Guo, Peng and Thomas, Christopher E., "Toward the excited isoscalar meson spectrum from lattice QCD," *Phys. Rev. D*, vol. 88, p. 094505, Nov 2013.

[184] M. Ablikim *et al.*, "Observation of a Resonance $X(1835)$ in $J/\psi \to \gamma\pi^{+}\pi^{-}\eta^{'}$," *Phys. Rev. Lett.*, vol. 95, p. 262001, Dec 2005.

[185] M. Ablikim *et al.*, "Observation of J/ψ Electromagnetic Dalitz Decays to $X(1835)$, $X(2120)$, and $X(2370)$," *Phys. Rev. Lett.*, vol. 129, p. 022002, Jul 2022.

[186] M. Ablikim *et al.*, "Search for the decay $h_c \to \pi^0 J/\psi$," *JHEP*, vol. 05, p. 003, 2022.

[187] M. Ablikim *et al.*, "Search for new hadronic decays of h_c and observation of $h_c \to p\bar{p}\eta$," *JHEP*, vol. 05, p. 108, 2022.

[188] M. Ablikim *et al.*, "Measurement of the Absolute Branching Fraction of $D_s^+ \to \tau^+\nu_\tau$ via $\tau^+ \to e^+\nu_e\overline{\nu}_\tau$," *Phys. Rev. Lett.*, vol. 127, p. 171801, Oct 2021.

[189] M. Ablikim *et al.*, "Measurement of the CP-even fraction of $D^0 \to \pi^+\pi^-\pi^+\pi^-$," 8 2022.

[190] M. Ablikim *et al.*, "Measurement of the absolute branching fractions for purely leptonic D_s^+ decays," *Phys. Rev. D*, vol. 104, p. 052009, Sep 2021.

[191] M. Ablikim *et al.*, "Measurement of the $e^+e^- \to \Sigma^0\bar{\Sigma}^0$ cross sections at center-of-mass energies from 2.3864 to 3.0200 GeV," *Phys. Lett. B*, vol. 831, p. 137187, 2022.

[192] Hand, L. N. and Miller, D. G. and Wilson, Richard, "Electric and Magnetic Form Factors of the Nucleon," *Rev. Mod. Phys.*, vol. 35, pp. 335–349, Apr 1963.

[193] Aubert, B. and others, "Study of $e^+e^- \to \Lambda\overline{\Lambda}$, $\Lambda\overline{\Sigma}^0$, $\Sigma^0\overline{\Sigma}^0$ using initial state radiation with BABAR," *Phys. Rev. D*, vol. 76, p. 092006, Nov 2007.

[194] S. Pacetti, R. Baldini Ferroli, and E. Tomasi-Gustafsson, "Proton electromagnetic form factors: Basic notions, present achievements and future perspectives," *Phys. Rept.*, vol. 550-551, pp. 1–103, 2015.

[195] Bob Holdom, "Two U(1)'s and ϵ charge shifts," *Physics Letters B*, vol. 166, no. 2, pp. 196–198, 1986.

[196] Pierre Fayet, "Extra U(1)'s and new forces," *Nuclear Physics B*, vol. 347, no. 3, pp. 743–768, 1990.

[197] Arkani-Hamed, Nima and Finkbeiner, Douglas P. and Slatyer, Tracy R. and Weiner, Neal, "A theory of dark matter," *Phys. Rev. D*, vol. 79, p. 015014, Jan 2009.

[198] M. Ablikim *et al.*, "Dark Photon Search in the Mass Range Between 1.5 and 3.4 GeV/c^2," *Phys. Lett. B*, vol. 774, pp. 252–257, 2017.

[199] P. Fayet, "Spontaneously broken supersymmetric theories of weak, electromagnetic and strong interactions," *Physics Letters B*, vol. 69, no. 4, pp. 489–494, 1977.

[200] Ulrich Ellwanger and Cyril Hugonie and Ana M. Teixeira, "The Next-to-Minimal Supersymmetric Standard Model," *Physics Reports*, vol. 496, no. 1, pp. 1–77, 2010.

[201] M. Ablikim *et al.*, "Search for the decay $J/\psi \to \gamma+$ invisible," *Phys. Rev. D*, vol. 101, p. 112005, Jun 2020.

[202] M. Ablikim *et al.*, "Search for baryon- and lepton-number violating decays $D^0 \to \overline{p}e^+$ and $D^0 \to pe^-$," *Phys. Rev. D*, vol. 105, p. 032006, Feb 2022.

[203] M. Ablikim *et al.*, "Search for baryon and lepton number violating decays $D^+ \to \overline{\Lambda}(\overline{\Sigma}^0)e^+$ and $D^+ \to \Lambda(\Sigma^0)e^+$," *Phys. Rev. D*, vol. 101, p. 031102, Feb 2020.

[204] M. Ablikim *et al.*, "Search for baryon and lepton number violation in $J/\psi \to \Lambda_c^+ e^- +$ c.c.," *Phys. Rev. D*, vol. 99, p. 072006, Apr 2019.

[205] F. Sauli, "GEM: A new concept for electron amplification in gas detectors," *Nucl. Instrum. Meth. A*, vol. 386, pp. 531–534, 1997.

[206] M. Poli Lener, "Triple-GEM detectors for the innermost region of the LHCb muon apparatus," *AIP Conf. Proc.*, vol. 794, no. 1, pp. 311–314, 2005.

[207] I. Vai, "The GEM (GE1/1) Phase II Upgrade for the CMS muon system: results from in-situ tests, production detector qualification, and commissioning plans," *PoS*, vol. EPS-HEP2019, p. 123, 2020.

[208] P. Hauer, "The upgraded ALICE TPC," *Nucl. Instrum. Meth. A*, vol. 1039, p. 167023, 2022.

[209] F. Sauli, "The gas electron multiplier (GEM): Operating principles and applications," *Nucl. Instrum. Meth. A*, vol. 805, pp. 2–24, 2016.

[210] S. Bachmann *et al.*, "Discharge mechanisms and their prevention in the gas electron multiplier (GEM)," *Nucl. Instrum. Meth. A*, vol. 479, pp. 294–308, 2002.

[211] M. P. Titov, "New Developments and Future Perspectives of Gaseous Detectors," *Nucl. Instrum. Meth. A*, vol. 581, pp. 25–37, 2007.

[212] M. Alexeev *et al.*, "Triple GEM performance in magnetic field," *JINST*, vol. 14, no. 08, p. P08018, 2019.

[213] F. Archilli *et al.*, "Technical Design Report of the Inner Tracker for the KLOE-2 experiment," 2 2010.

[214] I. Balossino, F. Cossio, R. Farinelli, and L. Lavezzi, "The CGEM-IT: An Upgrade for the BESIII Experiment," *Symmetry*, vol. 14, no. 5, p. 905, 2022.

[215] G. Barrand *et al.*, "GAUDI - A software architecture and framework for building HEP data processing applications," *Comput. Phys. Commun.*, vol. 140, pp. 45–55, 2001.

[216] W. D. Li *et al.*, "The Offline Software for the BESIII Experiment," in *15th International Conference on Computing in High Energy and Nuclear Physics*, 2006.

[217] S. Agostinelli *et al.*, "GEANT4: A Simulation toolkit," *Nucl. Instrum. Methods Phys. Res., Sect. A*, vol. 506, pp. 250–303, 2003.

[218] S. Jadach, B. F. L. Ward, and Z. Wąs, "Coherent exclusive exponentiation for precision monte carlo calculations," *Phys. Rev. D*, vol. 63, p. 113009, May 2001.

[219] S. Jadach, B. F. L. Ward, and Z. Was, "The Precision Monte Carlo event generator K K for two fermion final states in e^+e^- collisions," *Comput. Phys. Commun.*, vol. 130, pp. 260–325, 2000.

[220] D. J. Lange, "The EvtGen particle decay simulation package," *Nucl. Instrum. Methods Phys. Res., Sect. A*, vol. 462, pp. 152–155, 2001.

[221] R.-G. Ping, "Event generators at BESIII," *Chin. Phys. C*, vol. 32, no. 2007-0205, p. 599, 2008.

[222] J. C. Chen, G. S. Huang, X. R. Qi, D. H. Zhang, and Y. S. Zhu, "Event generator for J/ψ and $\psi(2s)$ decay," *Phys. Rev. D*, vol. 62, p. 034003, Jun 2000.

[223] R.-L. Yang, R.-G. Ping, and H. Chen, "Tuning and Validation of the Lundcharm Model with J/ψ Decays," *Chin. Phys. Lett.*, vol. 31, p. 061301, 2014.

[224] E. Richter-Was, "QED bremsstrahlung in semileptonic B and leptonic tau decays," *Phys. Lett. B*, vol. 303, pp. 163–169, 1993.

[225] R.-G. Ping, "An exclusive event generator for e^+e^- scan experiments," *Chinese Physics C*, vol. 38, p. 083001, aug 2014.

[226] S. Actis *et al.*, "Quest for precision in hadronic cross sections at low energy: Monte Carlo tools vs. experimental data," *The European Physical Journal C*, vol. 66, no. 3, pp. 585–686, 2010.

[227] M. Ablikim *et al.*, "Luminosities and energies of e $^+$ e $^-$ collision data taken between $\sqrt{s}$=4.61 GeV and 4.95 GeV at BESIII," *Chin. Phys. C*, vol. 46, no. 11, p. 113003, 2022.

[228] M. Oreglia, "A Study of the Reactions $\psi' \to \gamma\gamma\psi$," master thesis, 12 1980.

[229] Xingyu Zhou and Shuxian Du and Gang Li and Chengping Shen, "TopoAna: A generic tool for the event type analysis of inclusive Monte-Carlo samples in high energy physics experiments," *Computer Physics Communications*, vol. 258, p. 107540, 2021.

[230] S.M. Flatté, "Coupled-channel analysis of the $\pi\eta$ and $K\bar{K}$ systems near $K\bar{K}$ threshold," *Physics Letters B*, vol. 63, no. 2, pp. 224–227, 1976.

[231] M. Ablikim *et al.*, "Resonances in $J/\psi \to \phi\pi^+\pi^-$ and ϕK^+K^-," *Physics Letters B*, vol. 607, no. 3, pp. 243–253, 2005.

[232] E. A. Kuraev and V. S. Fadin, "On Radiative Corrections to e^+e^- Single Photon Annihilation at High-Energy," *Sov. J. Nucl. Phys.*, vol. 41, pp. 466–472, 1985.

Acknowledgements

So long, and thanks for all the fish...